uOttawa

L'Université canadienne
Canada's university

FACULTÉ DES ÉTUDES SUPÉRIEURES ET POSTOCTORALES

uOttawa

L'Université canadienne
Canada's university

FACULTY OF GRADUATE AND POSDOCTORAL STUDIES

Michael Greene

AUTEUR DE LA THÈSE / AUTHOR OF THESIS

M.Sc. (Cellular and Molecular Medicine)

GRADE / DEGREE

Department of Cellular and Molecular Medicine

FACULTÉ, ÉCOLE, DÉPARTEMENT / FACULTY, SCHOOL, DEPARTMENT

Binding of Phosphodiesterase-4 Inhibitor (R)-(11c) Rolipram in Obese and Diabetic Rats : Effect of Diet and Noradrenergic Modulation

TITRE DE LA THÈSE / TITLE OF THESIS

Dr. J. DaSilva

DIRECTEUR (DIRECTRICE) DE LA THÈSE / THESIS SUPERVISOR

CO-DIRECTEUR (CO-DIRECTRICE) DE LA THÈSE / THESIS CO-SUPERVISOR

EXAMINATEURS (EXAMINATRICES) DE LA THÈSE / THESIS EXAMINERS

Dr. Mary-Ellen Harper

Dr. M. Mbikay

Gary W. Slater

Le Doyen de la Faculté des études supérieures et postdoctorales / Dean of the Faculty of Graduate and Postdoctoral Studies

BINDING OF PHOSPHODIESTERASE-4 INHIBITOR (*R*)-[^{11}C]ROLIPRAM IN OBESE AND DIABETIC RATS: EFFECT OF DIET AND NORADRENERGIC MODULATION

by

Michael Greene

A thesis submitted in conformity with the requirements
for the degree of Master of Science
in the Graduate Department of Cellular and Molecular Medicine
University of Ottawa

Your file Votre référence
ISBN: 978-0-494-25779-1
Our file Notre référence
ISBN: 978-0-494-25779-1

Binding of Phosphodiesterase-4 Inhibitor (*R*)-[^{11}C]Rolipram in Obese and Diabetic Rats: Effect of Diet and Noradrenergic Modulation

M.Sc. in Cellular and Molecular Medicine 2006, Michael Greene,

Department of Cellular and Molecular Medicine, University of Ottawa

Phosphodiesterase type-4 (PDE4) belongs to a family of enzymes responsible for the hydrolysis of cyclic adenosine 3',5'-monophosphate (cAMP) in the body. Activity and density of PDE4 are regulated by endogenous cAMP. The obese and diabetic disease states are associated with sympathetic nervous system dysfunction culminating in altered cAMP-mediated signaling. Our group has previously developed a selective PDE4 inhibitor (*R*)-rolipram labeled with carbon-11 for imaging PDE4 and cAMP-mediated signaling *in vivo* using positron emission tomography (PET). Utilizing (*R*)-[^{11}C]rolipram in biodistribution experiments, rodent models of diet-induced obesity exhibited a dysfunctional PDE4 response to acute noradrenaline reuptake inhibitor desipramine treatment in brain and periphery compared to diet-resistant lean rats; streptozocin-treated type 2 diabetic rats had reduced brain and heart PDE4 levels compared to citrate-treated controls. Overall, these studies support the ability of (*R*)-[^{11}C]rolipram to measure central and peripheral tissue PDE4 levels and dysfunctional cAMP-mediated signaling in the obese and diabetic states using PET.

ACKNOWLEDGEMENTS

I would like to express my sincerest gratitude and thanks to a number of people who have assisted my research and work described in this thesis. Firstly, I would like to thank my supervisor, Dr. Jean DaSilva, whose guidance, endless support, and encouragement has developed me into the scientist that I am today. I would like to show my appreciation to my graduate supervisory committee members Dr. Rob Beanlands, Dr. Mary-Ellen Harper, and Dr. Jerry Radziuk for their involvement, assistance, and special interest of this work. To my co-workers Miran Kenk, James Thackeray, Stephanie Thorn, and Maryam Parsanejad, whom I have had the pleasure of working with, thank you for your immense help in the realization of this research, collective inputs, and also for your friendship. Our radiochemistry technicians Samantha Mason and Jeffrey Collins and engineer Paul Coletta deserve great recognition for the technical assistance provided. Proper statistical analysis of data was conducted in part due to the assistance and insight of the University of Ottawa Heart Institute's biostatistician Kathryn Williams. I would also like to thank the Ontario Graduate Student Scholarship in Science and Technology: Heart and Stroke foundation for the financial support of this work.

I would also like to express thanks to the foremost people in my life, my mother Shirley, father Tony, and grandmother Hilda whose love and guidance have helped me realize the rewards of hard work and perseverance. I deeply thank all of my family and loved ones for making me understand the importance of a strong education and providing me the support and encouragement to achieve this degree.

I would like to dedicate this thesis to my dear fiancée Jennifer, whose dear love, strength, and comfort have guided me through the difficulties of this passage. I look forward to our many journeys together through life. You inspire me every day and I love you with all of my heart.

TABLE OF CONTENTS

LIST OF TABLES

LIST OF FIGURES

ABBREVIATIONS

%AUC	percent area under the curve
$\%ID_{blood}/g_{blood}$	percent of injected dose per gram of blood
$\%ID_{tissue}/g_{tissue}$	percent of injected dose per gram of tissue
^{11}C	carbon-11
^{18}F	fluorine-18
^{3}H	hydrogen-3
^{125}I	iodine-125
^{13}N	nitrogen-13
^{15}O	oxygen-15
β+	positron
β-AR	beta-adrenergic receptor
β-ox	beta-oxidation
AC	adenylyl cyclase
AcCoA	acyl coenzyme-A
ACN	acetonitrile
AKAP	A-kinase anchor protein
AmF	ammonium formate
ANOVA	analysis of variance
ATF2	activating transcription factor 2
ATP	adenosine triphosphate
BAT	brown adipose tissue
B_{max}	maximal binding density
cAMP	cyclic adenosine 3',5'-monophosphate
cGMP	cyclic guanosine 3',5'-monophosphate
CNS	central nervous system
CRE	cAMP-response element
CREB	cAMP-response element binding protein
C-terminal	carboxy-terminal
DIO	diet-induced obese

DM	diabetes mellitus
DM1	type 1 diabetes mellitus
DM2	type 2 diabetes mellitus
DMI	desipramine
DR	diet-resistant
e^-	electron
EC_{50}	median effective concentration
ERK	extracellular-signal-related protein kinase
ETC	electron transport chain
FADH	reduced flavin adenine dinucleotide
FFA	free fatty acid
G	guanine nucleotide binding
G_s	stimulatory G-protein
G_i	inhibitory G-protein
GLM	general linear model
GPCR	G-protein-coupled receptor
HARBS	high-affinity rolipram binding site
HCl	hydrochloric acid
HFD	high-fat diet
HPLC	high performance liquid chromatography
HSL	hormone sensitive lipase
HYPO	hypothalamus
IC_{50}	median inhibitory concentration
ip	intraperitoneal
K_d	dissociation constant
K_i	inhibition constant
K_m	Michaelis-Menten constant
LARBS	low-affinity rolipram binding site
LFD	low-fat diet
LVS	left ventricle and septum
MAPK	mitogen-activated protein kinase

NA	noradrenaline
NADH	reduced nicotinamide adenine dinucleotide
NAT	noradrenaline-reuptake transporter
NORM	Sprague-Dawley
NSB	non-specific binding
N-terminal	amino-terminal
PDE	phosphodiesterase
PDE4	phosphodiesterase type-4
PET	positron emission tomography
PGC1	peroxisome proliferators activated receptor gamma coactivator-1
PPAR	peroxisome proliferators activated receptor
PKA	protein kinase-A
RER	respiratory exchange ratio
RIA	radioimmunoassay
R_t	retention time
SD	standard deviation
Ser	serine
SkM	skeletal muscle
SNS	sympathetic nervous system
STZ	streptozocin
T	total binding
TCA	tricarboxylic acid
tissue:blood	$(\%ID_{tissue}/g_{tissue})/(\%ID_{blood}/g_{blood})$
UCP	uncoupling protein
UCR	upstream conserved region
$\dot{V}_{CO2}$	carbon dioxide production
$\dot{V}_{O2}$	oxygen consumption
$\dot{V}_{O2}$/kgBW	oxygen consumption divided by kilogram body weight
V_{max}	maximal velocity
WAT	white adipose tissue

1.0: INTRODUCTION

1.1 General introduction

The development of novel positron emission tomography (PET) radioligands has placed PET technology at the forefront of medical imaging and scientific research by allowing non-invasive measurement of diverse physiological and biochemical processes in living subjects. Imaging with PET technology is widely employed as a diagnostic tool to examine tumors, heart, respiratory, and neuropsychiatric diseases. In addition, PET has been directed towards the exploration of various neurotransmitter systems in both healthy and pathological states. Recently, a selective phosphodiesterase type-4 (PDE4) inhibitor (*R*)-rolipram ((*R*)-4-(3-cyclopentyloxy-4-methoxy-phenyl-2-pyrrolidone) labeled with carbon-11 has been produced and characterized for imaging PDE4 in the brain, heart, and lungs (DaSilva et al., 2001; Lourenco et al., 2006) and this thesis is concerned with its application in obesity and diabetes.

The cyclic adenosine 3',5'-monophosphate (cAMP)-specific PDE4 enzyme is affiliated with a diverse family of PDEs possessing the ability to hydrolyze cAMP into 5'AMP following stimulation of various guanine nucleotide-binding (G) protein-coupled receptors (GPCRs), including β-adrenergic receptors (β-AR) (Houslay et al., 1998; Ye and O'Donnell, 1996). It has been established that endogenous cAMP levels control PDE4 by regulatory processes involving short-term phosphorylation and long-term gene expression. Phosphorylation of PDE4 by cAMP-dependent protein kinase-A (PKA) has been observed to augment PDE4 activity within 10-15 min of cAMP cascade activation (Alvarez et al., 1995; Sette and Conti, 1996). PDE4 density has been found to increase

via enhanced gene transcription following prolonged (hours to days) increases in cAMP (Manning et al., 1996; Miro et al., 2002). By terminating the actions of intracellular cAMP, PDE4 acts in a key role to regulate cAMP-mediated signaling pathways in many neurotransmitter systems and tissues.

Obesity and diabetes mellitus (DM) are problems that affect millions worldwide (Yach et al., 2006). Both obesity and DM are related to sympathetic nervous system (SNS) dysfunction (Bachman et al., 2002; Dagogo-Jack et al., 1993; Dulloo, 2002; Schmid et al., 1999). The objectives of this thesis are aimed at the pharmacological evaluation of (*R*)-[^{11}C]rolipram, as a potential radiotracer for imaging dysfunctional cAMP-mediated signaling in the obese and diabetic states. Perhaps, this work will inspire future research to enlighten the role of PDE4 in thermogenesis, and utilize PET imaging as a tool to study the progression and etiology of SNS dysfunction in obesity and diabetes *in vivo*.

1.2 The sympathetic nervous system

The SNS innervates almost all vital organs and tissues in the body with its post-gangionic nerves, and represents the efferent part of the autonomic nervous system. Activation of these nerves usually occurs as reflex mechanisms that involve afferent signals and some processing in the central nervous system (CNS). The hypothalamus (HYPO) is the main locus of afferent signal integration in the CNS (Forster, 1998) and is involved in the central regulation of SNS activity in the body (Snitker et al., 2000). Sympathetic neuronal activation leads to the release of noradrenaline (NA) from storage vesicles in the terminal axon which act via adrenergic receptors ultimately affecting the

production of cAMP (Brodde and Michel, 1999). Synaptic NA levels are regulated by negative feedback mechanisms such as the NA-reuptake transporter (NAT), which recycle excess synaptic NA back into the terminal axon, and α_2-ARs which inhibit the release of NA (Molenaar and Parsonage, 2005; O'Donnell and Zhang, 2004).

1.2.1 β-adrenergic signal transduction

All members of the GPCR superfamily possess the common structural feature of seven-transmembrane helices connected by three intracellular and three extracellular loops with an extracellular amino- (N) and an intracellular carboxy- (C) terminus (Palczewski et al., 2000; Pierce et al., 2002). A general model of GPCR activation proposes that GPCRs are in equilibrium between an activated state and an inactive state (Seifert and Wenzel-Seifert, 2002). These states presumptively differ in the disposition of the transmembrane helices, and in turn, the cytoplasmic domains that determine G-protein coupling. Agonists stimulate the activated state. GPCRs act as guanine nucleotide exchange factors. In their activated conformation, GPCRs catalyze exchange of guanosine diphosphate tightly bound to the α subunit of the heterotrimeric G-proteins for guanosine triphosphate. This leads to activation of the α subunit and its dissociation from the G-protein βγ dimmer. Both G-protein subunits are capable of regulating effector activity (Hamm, 2001). Activation of the GPCR β-AR regulates a variety of cAMP-mediated signal cascades in a range of tissues. β-ARs ($\beta_{1\text{-}3}$-ARs) are positively coupled to the stimulatory G-protein (G_s) and following agonist binding, activate adenylyl cyclase (AC) to convert adenosine triphosphate (ATP) into cAMP. Subsequent activation of PKA leads to phosphorylation of regulatory proteins, activating a multitude of signal cascades in assorted tissues (Dzimiri, 1999; Klein et al., 2000; Maltsev et al.,

1999). β_2-AR and β_3-AR are also coupled to the inhibitory G-protein (G_i), and once activated, reduce AC stimulation and cAMP production (Communal et al., 1999; Dzimiri, 1999; Koch et al., 2000; Soeder et al., 1999; Tseng et al., 2001). Included consequences of cAMP-mediated signal cascades following stimulation of β-ARs are cardiac performance, lipolysis in white adipose tissue (WAT), and thermogenesis in brown adipose tissue (BAT) and skeletal muscle (SkM) (Astrup et al., 1985; Collins and Surwit, 2001; Robidoux et al., 2004; Rohrer et al., 1999). Specific β-AR isoform localization, as well as differential coupling to G_s and G_i can lead to tissue specific sympathetic responses following SNS activation. PDE hydrolysis is a critical component of the cAMP-mediated signals.

1.3 PDE characteristics

Butcher and coworkers identified PDEs as the enzymes responsible for the breakdown of cAMP and cyclic guanosine 3',5'-monophosphate (cGMP) (Butcher and Sutherland, 1962; Robison et al., 1968). The cellular content and biological effects of cAMP or cGMP are defined by the balance between activities of synthesizing enzyme cyclases, AC, and guanylate cyclase, respectively; and catabolizing enzymes, the PDEs that hydrolyze the 3'-phosphoester bonds producing inactive noncyclic nucleotides 5'AMP and 5'GMP (Conti, 2000; Dousa, 1999). A collection of biochemical studies have discovered the existence of at least eleven various PDE families with a 20-25% sequence homology that differ with respect to substrate specificity, allosteric regulators, protein sequence, and sensitivity to inhibitors (Table I) (Beavo, 1995; Conti and Jin, 1999; Fawcett et al., 2000; Soderling et al., 1999). The types of PDE that hydrolyze only

Table I: The phosphodiesterase superfamily*.

Nomenclature	Gene Family (preferred substrate)	No. of Gene Products (splice variants)	Distribution	Inhibitors
PDE1	Ca2+/calmodulin stimulated (cGMP>cAMP)	3 (>9)	Brain, heart, kidney, pancreas, thyroid, testis, lymphocytes	Vinpocetine, SCH51866, zaprinast, 8-MM-IBMX
PDE2	cGMP-stimulated (cGMP≈cAMP)	1 (3)	Brain, heart, platelets, liver, thymocytes, adrenals, adipocytes	MEP-1, EHNA
PDE3	cGMP-inhibited (cGMP≈cAMP)	2 (3)	Heart, liver, pancreas, smooth muscle, adipocytes, tissue, lymphocytes	Milrinone, siguazodan (SKF94120), cilostamide, enoximone, OPC3911
PDE4	cAMP-specific (cAMP only)	4 (20)	Brain, immune system, lung, heart, pancreas, testis, smooth muscle, adipocytes	Rolipram, denbufylline, Ro20-1724, , LAS31025, SB207499
PDE5	cGMP-specific (cGMP only)	1 (3)	Smooth muscle, lung platelets, spleen	Zaprinast, sildenafil, dypyridamole, SCH51866
PDE6	Photoreceptor (cGMP only)	3 (3)	Retina	Zaprinast, dypyridamole
PDE7	cAMP-specific, rolipram-insensitive (cAMP only)	2 (3)	Skeletal muscle, brain, heart, liver, lymphocytes, kidney, pancreas	Dipyridamole
PDE8	cAMP-specific, IBMX-insensitive (cAMP only)	2 (>2)	Gonads, intestines, thyroid	Dipyridamole
PDE9	cGMP-specific (cGMP only)	1 (4)	Spleen, small intestine, brain, heart, kidney	SCH51866
PDE10	Dual substrate, cAMP/cGMP-specific (cAMP=cGMP)	1 (1)	Brain, testis	SCH51866, dipyridamole
PDE11	Dual substrate, cAMP/cGMP-specific (cAMP=cGMP)	1 (3)	Skeletal muscle, prostate, kidney, liver, testes	Zaprinast, dipyridamole

* Data obtained from (Conti et al., 1995b; Coudray et al., 1999; Essayan, 2001; Fawcett et al., 2000; Fisher et al., 1998a; Fisher et al., 1998b; Hayashi et al., 1998; Maurice et al., 2003; Pyne and Furman, 2003; Soderling et al., 1999; Spina et al., 1998).

cAMP are PDE4, PDE7, and PDE8; while PDE5, PDE6, and PDE9 are cGMP specific. PDE1, PDE2, PDE3, PDE10, and PDE11 hydrolyze both cAMP and cGMP (Maurice et al., 2003). Each family of PDE exhibits distinctive tissue, cell, and subcellular expression patterns, and are likely to participate in discrete signal transduction pathways involved in physiological and pathophysiological processes (Langin et al., 1992; Steinberg and Brunton, 2001). The cAMP-specific PDE4 enzymes present particular interest due to their function in the regulation of cardiac contraction, lipolysis, and thermogenesis (Collins and Surwit, 2001; Coudray et al., 1999; Müller et al., 1990; Nagaoka et al., 1998; Robidoux et al., 2004).

1.3.1 Characteristics of PDE4 and family isoforms

First identified in 1985 (Némoz et al., 1985), the PDE4 enzyme is characterized by selective inhibition by rolipram, a compound synthesized in 1976 (Schwabe et al., 1976). PDE4 is the most studied family of PDEs (Conti et al., 2003). The complexity achieved through the assortment of cAMP-signaling components, involves a diverse range of receptors, and multiple forms of AC, PKA and PDEs. Diversity of the second messenger signal termination is particularly evident with PDE4s, which are activated following induction of at least β-AR (Whalin et al., 1989), A_2-adenosine (Borisy et al., 1993), H_2-histamine (Holden et al., 1987), and serotonin (Takahashi et al., 1999) receptors linked to AC in the brain and peripheral tissues (Lourenco et al., 2006).

Diversifying the intricacy of this signaling system, the PDE4 family encodes four distinct isoforms, PDE4A, B, C, and D, which produce some 20 different splice variants that are widely distributed (Engels et al., 1994; Houslay et al., 1998). All PDE4 isoforms selectively hydrolyze cAMP, thus terminating the action of the second messenger. The

isozymes of PDE4 also exhibit similar kinetics for cAMP hydrolysis with a V_{max} ranging from 0.15 μmol/min/mg of protein to 11.5 μmol/min/mg of protein and a low K_m value (0.6-7.6 μM) (Houslay et al., 1998; Hughes et al., 1997).

1.3.2 Distribution and compartmentalization of PDE4

PDE4 enzymes are distributed throughout the body, being present in all major organs (Engels et al., 1994; Hughes et al., 1997; Lourenco et al., 2001). In the rat, the greatest concentrations of these enzymes are expressed in the brain (Lourenco et al., 2001; Schneider et al., 1986). High concentrations of PDE4 are also contained in the lungs, heart (Engels et al., 1994; Lourenco et al., 2006; Schudt et al., 1991), and SkM (Enoksson et al., 1998; Nevzorova et al., 2006). The pancreas is reported to express PDE4 enzymes (Han et al., 1999; Hughes et al., 1997) as do types of cells in the immune system (Nicholson et al., 1991); however, platelets and red blood cells are devoid of PDE4 activity (Beavo, 1995; Maurice et al., 2003; Tenor and Schudt, 1996). PDE4 has been shown to be expressed in WAT and BAT, but to a much lesser extent than PDE3 (Coudray et al., 1999; Nagaoka et al., 1998). The four distinct genes, PDE4A, B, C, and D are widely expressed in the human brain and SkM, whereas PDE4C is absent in the remainder of the above mentioned tissues (Engels et al., 1995; Han et al., 1999; Houslay et al., 1998; Hughes et al., 1997). Both particulate (cell membranes and cytoskeleton) and soluble (cytosol) cellular fractions of many different tissues and cell lines contain localizations of PDE4 enzymes (Schneider et al., 1986; Tenor and Schudt, 1996). The proportions between cell membrane and cytosol fractions depend on the PDE4 isoform expression (Lobban et al., 1994).

It is now recognized that cAMP signaling responses are likely compartmentalized. The compartmentalization of cAMP-mediated signaling is a foremost factor in the generation of a non-uniform intracellular allocation of cAMP, leading to distinct alterations in cell activity. Specific PDE isoforms display decidedly selective cellular and sub-cellular localizations (Bolger et al., 1997; Jin et al., 1998; Lobban et al., 1994). This concept allows spatially distinct cellular regions of PKA to be differentially activated by cAMP concentration gradients (Steinberg and Brunton, 2001). Based on the principle that PKA isoforms are anchored at specific intracellular sites by A-kinase anchoring proteins (AKAPs) in distinct patterns of association with cAMP production, AKAP-bound PKA populations have the ability to respond to concentrations of cAMP in cells and modify localized target proteins (Colledge and Scott, 1999; Houslay and Adams, 2003). The basis of such gradients depends upon the spatial and temporal characteristics of both AC production and PDE degradation of cAMP (Houslay and Milligan, 1997). Thus, PDE compartmentation activities possessing distinct pharmacokinetic and regulatory properties likely play an important role in the regulation of cAMP-mediated signaling and maintenance of cellular homeostasis.

1.4 PDE4 structure

Structurally, PDE4 enzymes share similar patterns consisting of distinct regions. PDEs are composed of a highly conserved catalytic domain of ~300 amino acids flanked by regulatory C- and N-terminal ends which are variant specific (Francis et al., 2001; Huai et al., 2003). The structure of the PDE4B and D isozymes have been analyzed at the atomic level (Huai et al., 2003; Lee et al., 2002; Xu et al., 2000). The catalytic

domain is composed of 17 α helices connected by loops, with helices 6-13 containing residues critical for substrate binding and coordination of two metal ions involved in nucleotide hydrolysis (Xu et al., 2000). The cations Zn^{2+} and Mg^{2+} are known to be present at the catalytic site of the PDE4 enzyme (Liu et al., 2001; Xu et al., 2000) and appear to be involved in high-affinity drug binding as well as catalytic activity toward the substrate (Laliberte et al., 2000).

The C-terminal region found downstream of the catalytic core appears to be alike all active isoforms generated by a particular PDE4 gene and distinct for each of the PDE4 genes. Within the catalytic unit, a catalytic pocket is suggested to inactivate the second messenger cAMP and present a binding region for exogenous inhibitors such as rolipram (Charbonneau et al., 1986; Dym et al., 2002; Huai et al., 2003; Xu et al., 2000). Structural features unique to PDE4 enzymes are the presence of two domains on the N-terminus side of the catalytic region, the upstream conserved region (UCR) 1 and 2 (Fig. 1). The four isozymes of PDE4 are each expressed as various splice variants that are further classified as either long (85-100 kDa) or short (68-75 kDA) forms depending on the presence of the UCRs (Beard et al., 2000; Bolger et al., 1997; Houslay, 2001; Houslay et al., 1998). Long splice variants of PDE4 contain units of UCR1 and 2, whereas the short forms lack UCR1 but still possess all or a portion of UCR2 (Richter and Conti, 2002). The UCR1/2 modules of the long forms function as a regulatory domain that controls the catalytic region. Long forms are reported to be a target of PKA at a serine (Ser)-54 residue in UCR1 in PDE4D3 which increases V_{max} of the enzyme 4-fold (Conti et al., 2003; Lim et al., 1999; Sette and Conti, 1996). Additionally, increased nucleotide hydrolysis has been observed following nested deletions or controlled

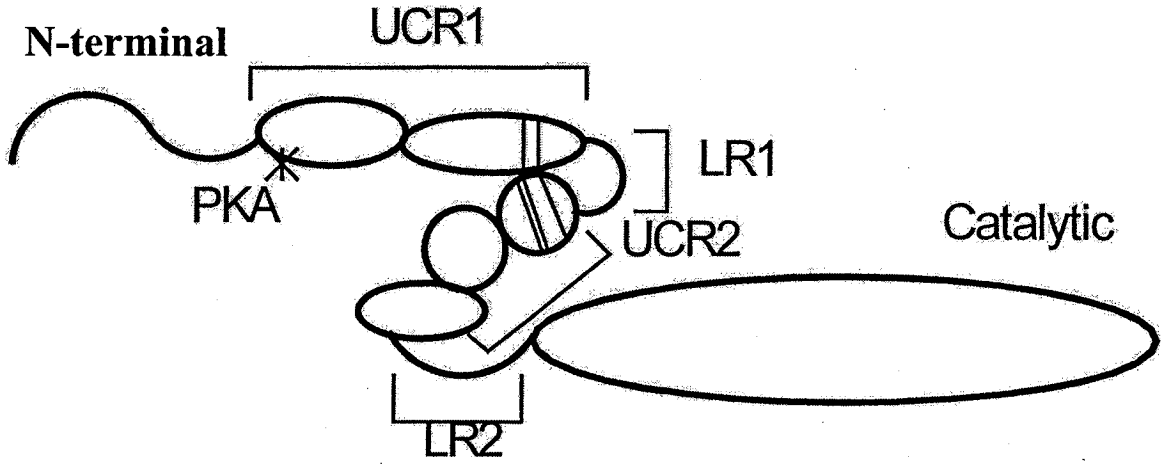

Fig. 1: Various regions of the PDE4D3 isoform are described. UCR1 is divided into two domains, with the N-terminal domain containing the PKA phosphorylation site and the C-terminal domains interacting with UCR2. LR1 and LR2 refer to linker regions 1 and 2, which connect UCR1 with UCR2, and UCR2 with the catalytic region, respectively (Beard et al., 2000).

proteolysis of PDE4D, causing cleavage of UCR1 and 2 away from the catalytic region inducing a pronounced increase in catalytic activity (Jin et al., 1992; Kovala et al., 1997; Lim et al., 1999). The UCR1/2 domain has an important role in the quaternary structure of PDE4. Long splice variants behave as dimers, whereas short forms behave as monomers (Richter and Conti, 2002). This dimerization is a key element for transmitting the conformational changes at the N-terminus to changes in conformation of the catalytic domain. Dimerization of UCR1/2 is an essential structural element that determines the regulatory properties and inhibitor sensitivities of PDE4 enzymes (Richter and Conti, 2004).

1.5 PDE4 regulation

1.5.1 Short-term regulation of activity

In most cells and tissues, the maximal capacity of cAMP and cGMP production is less (~10 times) than the capacity for hydrolysis by PDEs and is an essential feature in determining turnover of cAMP (Dousa, 1999). This characteristic is consistent with the general observations that partial inhibition of PDE results in a dramatic increase in intracellular concentration of cAMP and activation of the PKA signaling system (Beavo and Reifsnyder, 1990; Houslay and Milligan, 1997; Nicholson et al., 1991). It follows that PDEs must operate at sub-maximal capacity and should be tightly regulated. Elevated cAMP levels up-regulate PDE4 isozymes through two different means; short-term phosphorylation or long-term increased transcription and expression (Fig. 2).

Stimuli that increase intracellular cAMP lead to short-term (within 15 min) regulation of long PDE4 isoforms (Alvarez et al., 1995; Baillie et al., 2001; Chang et al., 1997;

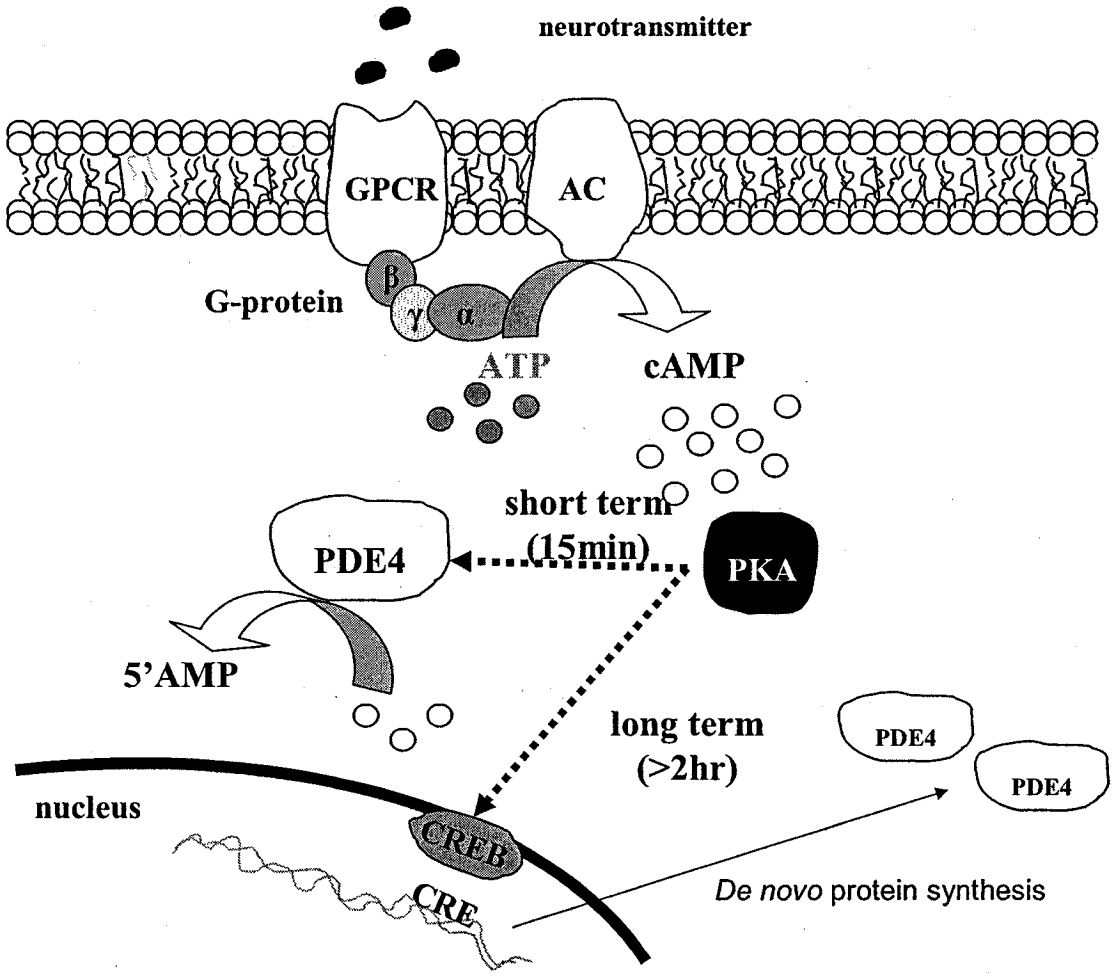

Fig. 2: Illustration of the two main mechanisms of PDE4 regulation: (1) short-term phosphorylation of some PDE4 subtypes by cAMP-dependent protein kinase A (PKA) occurring within approximately 15 min of stimulation of cAMP synthesis, leading to an increase in PDE4 activity and (2) increase in *de novo* PDE4 protein synthesis as a result of long-term (>2 hours) incubation of cells with agents augmenting cAMP levels (adapted from Conti et al., 1995a).

Conti et al., 1995a; Ekholm et al., 1997; MacKenzie et al., 2002; Madelian and La Vigne, 1996; Sette and Conti, 1996; Sette et al., 1994a; Sette et al., 1994b). Phosphorylation of PDE4D3 at the Ser-13 of the N-terminal region and the Ser-54 in UCR1 is accomplished through direct PKA-mediated phosphorylation. However, only alteration of Ser-54 in UCR1 is required to elicit activation of PDE4 (Hoffmann et al., 1998; Sette and Conti, 1996). Forskolin challenge of COS1 cells has lead to the rapid activation of PDE4A8, PDE4B1, PDE4C2, and PDE4D5 long isoforms (MacKenzie et al., 2002). The same activation coincided in astroglial (Madelian and La Vigne, 1996) and vascular smooth muscle cells (Ekholm et al., 1997). PKA-mediated phosphorylation of PDE4s can thus provide part of the cellular desensitization mechanism to cAMP signaling. Additionally, PKA phosphorylation of PDEs can affect the catalytic site. Decreased Mg^{2+} concentrations at the catalytic site were required for cAMP hydrolysis following PKA phosphorylation of PDE4D3 *in vitro* (Sette and Conti, 1996), indicating an increased capacity to break down cAMP produced by Mg^{2+}-PKA mediated phosphorylation changes.

Several observations suggest the involvement of other protein kinases in the short-term phosphorylation of cAMP-PDE enzymes. The extracellular-signal-related protein kinase (ERK) mitogen-activated protein kinase signaling pathway provides a pivotal route whereby various hormones and growth factors exert key effects on cell growth and survival. The catalytic unit of all PDE4 subfamilies, except PDE4A, contain a Ser-579 residue which can be phosphorylated, both *in vitro* and *in vivo*, by ERK within 30 min (Baillie et al., 2000; Hoffmann et al., 1999; MacKenzie et al., 2000). This inhibitory phosphorylation of PDE4 isoforms by ERK can cause localized increases in cAMP

levels, allowing activation of PKA and subsequent stimulatory phosphorylation of PDE4 (Hoffmann et al., 1999; Houslay and Kolch, 2000). As well, 20 min treatment of protein kinase-C stimulators phorbol 12-myristate and diacylglycerol 13-acetate were observed to cause rapid increases in cAMP-PDE activity of rat renal collecting tubules (Tetsuka et al., 1995). Administration of insulin to intact hepatocytes has been reported to cause tyrosine-kinase phosphorylation of cAMP-PDE (Pyne et al., 1989). Taken together, these results indicate that PDE4 enzymes have a wide spectrum of phosphorylation sites for various kinases, allowing prompt activation of the enzyme and rapid regulation of cyclic nucleotides.

1.5.2 Long-term regulation of expression

In addition to short-term regulation of PDE4 due to post-translational modifications, the expression of PDE4 is regulated at the transcriptional level. Long-term (hours to days) elevation of intracellular cAMP levels have been found to cause increases in the levels of mRNA and protein expression of various PDE4 isoforms both *in vitro* and *in vivo*. Elevated cAMP, via AC activity, cause increased PKA-mediated phosphorylation of the cAMP-response element binding (CREB) protein which upon binding to CRE mediates augmented PDE4 gene transcription (Erdogan and Houslay, 1997; Monaco et al., 1994; Swinnen et al., 1989; Vicini and Conti, 1997). In the brain, CREB expression and function were reported to be up-regulated following 3 week antidepressant treatment in rats (Nibuya et al., 1996). Indeed, several *in vitro* and *in vivo* studies support the notion that cAMP-signaling pathway regulates the long-term expression of PDE4 subtypes. Prolonged monocyte β-AR stimulation with salbutamol for 4 hours, enhanced PDE4A and β-AR density with no effect on PDE4D (Manning et al., 1996). As well,

increased cAMP following extended treatment of PC12 cells for 16 hours with A_2-receptor agonist CGS 21680, caused a dose-dependent elevation in PDE4 density which was abolished by inhibitors of transcription or protein synthesis (Chang et al., 1997). Conversely, decreased cAMP production following β-AR blockade with propranolol for 14 days or neuronal lesioning caused significant reductions in cerebral PDE4 activity (Ye and O'Donnell, 1996). Stimulation of AC is described to induce PDE4D1 and D2 expression within three hours in human Jurkat T-cells (Erdogan and Houslay, 1997). Intriguingly, the PDE4A4 splice variant was down-regulated following this treatment (Erdogan and Houslay, 1997), illustrating that PDE4 variants may also be down-regulated by certain cAMP-enhancing treatments. Up-regulation of PDE4 synthesis in response to extended activation of the cAMP pathway may represent a compensatory adaptive mechanism to reduce cAMP levels back to baseline (Conti et al., 1995b; Houslay and Milligan, 1997; MacKenzie et al., 2002).

1.6 High affinity rolipram binding site

Rolipram is one of the most potent and widely studied compounds in the group of neuroactive cAMP-PDE inhibitors. Rolipram is a selective inhibitor of PDE4 that preferentially inhibits cAMP hydrolysis (K_i ~1 μM) in the brain and periphery, thus enhancing the intracellular availability of cAMP in the absence of direct stimulation of neurotransmitter receptors (Jacobitz et al., 1996; Lourenco et al., 2006; Schneider, 1984; Schneider et al., 1986). The chiral compound rolipram binds with stereospecificity to PDE4. In intact eosinophils, (*R*)-rolipram (EC_{50} ~0.19 μM) was 10 times more potent than (*S*)-rolipram (EC_{50} ~1.87 μM) at displacing tritiated (*R/S*)-rolipram (Souness et al.,

1990). The active (*R*)-rolipram was previously reported to bind to PDE4 with 10-30 fold higher potency than (*S*)-rolipram (Hughes et al., 1997; Schmiechen et al., 1990; Schneider et al., 1986). Studies have shown that (*R*)-rolipram binds reversibly and stereospecifically with high affinity (K_d 1-5 nM) to the active Mg^{2+}-induced PDE4 holoenzyme conformation (Houslay et al., 1998; Laliberte et al., 2000).

One of the unique characteristics of PDE4 is that the binding of rolipram, is to two sites, called the high-affinity rolipram binding site (HARBS) and the low-affinity rolipram binding site (LARBS) in *in vitro* studies (Jacobitz et al., 1996; Schneider et al., 1986). The tritiated form of the more active enantiomer of (*R*)-rolipram was shown to bind the two affinity states with K_d values approximately 0.7 and 34 nM, respectively (Jacobitz et al., 1996; Souness and Rao, 1997). It has been shown *in vitro* that rolipram binds preferentially to HARBS, piclamilast binds with equal high affinity to both HARBS and LARBS, whereas CDP840 binds preferentially to LARBS (Zhao et al., 2003). Tritiated (*R*)-rolipram has shown similar binding potency (K_d ~2 nM) to the HARBS on both PDE4A and B (Amegadzie et al., 1995). Previous reports have shown that rolipram was five times more potent at inhibiting the catalytic site of PDE4A, B, and D, as compared to C (Hughes et al., 1996; Wang et al., 1997), while other reports showed it binds to all subtypes relatively equally (Müller et al., 1996). A study using a series of truncated PDE4A mutants showed that inhibitor binding to both the HARBS and the LARBS is to the catalytic site (Jacobitz et al., 1996). Studies have revealed that the Mg^{2+} ion at the catalytic site affects cAMP binding and the high-affinity interactions of many PDE4 inhibitors (Laliberte et al., 2000; Liu et al., 2001). For example, upon removal of Mg^{2+}-bound water from recombinant PDE4, the high-affinity cAMP binding of PDE4

decreased from 2 μM to 179 μM, and the binding of the PDE4 inhibitor cilomilast decreased from a K_d value of 42 nM to >4000 nM (Huai et al., 2006). It has been proposed that the hydrophilic interaction in the metal pocket acts as a key factor eliciting the high-affinity binding of PDE4 inhibitors (Card et al., 2005; Huai et al., 2006). Binding to the HARBS also depends on the presence of the N-terminal region of the protein (Lobban et al., 1994; Shakur et al., 1995; Torphy et al., 1992a), whereas the LARBS requires only the residues within the catalytic site of PDE4 (Hughes et al., 1997).

In vitro analyses suggest that while LARBS are present in both peripheral and central tissues (Zhao et al., 2003), HARBS may be exclusively distributed in the brain regions known to be important for mediation of antidepressant effects (Kaulen et al., 1989; Zhang et al., 2001; Zhang et al., 2006). It has been proposed that the HARBS and the LARBS mediate distinct effects of PDE4 inhibitors. The differential distributions of the two affinity states signify that they may have diverse contributions to antidepressant actions. Consistent with this distribution, it appears that HARBS mediates central effects such as emesis (Duplantier et al., 1996), head twitches, and tremors (Schmiechen et al., 1990), whereas LARBS is primarily involved in peripheral responses resembling suppression of inflammatory reactions (Souness and Rao, 1997). Although the exact function of HARBS and LARBS are unknown, it is recognized that all PDE4 subtypes possess HARBS (Amegadzie et al., 1995; Hughes et al., 1997; McLaughlin et al., 1993; Pillai et al., 1993). Accordingly, it is reasonable to assume that the (*R*)-[^{11}C]rolipram PET radiotracer labels all types of PDE4 isozymes.

1.7 Obesity

In Canada, reports have revealed that 35% of adult women and 57% of adult men are overweight or obese (Canning et al., 2004). The escalating prevalence of obesity is problematic as it is associated with various health complications such as diabetes and cardiovascular diseases. While there has been much progress over the last few decades in achieving many health goals, the occurrence of obesity has steadily increased. If this situation is not reversed, it could wipe out the gains made in areas of heart disease, diabetes, and other chronic health problems (U.S. Department of Health and Human Services., 2001). It has been suggested that obesity is second only to smoking as a preventable cause of death (Flegal et al., 2004). The development of obesity is greatly effected by various contributions such as genetics, diet, lifestyle, and SNS signaling.

1.7.1 SNS dysfunction in obesity

The ability to stimulate lipolysis and thermogenesis (production of heat) is impaired in many animal models of obesity. The nature of this thermogenic defect is not fully understood, however, there is compelling evidence pointing to defective reactivity of the SNS. (Levin and Sullivan, 1987; Levin et al., 1983; Nagai et al., 2005; Reynisdottir et al., 1994; Sharma et al., 2001; Tentolouris et al., 2003). β-AR signaling is required for heat production (thermogenesis) in the prevention of obesity (Bachman et al., 2002; Lowell et al., 1993). Changes in weight gain profiles can alter expression of β-ARs (Reynisdottir et al., 1994). Clinical trials using chronic β-blocking agents have shown increased propensity to obesity during therapy (Rossner et al., 1990; Sharma et al., 2001). Indeed, cAMP-mediated signaling plays a key function in the initiation of thermogenesis and the regulation of body weight. Observations that animals subjected to HYPO-lesions

become obese (Lowell and Bachman, 2003) confirm the importance of the HYPO in coordinating weight regulation. Furthermore, SNS activity was found to be elevated following overfeeding and diminished after starvation, linking the efferent involvement of SNS signals to diet and thermogenesis (Landsberg et al., 1984). Subsequently, investigations revealed that the SNS was certainly the prime mediator of thermogenesis, as mice lacking all β-ARs were observed to become severely obese in contrast to wild-type mice that were resistant to obesity following overfeeding (Bachman et al., 2002). Interestingly, there are knock-out rodent models of uncoupling protein (UCP) (Enerback et al., 1997; Gong et al., 2000) or β_3-ARs (Harper and Himms-Hagen, 2001) who fail to become obese suggesting an intrinsic compensatory mechanism involved in thermogenesis (Dulloo, 2002). This cAMP signaling system is tightly regulated and also concerns hydrolysis by PDEs.

1.7.2 The SNS in thermogenesis

Thermogenesis is thought to be a mechanism of body weight regulation. Body weight homeostasis is regulated between a balance of energy intake and expenditure. The SNS is considered to be the efferent pathway by which the brain (HYPO) regulates thermogenesis. This mechanism of energy expenditure can occur in response to dietary intake, temperature (Fig. 3), or neuropeptide influences such as leptin, ghrelin, and melanocortin (Hall et al., 2000; Haynes et al., 1999; Himms-Hagen et al., 1978). The SNS is responsible for systemic signaling to cellular processes that generate heat such as cardiac contraction, protein synthesis, and thermogenesis. The indirect activation of thermogenesis by the SNS occurs at the mitochondrial level, beginning with the NA-

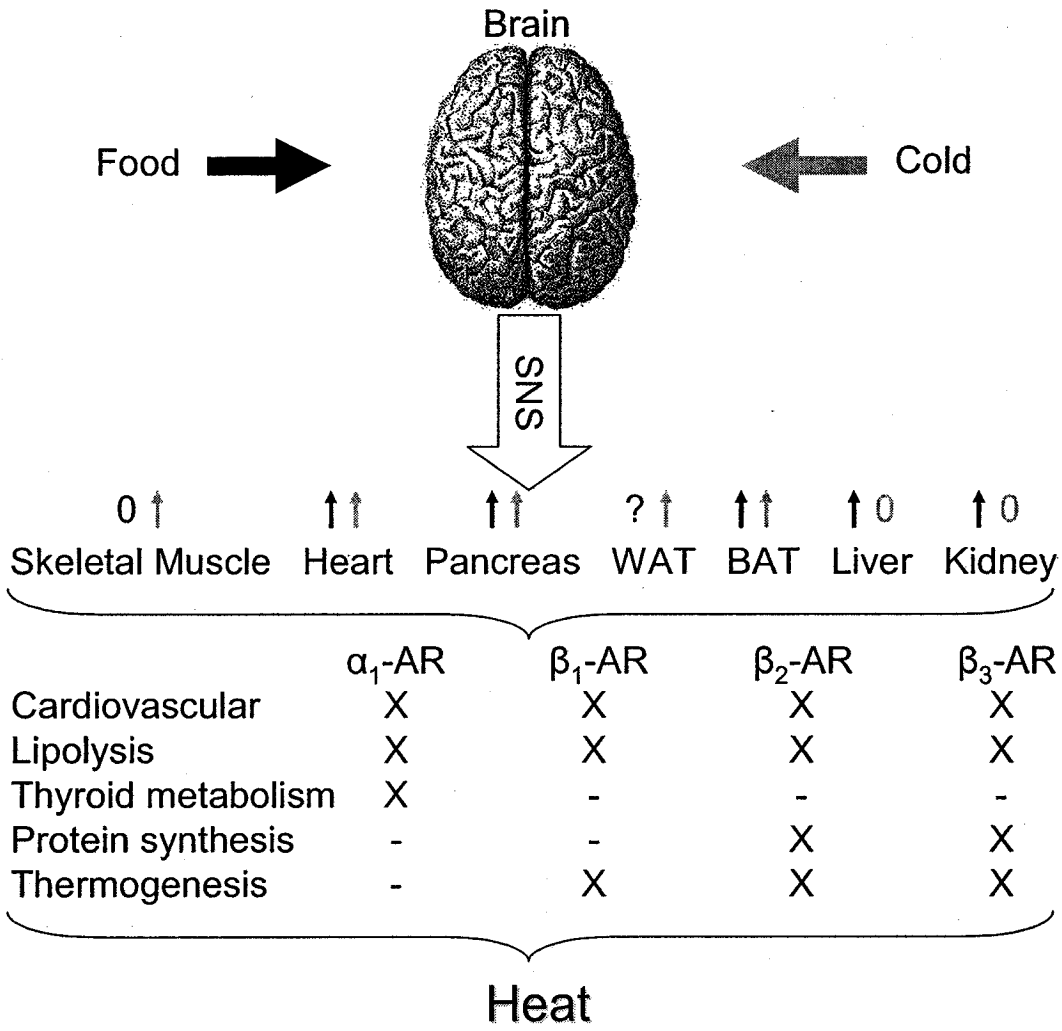

Fig. 3: Activation of the sympathetic nervous system (SNS) in response to food or cold stimuli. SNS signaling to diverse tissues causing alpha- (α) and beta- (β) adrenoceptor (AR) stimulation. Activation (X) of various intracellular processes generates heat (adapted from Dulloo, 2002).

induced stimulation of UCP1, UCP2, and UCP3 (Collins and Surwit, 2001; Yoshitomi et al., 1998a).

UCPs are anion transporters that dissipate the proton gradient across the inner mitochondrial membrane, uncoupling oxidative phosphorylation by circumventing the ATP-synthase enzyme complex. The sole byproduct of this reaction is the generation of heat from stored energy (Dulloo, 2002). In BAT, UCP1 is activated via cAMP-mediated PKA that can access both hormone sensitive lipase, and perilipin, resulting in the liberation of free fatty acid (FFA). PKA stimulates the p38 mitogen-activated protein kinase pathway, culminating in the activation of transcription factor 2 and newly transcribed peroxisome proliferator activated receptor coactivator-1, transactivating members of the peroxisome proliferators activated receptor family and therefore generating UCP1 expression (Fig. 4) (Robidoux et al., 2004). FFAs are activated by synthase enzymes and enter β-oxidation as well as the tricarboxylic acid cycle, leading to the formation of the reduced electron carriers flavin (FADH) and nicotimamide adenine dinucleotide (NADH). Electron carriers are then oxidized by the electron transport chain (ETC), resulting in protons being pumped out of the mitochondria and the formation of a protonmotive force. The protonmotive force drives the protons back into the mitochondrial matrix through UCP1. The energy stored in the protonmotive force is then released as heat (Cannon and Nedergaard, 2004; Robidoux et al., 2004)

Alteration of the expression of UCP1, UCP2, and UCP3 has been demonstrated to preserve weight homeostasis in response to changes in environmental temperature or variation in food intake (Lowell and Flier, 1997; Yoshitomi et al., 1998a; Yoshitomi et al., 1998b). In rodents, UCP1 is the major contributor to thermogenesis, found

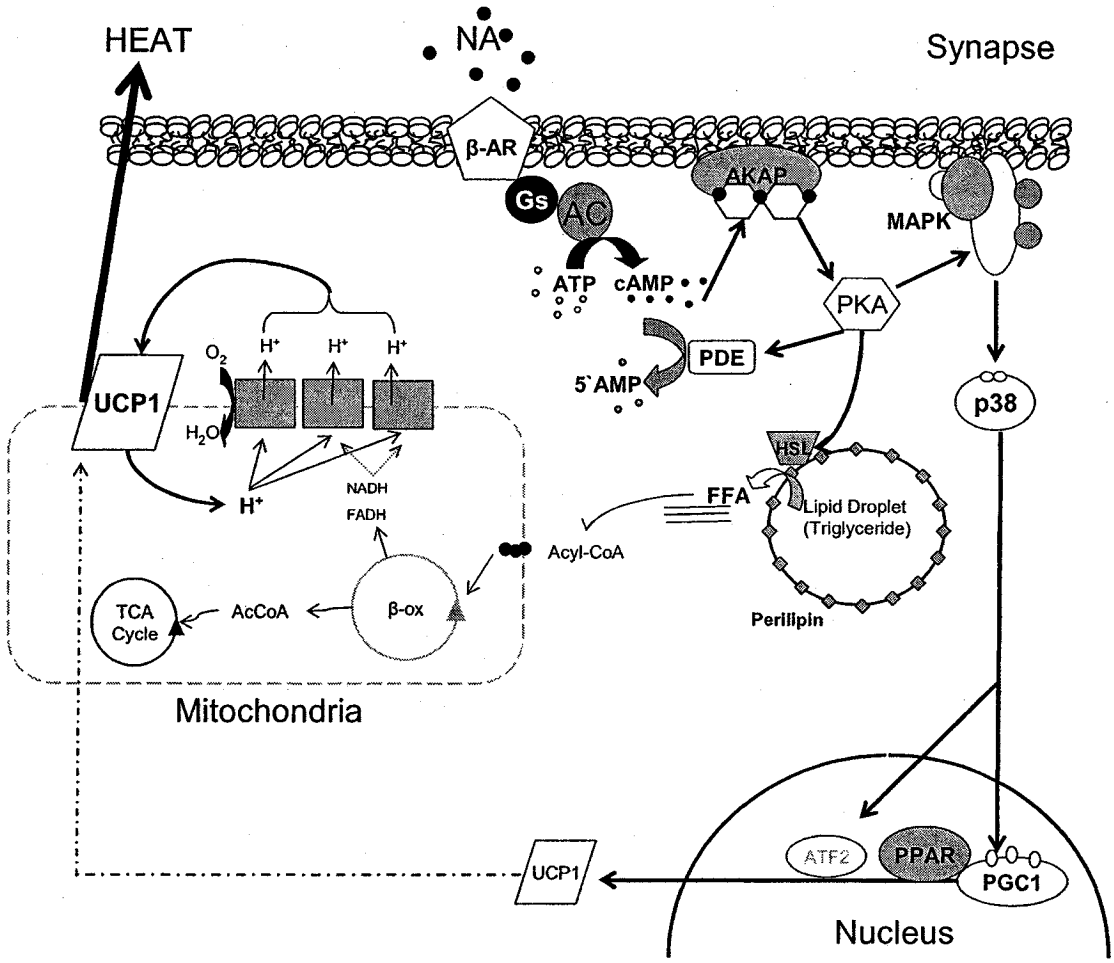

Fig. 4: NA-induced stimulation of thermogenesis in BAT. NA couples to G_s leading to the stimulation of AC and PKA which is bound via regulatory subunits to A-kinase anchor proteins (AKAP). PKA can access both hormone sensitive lipase (HSL), and perilipin, resulting in the liberation of free fatty acid (FFA). PKA also phosphorylates PDE, degrading cAMP to 5`AMP. PKA stimulates the p38 mitogen-activated protein kinase (MAPK) pathway, culminating in stimulation of activating transcription factor 2 (ATF2) and newly transcribed peroxisome proliferators activated receptor gamma coactivator-1 (PGC1), transactivating members of the peroxisome proliferators activated receptor (PPAR) family and therefore generating UCP1 expression. FFA is activated to acyl CoAs (AcCoA) by acyl-CoA synthase and enters β–oxidation (β-ox) as well as the tricarboxylic acid (TCA) cycle, leading to the formation of the reduced electron carriers FADH and NADH. Electron carriers are then oxidized by the electron transport chain, resulting in protons being pumped out of the mitochondria and the formation of a proton motive force. The proton motive force drives the protons back into the mitochondrial matrix through UCP1. The energy stored in the proton-motive force is then released as heat (adapted from Cannon et al., 2004, and Robidoux et al. 2004).

predominantly in BAT (Ricquier et al., 1999). Other UCPs have been characterized in specific tissues such as UCP2 in visceral organs. UCP3 expression is found in rodent BAT and both in human and rodent SkM (Astrup et al., 1985; Clapham et al., 2000; Wang et al., 2003). In large mammals whose BAT decreases with maturity, UCP3 in SkM may be more important for heat production (Astrup et al., 1985; Wang et al., 2003). In addition, muscle UCP3 has been shown to produce enhanced energy dissipation in UCP3 transgenic mice (Clapham et al., 2000), supporting the concept of thermogenesis in mammals with only small deposits of BAT. However, there is controversy in this area as many experts are now doubtful that the novel UCPs actually function like UCP1 (Nedergaard and Cannon, 2003).

1.7.3 PDE4 in obesity

The contribution of PDEs to cAMP-mediated signaling in obese models has not been greatly explored in detail. However, most of the focus of investigation has been directed towards the metabolic abnormalities associated with PDEs in BAT and lipolysis in WAT. *In vitro* analyses confirm the presence of both PDE3 and 4 in BAT and WAT with PDE3 being more predominant in these tissues (Nagaoka et al., 1998). PDE levels in these tissues have been reported to be modulated by temperature induced alterations in SNS activity. Total BAT PDE levels were described to be decreased in cold-acclimatized animals compared to control rats demonstrating the modulation of PDE involvement in thermogenesis (Bertin and Portet, 1975). In obese Zucker fa/fa rats, basal *in vitro* concentrations of BAT PDE4 where greater than lean Fa/fa controls indicating an increased capacity to degrade cAMP (Coudray et al., 1999). However, little is known about the central and peripheral effects that obesity has on the body with respect to

cAMP-mediated signaling and the negative feedback of PDE4. Investigation of PDE4 binding in obese animal models has yet to be performed *in vivo*.

1.7.4 Animal models

An ideal animal model for a disease is one that closely represents most or all of the pathophysiological characteristics desired. There are many animal models of obesity including the Zucker, Zucker diabetic fatty, and Koletsky rats which have mutations in the extracellular domain of the leptin receptor conferring them with morbid obesity, dyslipidemia, and hyperphagia (Tschop and Heiman, 2001). However, leptin receptor mutations are rare sources of obesity in humans. Human obesity appears to be a result of polygenic factors and imbalance between energy intake and expenditure (West and York, 1998). The diet-induced obese (DIO) and diet-resistant (DR) rat models are natural controls of each other, and represent an obesity model that parallels the human condition. The original DIO and DR models were developed from Sprague-Dawley subsets of top and bottom percent weight gainers fed high-fat diet (HFD). The top and bottom weight gainers were classified as DIO and DR rats (Levin et al., 1989; Levin et al., 1983). The DIO rats are reported to become obese, hyperphagic, hyperleptinemic, and hyperinsulinemic following consumption of HFD, while DR rats are resistant to the onset of obesity induced by HFD (Farley et al., 2003; Gao et al., 2002; Ricci and Levin, 2003). In addition, DIO rats are described to possess a dysfunctional NA response to glucose and have increased respiratory exchange ratios (RER) indicating predisposition to store fat (Gao et al., 2002; Levin et al., 1998; Levin and Sullivan, 1987; Levin and Sullivan, 1989). Current inbred DIO and DR rats breed true to all the weight gain patterns and phenotypes of the original DIO and DR rats fed HFD and separated by their propensity to

gain weight (Levin and Keesey, 1998). The advantage of dietary obese susceptible rats is that this model is much more prone to mechanisms underlying obesity that are applicable to humans in comparison with other obese rodent models (Lauterio et al., 1994), and is the reason the DR and DIO rat models were chosen for this research.

1.8 Indirect calorimetry

Indirect calorimetry has long been an essential tool in studies of overall energy expenditure and substrate balances in animals. As opposed to the experimentally challenging direct calorimetry which assesses body heat dissipation, indirect calorimetry measures heat released by oxidative processes using measurements of inspired and expired gases. The body continuously generates energy by oxidative metabolism in order to assure physiological homeostasis. This energy is used for biosynthesis, muscular contractions, and to maintain chemical and electrochemical gradients across cellular membranes. Additionally, part of this energy is lost to the inefficiency of metabolic transformations. Ultimately, all energy produced by the organism is dissipated as heat. The heat production generated by the biochemical processes within the body can be assessed from the measurements of oxygen consumption ($\dot{V}_{O2}$) and carbon dioxide production ($\dot{V}_{CO2}$) (Schutz, 1995). The oxidation of fixed amounts of fuel leads to set amounts of ATP being produced. Accordingly, utilization of ATP leads to a fixed amount of work being performed. Indirect calorimetry utilizes these principles in assessing energy expenditure and substrate utilization.

When two substrates are oxidized simultaneously (carbohydrate and fat), two measurement parameters are necessary to predict energy expenditure. The most

commonly evaluated parameters are $\dot{V}_{O2}$ and $\dot{V}_{CO2}$ (Elia and Livesey, 1992). Using this model, $\dot{V}_{O2}$ measurements can be utilized as an expression of energy expenditure, while a ratio of $\dot{V}_{CO2}/\dot{V}_{O2}$ is used as an indication of substrate metabolism known as RER. The oxidation of carbohydrates result in RER values of ~1.00, whereas the oxidation of fatty acids results in a value of ~0.70 (Bezaire et al., 2001; Elia and Livesey, 1992). The oxidation of fuel results in electrons being transferred by means of NADH and FADH to the ETC. As these electrons move down the ETC, energy is used to pump protons outside the inner membrane, creating an electrochemical potential gradient (Schutz, 1995). Alterations of the normal electrochemical gradient at the mitochondrion by UCPs or SNS-mediated stimulation are suggested to lead to modifications in energy expenditure.

1.9 Type 2 diabetes

Diabetes is estimated to affect 200 to 300 million people by the end of the decade (Zimmet et al., 2001). Diabetes is a complex and diverse group of disorders characterized by hyperglycemia and autonomic neuropathy which has reached epidemic proportions in the present century (Vinik et al., 1992; Vinik et al., 2003; Yach et al., 2006). The incidence of type 2 DM (DM2) is closely linked to obesity. It has been estimated that 60-75% of Caucasian cases of DM2 could be avoided if the population not exceed a body mass index of 25 kg/m^2 (Seidell, 1997). A major distinction between type 1 DM (DM1) and DM2 is that the dysfunction in glucose regulation in DM1 results from the destruction of insulin secreting pancreatic β-cells, theorized to be caused by genetic or autoimmune dysfunction (Lee et al., 2004). DM2 is distinguished by peripheral insulin

resistance and compensatory over-production of β-cell insulin production in response to chronic glucose stimulation. Increased workload by the pancreas ultimately leads to apoptosis and loss of β-cell function (Abel, 2005; Elder et al., 2005; Harris, 1992; Saad et al., 1989). Impairment of the body to regulate glucose levels has widespread effects on the SNS.

1.9.1 Insulin, glucose and the SNS

In DM2, hyperglycemia and hyperinsulinemia have been observed to cause SNS overactivity in the central and peripheral tissues (Anderson et al., 1991; Esler et al., 2001; Fisher et al., 2005; Kern et al., 2005; Masuo et al., 1997). As insulin levels rise in response to unrelenting hyperglycemia, tissues become less responsive to insulin and both glucose and insulin contribute to elevated NA levels in DM2 subjects (Anderson et al., 1991; Esler et al., 2001). Administration of insulin into the brain increases SNS muscle activity in rats (Muntzel et al., 1994). Similar effects are observed in humans following intravenous insulin infusion, where muscle SNS activity and plasma NA content increase (Berne et al., 1992). Moreover, administration of insulin has been shown to down-regulate β_3-AR in 3T3-F442A cells (Feve et al., 1994), an effect that has been reversed *in vivo* with monogenic obese mutant mice following treatment with K^+-ATP channel blocker diazoxide that suppresses insulin-resistance-driven hyperinsulinemia (Surwit et al., 2000). Adrenergic and insulin cross-talk have been postulated as a mechanism contributing to altered SNS signaling in DM2 (Morisco et al., 2005). Current theory suggests that short-term β-AR stimulation mediates PKA and Ca^{2+}-calmodulin dependent activation of the Akt protein which in turn promotes glucose uptake through activation of insulin receptors; however, long-term β-AR stimulation

inhibits glucose uptake (Morisco et al., 2005). This appears to be an alternate regulatory mechanism in response to increased glucose mediated by β-AR activation. The dysfunction of blood glucose and insulin regulation has wide effects on the SNS in DM2 which culminate in variability of cAMP-mediated signaling and PDEs.

1.9.2 PDEs in diabetes

PDE involvement in diabetic cAMP-mediated signaling has been principally explored with respect to arthrosclerosis in cardiovascular tissues and antilipolytic effects of insulin in peripheral tissues. The atherosclerosis-prone insulin-resistant JCR:LA-cp rat was revealed to express increased PDE3 and PDE4 activities compared with aorta from age-matched control +/- littermates (Nagaoka et al., 1998). Only particulate PDE3B activity was reported to be increased in this diabetic model (Netherton et al., 2002). As well, both PDE3 and PDE4 activity were decreased in JCR:LA-cp heart samples, while contributing equally to total PDE activity (Nagaoka et al., 1998). Little is known about the action of insulin on lipid metabolism. However, the major mechanism for the antilipolytic effect of insulin in adipose tissue is stimulation of PDE3 to inhibit cAMP phosphorylation of hormone sensitive lipase (Degerman et al., 1997; Hagstrom-Toft et al., 1995; Nagaoka et al., 1998). In contrast, the *in vivo* regulation of lypolysis in human SkM was reported not to be mediated by PDE3, PDE4 or PDE5 (Enoksson et al., 1998). Accordingly, insulin has diverse effects on PDE regulation which may be tissue specific.

While it is well established that cAMP plays a modulatory role in insulin secretion (Sharp, 1979), the contribution of the various PDE isoenzymes to islet cAMP metabolism and to the regulation of insulin secretion is less understood. In the pancreas, PDE3, PDE4 (Parker et al., 1995), and PDE7 (Hetman et al., 2000) were found to be present *in*

vitro. Selective inhibition of PDE3 but not PDE4 was found to stimulate insulin secretion in human and rat islet of Langerhans cells *in vitro* (Parker et al., 1995; Parker et al., 1997). Importantly, the inhibition of PDE4 with rolipram was found to prevent the onset of diabetes in non-obese diabetic (NOD) mice by blocking the destructive inflammatory cytokine production in the pancreas (Liang et al., 1998). The specific role that PDE4 provides in cAMP-mediated signaling in the pancreas is unclear, however, its plausible function as an immunoprotective force may be altered in the diabetic state and further investigation needs to be explored.

1.9.3 Animal models

Numerous animal models resembling DM2 either occur spontaneously or can be induced experimentally. Most of the commonly used models of DM2 are genetic and have the disadvantage of prohibitive costs, unavailability, and failure to represent the human condition. Prolonged consumption of HFD leads to insulin resistance and is considered the predisposing factor for DM2 (Kraegen et al., 1991; Storlien et al., 1986). Models of HFD take many months to develop diabetes and yield only moderate hyperglycemia (Pascoe et al., 1992; Reed et al., 2000; Surwit et al., 1988). There also exists a rapidly induced DM2 model developed from short-term (2-week) HFD to elicit insulin resistance followed by a single low dose (<50 mg/kg) of the toxic alkylating agent streptozocin (STZ), to destroy pancreatic β-cells, and create a representative model of the human DM2 condition (Reed et al., 2000; Sawant et al., 2004). This cost-effective DM2 model (due to lower time period needed to achieve DM2) was reported to demonstrate hyperglycemia with insulin levels comparable to normal control rats ten days after STZ administration (Sawant et al., 2004), as well as sympathetic cardiac denervation after 9

months (Schmid et al., 1999). However, low dose STZ administration was also found to yield non-diabetic STZ-treated animals in ~50% of the cases (Sawant et al., 2004), possibly due to insufficient pancreatic β-cell destruction. The HFD fed low dose STZ-treated DM2 rat model was used in my project for its advantageous low cost and rapid induction of DM2 for scientific experimentation.

1.10 Positron emission tomography imaging and second messenger systems

PET is a non-invasive medical imaging technology with the ability to produce images of selective physiological and biochemical body functions. PET can often differentiate between the normal and pathological states in the absence of major anatomical changes (Frey, 1989; Herscovitch, 1990; Sedvall et al., 1988). Positron emitting isotopes such as ^{15}O, ^{11}C, ^{13}N, and ^{18}F are incorporated into PET tracers and decay rapidly (within minutes to hours). The unstable nature of these isotopes cause positively charged positron release from the labeled atomic nucleus (Fig. 5). The positron travels a short distance until it encounters and collides with a negatively charged electron, resulting in annihilation and the release of two high energy photons antiparallel to one another. Scintillation crystal detection of the photon pairs are used to measure both the amount and location of coincidence of annihilations traveling through biological tissues with minimal absorption. This information is processed and used to reconstruct a diagnostic image.

In recent years, PET scanners have become increasingly sophisticated and current models possess both PET and computer assisted tomography technology to acquire functional and structural diagnostic images. In conjunction with increasing resolution technologies (3-5 mm^3), PET has become recognized as a useful tool in oncology,

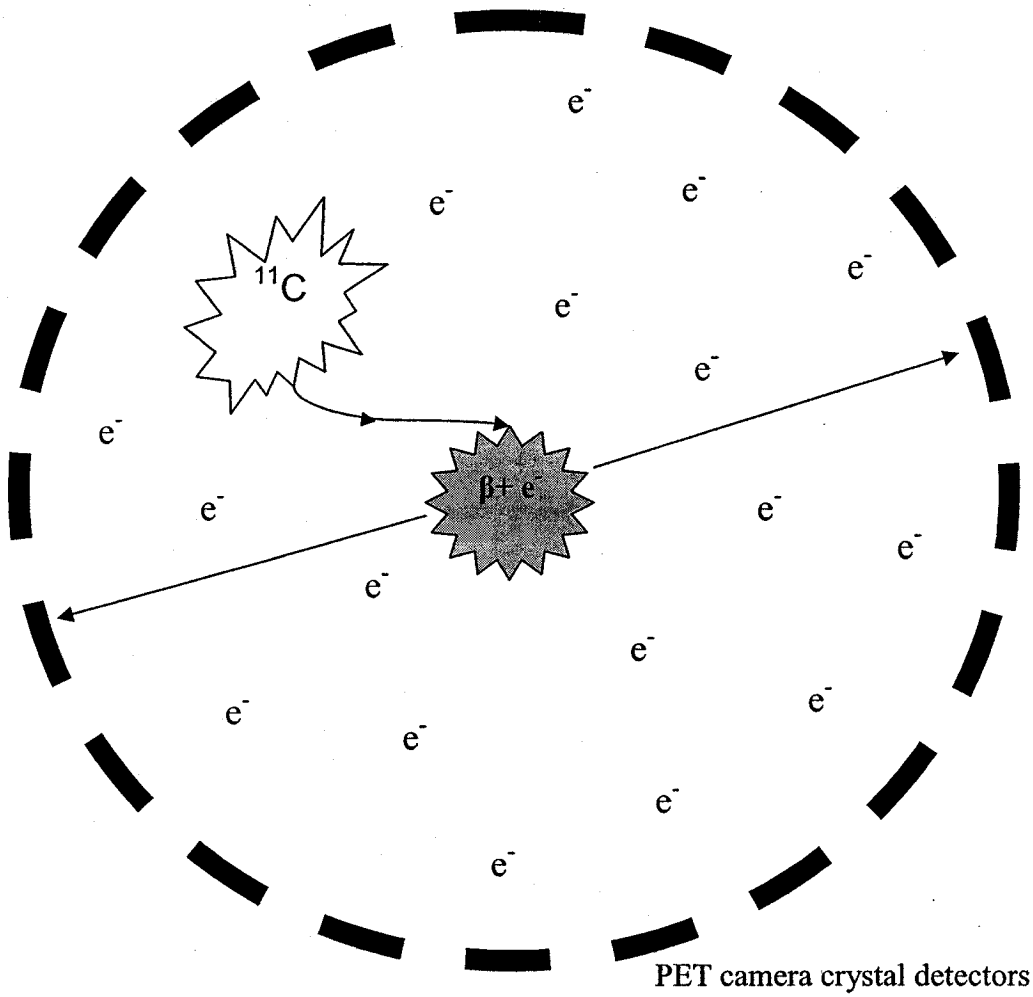

Fig. 5: The ^{11}C nucleus (half-life 20.4 min) decays releasing a positron (β+) which travels through tissues until it encounters its antiparticle, an electron (e^-). The β+ annihilates with the e^- releasing two photons of 511 Kev at 180° to each other. The photons are detected by the PET camera crystal detectors (adapted from Sedvall et al., 1988).

cardiology, and neurology providing pathological and pharmacological information used in patient treatment. A new potential area of molecular imaging is emerging in the field of PET due to the availability of radioligands capable of imaging the cAMP signaling system both pre- (Luisi et al., 2005) and post-synaptically (DaSilva et al., 2002; Fujita and Innis, 2000; Kopka et al., 2005) and described in this thesis.

In general, the employment of PET and receptor-ligands requires three components: (1) subject administration of radiotracer to bind a receptor/enzyme/transporter site; (2) tissue-tracer concentration imaging using a positron emission tomograph; and (3) a mathematical model describing *in vivo* tracer kinetics. The quantitative measurement and detection of radiotracer emission by highly sensitive radiation detectors arranged around the body result in a four-dimensional image of distribution through time. By pursuing the path of the radioactive tracer, the normal and pathological functions can be identified in tissues.

1.10.1 Positron emission tomography imaging of signal transduction systems

Interest in imaging molecular signal transduction systems has led to the synthesis of novel PET radiotracers capable of imaging changes in pre- and postsynaptic signaling at both the membrane and intracellular level. Presynaptically, NAT and vesicular monoamine transporters can be measured with [^{11}C]hydroxyephedrine (Stevens, 2001; Vesalainen et al., 1999) and [^{11}C]tetrabenazine (DaSilva and Kilbourn, 1992), respectively. Postsynaptically, radioligands have been developed to measure membrane β-AR densities such as (*S*)-[^{11}C]CGP 12177 (Ueki et al., 1993; van Waarde et al., 1995). However, measurements of cellular membrane receptor density ignore the multitude of intracellular mechanisms and signaling required for biological effects. Limited PET

studies have been carried out using intracellular signaling radiotracers. Radioligands measuring AC and PKC second messenger systems have been studied using [^{11}C]forskolin (Sasaki et al., 1995; Sasaki et al., 1991) and [^{18}F]- or [^{11}C]-1,2-diacylglycerol (Hammadi et al., 1994; Takahashi et al., 1994). Unfortunately, little data has been published on these radiotracers possibly due to complex radiosynthesis and low radiochemical yields. There has however been success imaging PDE4. In addition to the development of PDE4 inhibitor (*R*)-[^{11}C]rolipram, further examined in this thesis (DaSilva et al., 1999; DaSilva et al., 2002; Lourenco et al., 2006), another group in Japan has synthesized and analyzed *in vivo* mice with PDE4 inhibitor [^{18}F]KF 19316 (Hatano et al., 1999). The successful development of radioligands for imaging post-synaptic cAMP-mediated signaling may permit innovative discoveries in the etiology and pathogenesis involved in obesity and diabetes as well as other disorders.

1.10.2 Characteristics of (R)-[^{11}C]rolipram

Our group has previously synthesized and evaluated the binding characteristics of the most active (*R*)-enantiomer of the PDE4 inhibitor rolipram, labeled with carbon-11 (Fig. 6), *in vivo* in the rat and human brain (DaSilva et al., 2002; Lourenco et al., 2001), as well as the rat heart and lungs (Lourenco et al., 2006). Other groups have utilized (*R*)-[^{11}C]rolipram as an *in vivo* index of brain cAMP signaling using PET (Fujita et al., 2005; Harada et al., 2002; Parker et al., 2005; Tsukada et al., 2004; Tsukada et al., 2001a; Tsukada et al., 2001b). Regional brain uptake has been proven to be in accordance with the HARBS in rats (Kaulen et al., 1989; Schneider et al., 1986). Distribution of (*R*)-[^{11}C]rolipram retention was found to be most delineated for central and peripheral tissues between the 30 and 45 min time point following tracer administration in rats (Lourenco et

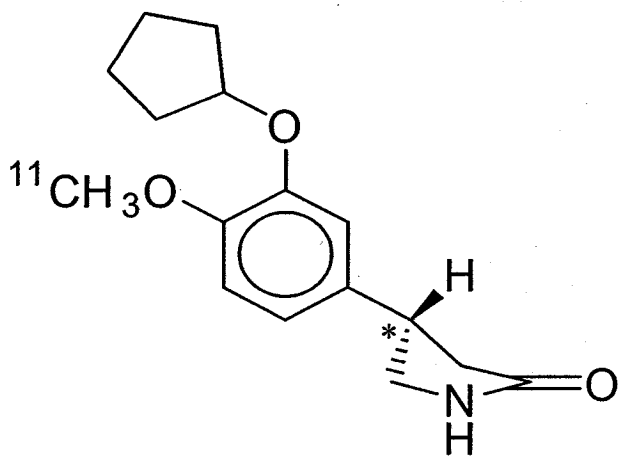

(*R*)-[^{11}C]Rolipram

Fig. 6: Chemical structure of the carbon-11 labeled (*R*)-enantiomer rolipram (*denotes the chiral centre).

al., 2001). Furthermore, co-injection with unlabeled selective PDE4 inhibitors (*R*)-rolipram or Ro20-1724 lead to a dose-dependent reduction in (*R*)-[^{11}C]rolipram retention, significantly reducing tracer uptake to non-specific levels throughout tissue regions (Lourenco et al., 2001). Pretreatment of rats with NAT inhibitor desipramine (DMI) or tranylcypromine causes significant dose-dependent increases in (*R*)-[^{11}C]rolipram binding in rat brain and heart tissues (Lourenco et al., 2006), indicating an association between synaptic NA levels and PDE4 activity and expression.

Metabolism studies have revealed considerable tritiated or carbon-11 labeled (*R*)-rolipram metabolism 30 to 45 min after injection, with radioactivity corresponding to both polar metabolites and unchanged radioligand. The radioactive metabolites do not cross the blood-brain barrier (Lourenco et al., 1999b) in agreement with previous exploration using [^{3}H]rolipram in brain homogenates (Krause and Kühne, 1988; Krause and Kühne, 1993). Based on reports regarding alterations in SNS signaling in various disease states like heart failure, obesity, and diabetes, our group has directed efforts towards studying PDE4 with (*R*)-[^{11}C]rolipram in pathological states. Collectively, the results of the *in vivo* binding, metabolism, and pharmacological studies in rats provide a multitude of strong support for the further employment of (*R*)-[^{11}C]rolipram as an agent for studying PDE4 and intracellular cAMP using PET.

1.11 Research rationale, hypotheses, and strategy

1.11.1 Previous results

(*R*)-[^{11}C]Rolipram binds selectively to intracellular PDE4 over PDE1 in rats since treatment with PDE4 competitors Ro20-1724, or (*R*)-, (*S*)- or (*R/S*)-rolipram, but not

PDE1 inhibitor vinpocetine, significantly reduces (*R*)-[^{11}C]rolipram radioactivity uptake to non-specific levels (Lourenco et al., 1999a; Lourenco et al., 2001). Administration of (*R*)-[^{11}C]rolipram was found to distribute in the brain and broadly to many peripheral organs and tissues (Lourenco et al., 2001). Previous *in vivo* pharmacological experiments have demonstrated modulation of (*R*)-[^{11}C]rolipram specific binding to PDE4 in both rat brain and heart following increased synaptic NA via administration of DMI or tranylcypromine in a dose-dependent manner (Lourenco et al., 2006). The binding of (*R*)-[^{11}C]rolipram in rat tissues has been modulated by agents affecting cAMP. Generally, it has been concluded that (*R*)-[^{11}C]rolipram appears to detect an increase in PDE4 binding.

1.11.2 Rationale and objectives

Based on previous results, (*R*)-[^{11}C]rolipram has the ability to measure alteration of PDE4 activity caused by modulation of cAMP-signaling. Additionally, insights of the pathological obese and diabetic states suggest alterations in cAMP-mediated signaling in central and peripheral tissues. The conducted research, described in this thesis, has been directed toward the accomplishment of two major objectives. The first objective has been to determine the presence of PDE4 specific binding as measured with (*R*)-[^{11}C]rolipram *in vivo* in tissues associated with thermogenesis and diabetes. The second objective of this research was directed towards assessing the functional states of cAMP-mediated signaling in NORM, obese, and diabetic rat models. This objective included the use of acute and chronic cAMP modulating agents such as DMI, α_2-AR antagonist yohimbine, and non-selective β-AR antagonist CGP 12177. Measurements of PDE4 with (*R*)-[^{11}C]rolipram following pretreatment of NA elevating agent DMI revealed post-

synaptic cAMP-mediated signaling function in comparison to untreated controls. The agents were chosen at doses that have previously shown or were expected to cause changes in (*R*)-[^{11}C]rolipram regional uptake. Acquisition of these objectives will further evaluate the potential of (*R*)-[^{11}C]rolipram in tracing central and peripheral disturbances of PDE4 binding and cAMP-mediated signaling in the obese and diabetic states using PET. Ultimately, future work would utilize this research as a foundation for unveiling the obscure etiology and treatment of SNS dysfunction in obesity and diabetes using (*R*)-[^{11}C]rolipram and PET.

1.11.3 Hypotheses

The main hypotheses that were tested in this research are the following:

1) (*R*)-[^{11}C]Rolipram quantifies PDE4 specific binding in the brain, SkM, heart, pancreas, adipose tissues, and lungs.
2) Dysfunctional cAMP-mediated signaling is observed in obese and DM2 rats.
3) (*R*)-[^{11}C]Rolipram can measure altered cAMP-mediated signaling in obesity and DM2.

1.11.4 Aims

The following main experiments were planned out and performed to test the presented hypotheses:

1) *In vivo* blocking studies will be conducted in normal Sprague-Dawley (NORM) rats co-administered with PDE4 inhibitors (*R*)-rolipram and Ro20-1724 to assess the presence of PDE4 specific binding in rat tissues. *Ex vivo* metabolism studies will be performed using (*R*)- and (*S*)-[^{11}C]rolipram to determine the identity of the labeled

products and to further confirm the presence of PDE4 specific binding in tissues of interest.

2) *In vivo* biodistribution studies will be performed in NORM rats using acute and chronic drug treatments that alter cAMP-mediated signaling in order to determine the pharmacological binding profile of our tracer.
3) Physiological measurements will be assessed for obese and diabetic rat body weight gain, dietary intake, blood glucose, plasma insulin, and metabolic $\dot{V}_{O2}$ and $\dot{V}_{CO2}$.
4) *In vivo* biodistribution studies will be conducted with obese and diabetic rat models using (*R*)-[^{11}C]rolipram with or without DMI assessing the functionality of cAMP-mediated signaling in disease states.

2.0: MATERIALS AND METHODS

2.1 Animals

Animal experiments were conducted in accordance with the guidelines of the Canadian Council on Animal Care and with approval from the Animal Care Committee at the University of Ottawa. Male NORM, DR, and DIO rats at five weeks of age were obtained from Charles River Laboratories (Montreal, Canada). Upon arrival, animals were allotted a five day acclimatization period for environmental stress adjustment. Following acclimatization period, six week old rats were placed on appropriate diet, and maintained on a 12 h light/dark cycle with food and water provided *ad libitum.*

2.1.1 NORM rats

Six week old NORM rats were placed on HFD (32% fat, 51% carbohydrate, 17% protein) (Research Diets D12266B) and weight matched to rats fed comparable control low-fat diet (LFD; 10% fat, 73% carbohydrate, 17% protein) (Research Diets D12489B) for 2- or 8-weeks (± 4 days) until used in biodistribution studies. NORM rats studied using HPLC analysis were fed regular chow diet (Harlan Teklad 2019). Body weight and food intake was monitored twice weekly among rat groups. Body weight results were expressed as weight gain over specified time periods (grams body weight – grams initial body weight). Final experimental fasted body weights for rats were also expressed. Dietary intake was expressed as total diet consumed over specified time period, as total diet consumed per day, and as total calories consumed. Fasting blood glucose measurements were taken following biodistribution experiment.

2.1.2 Obesity model

DR and DIO rats were purchased from Charles River Laboratories (Montreal, QC), and fed HFD (Research Diets D12266B) for a period of 2- or 8-weeks (± 4 days) until biodistribution studies. DR and DIO body weights and food intake were monitored twice weekly. Data was expressed as described above. Fasting blood glucose was obtained from trunk blood following biodistribution experiment.

2.1.3 DM2 model

Upon arrival at the University of Ottawa Heart Institute animal care facilities, baseline 6 week old NORM rats were fed HFD for a period of 14 days, followed by intraperitoneal (ip) administration of either 1 mL/kg 0.1M sodium citrate buffer in citrate control rats or 45 mg/kg STZ treatment to induce diabetes in DM2 rats (day 0). Rats were maintained on HFD for an additional 2- or 8-weeks (± 4 days) until used for biodistribution studies. Blood glucose levels were monitored via the saphenous vein on week -2 (prior to HFD), day 0 (prior to citrate or STZ treatment), and week 1, 3*, 6*, and 8* following citrate or STZ administration. Fasting blood glucose was also monitored on the day of experiments from trunk blood obtained following decapitation. As a measure to screen for DM2, rats exhibiting post-prandial blood glucose levels less than 11 mmol/L following STZ administration were separated and categorized into a STZ-treated DM2 (bg<11) sub-group; rats exhibiting blood glucose greater than 11 mmol/L were defined as DM2. Citrate control and DM2 rat body weights were monitored twice weekly and data was expressed as previously described above.

---

* 8-week model

2.2 General biodistribution

Rats were fasted from 16:00 overnight prior to experiments as to reduce circadian rhythm- and metabolic pattern-induced fluctuations. Experiments were conducted at approximately identical times (within 1.5 h of 12:00) to nullify increases in SNS signaling, NA levels, and blood marker secretion observed during the morning hours due to circadian rhythm effects (Martinez-Merlos et al., 2004). Animals in restraining cages (Harvard Apparatus, Canada) were warmed under an incandescent lamp to induce vein vasodilatation to facilitate (*R*)-[^{11}C]rolipram injection via the lateral tail vein. The dose of (*R*)-[^{11}C]rolipram administered varied between 0.9–1.9 mCi (33.3-70.3 MBq) in ~0.3 mL of the saline formulation. In each experiment, all animals received approximately equivalent mass doses (0.21-1.74 μg) of high specific activity (*R*)-[^{11}C]rolipram (300-1200 Ci/mmol at end-of-synthesis). The time point of 45 min post-tracer injection was determined to be ideal for rat sacrifice from previous studies in our laboratory (Lourenco et al., 2001; Lourenco et al., 2006). A blood sample (~1.0 mL) was collected from the rat trunk into 10.8 mg EDTA vacutainer tubes (BD). Fasting blood glucose measurements were taken using an Accu-Chek Advantage glucometer (Roche) from blood samples.

The following tissues were rapidly dissected out: HYPO, cerebellum, brain stem, SkM, atria, free wall of right ventricle, left ventricle and septum (LVS), pancreas, WAT, interscapular BAT, lung, liver, and blood sample. Tissues were placed in pre-weighed gamma counter tubes, evaluated in the gamma-counter (Canberra Packard, Cobra II) along with aliquots of the injected solution as standards and then weighed. Residual radioactivity remaining in the tails and syringes were counted in a dose-calibrator (Capintec CRC-712 M). Subtracting residual activity in tails and syringes indicate actual

injected dose entering the bloodstream. Degree of radiotracer retention was expressed as a tissue-to-blood (tissue:blood) ratio where percent injected dose per gram of tissue ($\%ID_{tissue}/g_{tissue}$) is divided by percent injected dose per gram of blood ($\%ID_{blood}/g_{blood}$) which takes into account the altered radioligand delivery caused by pharmacokinetic differences resulting from uneven animal sizes, and pharmacological agents (Law, 1993).

$$\text{Tissue:blood} = \frac{\%ID/g\ (tissue)}{\%ID/g\ (blood)}$$

2.3 Drugs

The following drugs were dissolved in warm sodium chloride 0.9% sterile saline or as otherwise indicated below: desipramine hydrochloride (Sigma), (±) CGP 12177 (Sigma). (*R*)-Rolipram (Tocris) was dissolved in warm 5/20/75 ethanol/1,2-propendiol/0.9% saline (v/v/v, pH≥4.4). Ro20-1724 (4-(3-Butoxy-4-methoxy-benzyl)imidazolidin-2-one) (Sigma) and yohimbine hydrocholide (Sigma) were dissolved in hydrochloric acid (HCl) acidified 5/20/75 ethanol/1,2-propendiol/0.9% saline (v/v/v, pH≥4.0). Streptozocin (Sigma) was dissolved in HCl acidified sterile 0.1M sodium citrate buffer (pH≥4.5).

2.4 Specific binding and metabolism in NORM rats

2.4.1 Biodistribution analysis of (R)-[^{11}C]rolipram PDE4 specific binding

Using the general biodistribution procedures, tracer doses of (*R*)-[^{11}C]rolipram were co-injected with unlabelled (*R*)-rolipram (1.0 mg/kg) (Lourenco et al., 2001) to measure non-specific binding in all rat models. This was repeated in 2-week HFD NORM rats with the PDE4 inhibitor Ro20-1724 (30 mg/kg) (Lourenco et al., 1999a). Results represented non-saturable, non-specific (*R*)-[^{11}C]rolipram binding. PDE4 specific

binding was calculated by subtracting non-specific binding from total tracer retention (without co-injection of saturating dose (1 mg/kg) of PDE4 inhibitor (*R*)-rolipram). Rats were killed at the defined ideal time point as previously determined in our laboratory (45 min).

2.4.2 Metabolite and specific binding analysis of (R)- and (S)-[^{11}C]rolipram in peripheral tissues using high performance liquid chromatography

Similar to protocols of the general procedures, tracer doses of (*R*)- or (*S*)-[^{11}C]rolipram were co-injected alone or in combination with unlabelled (*R*)-rolipram (1.0 mg/kg) into NORM rats as outlined with changes in Lourenco *et al.* (Lourenco et al., 2001). In addition to the competition studies using (*R*)-rolipram, (*S*)-[^{11}C]rolipram was also utilized as a measure of non-specific binding in comparison to the carbon-11 labeled (*R*)-enantiomer, and to compare both enantiomers. Rats were sacrificed 45 min post-tracer injection, and SkM, pancreas and BAT tissues were dissected rapidly. Tissues were individually homogenized (Polytron) in ice-cold 80% ethanol (8 mL). Residual tissue on the homogenizing apparatus was collected with 2 mL of 80% ethanol and placed in an open-top polyallomer tube and centrifuged at 60000 x g for 15 min (Beckman L8-80M). The supernatant was removed and evaporated to dryness under vacuum. The residue was resuspended in 0.25 mL acetonitrile (ACN) to lyse remaining proteins and cells, then 2.0 mL of 1/99 solution of ACN/water (v/v) was added. The solution was passed through a 0.2 μm syringe filter (PharmAssure) to remove the remaining proteins, then analyzed by high performance liquid chromatography (HPLC).

HPLC was carried out using an adapted methodology outlined by Hilton *et al.* (Hilton et al., 2000). Briefly, the system consisted of two Waters 510 pumps (Waters Co.), one

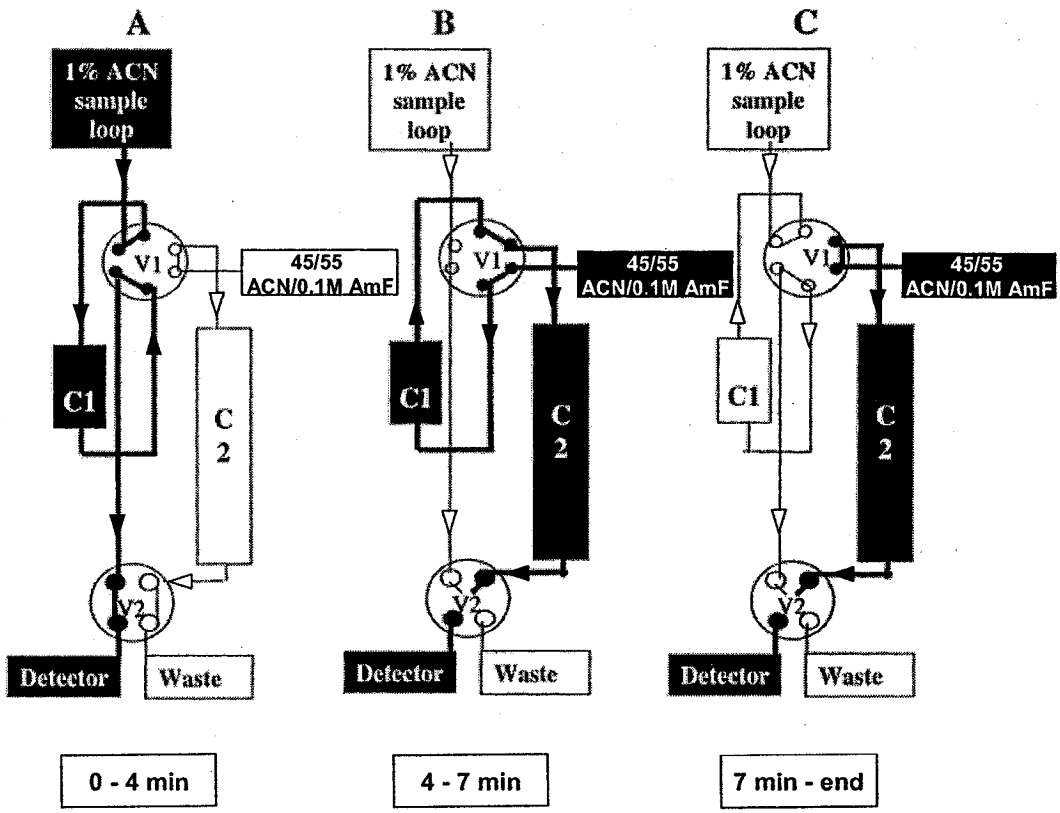

Fig. 7: Flow diagrams (heavy lines) for displacement of the injected sample from the injector loop by 1% ACN and its passage through the capture column C1 **(A)**; elution of analytes from C1 by the 45/55 ACN/0.1M AmF analytical mobile phase and chromatography on the analytical column C2 **(B)**; and reequilibration of the capture column during chromatography on the analytical column C2 **(C)** (adapted from Hilton et al., 2000).

delivering 1/99 ACN/water (v/v) at 2 mL/min, and the other carrying the 45/55 ACN/0.1M ammonium formate (AmF) (v/v) mobile phase at 1 mL/min (designated 45/55 ACN/0.1M AmF in Fig. 7). Samples were loaded into a 5 mL injector loop. At the time of injection, a six-port valve was positioned (Fig. 7A) to direct the sample, displaced by 1% ACN, to come in contact with the capture column (Oasis HLB). Compounds too polar and hydrophobic to bind the C_{18} Sep-pak sorbent (Waters) of the capture column were eluted and detected by a highly sensitive coincidence radioactivity detector (Bioscan). Four minutes after the sample injection, the valves were repositioned to allow the analytical mobile phase to back-flush the contents of the capture column onto the Aqua analytical column (Phenomenex, 250 x 4.6mm 5 micron), and to direct the effluent from the analytical column to the detector (Fig. 7B). Approximately 7 min after sample injection, the first valve was returned to its original position (Fig. 7C) allowing the capture column to equilibrate in original solvent in preparation for the next sample. At the end of the analysis, the second valve was returned to its original position (Fig. 7A). Metabolite radioactivity signals from the analytical HPLC detector were analyzed using PeakSimple software (SRI Inc.), and used to record the peak areas and retention times (R_t). Percentages of peak areas were background- and decay-corrected. Data was presented as averages of percent area under the curve (%AUC).

2.5 Physiological measurements

In addition to body weight gain, and dietary consumption previously described in the above sections, blood glucose and plasma insulin levels were also monitored in select animal models.

2.5.1 Blood glucose

Fasting blood glucose was obtained from trunk blood of untreated control NORM, DR, DIO, citrate control and DM2 rats. Postprandial blood glucose was monitored in DM2 and citrate control rats as described above in animal models. Blood glucose measurements were obtained using an Accu-Chek Advantage glucometer (Roche).

2.5.2 Plasma insulin

Plasma samples were obtained from residual remaining trunk blood collected in EDTA tubes. Blood samples were centrifuged at 2900 x g for 5 min and plasma samples pipetted into 2.0 mL eppendorf tubes and stored at -80°C. Obese and diabetic animal model fasting plasma insulin measurements were assessed using a sensitive rat insulin radioimmunoassay (RIA) kit (Linco) (Jang et al., 2003; Levin and Dunn-Meynell, 2000). Briefly, during the three day RIA procedure, known plasma volumes were diluted with 0.05M phosphosaline (0.025M EDTA, 0.08% sodium azide, 1% RIA grade bovine serum albumin) assay buffer (to 200 µL), then incubated with 100 µL of guinea pig anti-rat insulin serum in the buffer overnight for 24 h in the refrigerator. On the second day, 100 µL of ^{125}I-insulin was added to the plasma-antibody solution, and incubated overnight for 24 h in the refrigerator. The final step involved addition of 1.0 mL of cold (4°C) precipitating reagent (goat anti-guinea pig IgG serum, 3% polyethylene glycol and 0.05% Triton X-100 in 0.05M phosphosaline, 0.025M EDTA, 0.08% sodium azide), allowing 20 min of incubation, then centrifugation at 3000 x g for 20 min. Supernatants were decanted and pellets counted in the gamma-counter for radioactivity. The amount of tracer bound to antibody decreases as the concentration of unlabeled rat insulin bound antigen increases. An insulin standard curve of was created using increasing

concentrations of insulin provided in the RIA kit to evaluate final results of each assay. Final rat insulin results were then corrected for dilution factor of plasma in assay buffer.

2.6 Indirect calorimetry

Two- and 8-week DR, DIO, citrate control and DM2 rat models were subjected to indirect calorimetry measurements at 2-4 days prior to biodistribution studies. Rats were transported to Dr. Mary-Ellen Harper's laboratory in Roger Guindon Hall 5 days prior to biodistribution studies and allowed a 24 h acclimatization period upon arrival. Following acclimatization period, groups of 3-4 rats were placed individually into separate calorimetry chambers (each with a volume of 10 L) for a 24 h indirect calorimetry measurement period with *ad libitum* access to HFD and water. Temperature was maintained at 24°C, and lights set to be on from 07:00 to 19:00 (light phase) and off between 19:00 to 07:00 (dark phase). The indirect calorimetry detection used a four-chamber Oxymax system with automatic temperature and light controls (Columbus Instruments, Columbus, OH) (Bezaire et al., 2001; Riachi et al., 2004). System settings included a gas flow rate of 4.5 L/min. Gas concentrations of oxygen and carbon dioxide were analyzed using a limited diffusion, metal air battery sensor to measure $\dot{V}_{O2}$ while $\dot{V}_{CO2}$ was measured using a spectrophotometric sensor. Repeated sampling of $\dot{V}_{O2}$ and $\dot{V}_{CO2}$ over the 24 h period corresponded to RER measurements as an index of the utilization of energy fuel sources, as well as relative rate of heat production corrected to kilogram body weight ($\dot{V}_{O2}$/kgBW) and $\dot{V}_{O2}$ per whole rat. After completion of indirect calorimetry measurements, rats were returned to animal care facilities at the University of Ottawa Heart Institute and placed under quarantine for any pathogens acquired during

transfers between facilities. *In vivo* biodistribution studies using (*R*)-[^{11}C]rolipram of rats measured with indirect calorimetry were also completed under quanantine conditions.

2.7 (*R*)-[^{11}C]Rolipram baseline analyses of rat models

2.7.1 High-fat diet, low-fat diet, fasting, and fed states in NORM rats

Groups of 6 week old NORM rats were fed HFD or LFD for the required 2- and 8-week time periods until biodistribution studies. Subgroups of the 2-week HFD or LFD fed rats on each diet were either fasted overnight as described in general biodistribution procedures, or fed *ad libitum* until experiment. Rats were injected with radioligand and sacrificed. Tissues were dissected and counted for (*R*)-[^{11}C]rolipram binding as described above.

2.7.2 Baseline comparison of DR, DIO, citrate control and DM2 rats

Using the general biodistribution procedures, (*R*)-[^{11}C]rolipram was injected into 2- and 8-week DR, DIO, citrate control, and DM2 rat models. Tissues were dissected, weighed and counted for radioactivity with a gamma counter and expressed as previously stated in general biodistribution.

2.8 Effects of diverse treatments on *in vivo* (*R*)-[^{11}C]rolipram binding in rat models

2.8.1 Acute pharmacological treatments in NORM rats

Similar to protocols of the general procedures, the effects of acute pretreatment with various pharmacological agents on the regulation of (*R*)-[^{11}C]rolipram *in vivo* binding was assessed in 2-week diet fed NORM rats. At times following administration of drugs, determined from literature, rats were injected with (*R*)-[^{11}C]rolipram and tissues were

dissected out and analyzed as described above. Studies producing increases in (*R*)-[^{11}C]rolipram binding were repeated with co-injection of unlabelled (*R*)-rolipram (1 mg/kg) to assess increases in specific binding in all animal models.

Agents affecting cAMP production through agonism and antagonism of β-ARs were administered to rat models in acute treatments (ip). To directly elicit an increase synaptic NA, DMI (20 mg/kg 3 h prior) (Bodnar et al., 1985; Lourenco et al., 2006), or yohimbine (10 mg/kg 15 min prior) (van Oene et al., 1984) was administered (ip) to NORM rats. Acute blockade of β-ARs was produced with single administration of CGP 12177 (10 mg/kg ip, 3 h prior) (Hjeresen et al., 1989). Effects of increased synaptic NA following DMI treatment on β-ARs were blocked with CGP 12177 (10 mg/kg ip, 3 h 15 min prior). Following pharmacological treatments, rats were sacrificed and tissues analyzed as above.

2.8.2 Sub-chronic treatments in NORM rats

To assess the effect sub-chronic elevation in synaptic NA levels in 2-week diet fed NORM rats on (*R*)-[^{11}C]rolipram, 0.9% sterile saline (1 mL/kg) or DMI (10 mg/kg) was administered (ip) twice daily for 14 days (Lacroix et al., 1991; Ye et al., 2000). Allowing a 24 h wash-out period, rats were evaluated using the general biodistribution procedures mentioned above. This study was repeated on a small group of sub-chronic DMI rats also treated with co-injection of unlabelled (*R*)-rolipram (1mg/kg) during tracer administration to assess changes in specific binding.

2.8.3 Acute desipramine treatment in obese and diabetic rats

Post-synaptic cAMP-mediated functionality was assessed in 2- and 8-week HFD DR, and DIO rats, and 2-week STZ DM2 rats with (*R*)-[^{11}C]rolipram using the following

procedure. Rats were administered (ip) acute treatments of the NAT inhibitor DMI (20 mg/kg) 3 h prior to (*R*)-[^{11}C]rolipram injection. Treatments were repeated using co-injection of unlabelled (*R*)-rolipram (1 mg/kg) to assess changes in specific binding. Animals were sacrificed, tissues dissected, weighed and counted for radioactivity, expressed as previously stated in general biodistribution.

2.9 Statistical analysis

2.9.1 Physiological measurements

2.9.1.1 Body weight and diet

Statistical significance was determined utilizing the student's t-test comparing DIO and DM2 disease state rats to respective age matched controls (using SPSS software). All analyses of concerning final fasted body weight, diet consumed, calories consumed, and diet per day consumed utilized *n* values of total treated and untreated rats since treatments did not affect these values.

Statistical analysis of body weight gain for 8-week STZ DM2 rats compared to citrate control and DM2 (bg<11) rats was determined by One-way Analysis of Variance (ANOVA) followed by Dunnett post-hoc comparisons test (using SPSS software). All analyses of weight gain employed *n* values of total treated and untreated rats as different groups. Statistical significance comparing citrate controls to DM2 rats were indicated by asterisks (*), and DM2 (bg<11) to DM2 rats were indicated by a plus sign (+) with a criterion of probability < 0.05.

2.9.1.2 Blood glucose and plasma insulin

Analysis of fasted glucose and insulin utilized the student's t-test and concerned *n* values from untreated rat models (using SPSS software). Statistical significance (compared to control group) was indicated by asterisks (*) with a criterion of probability < 0.05.

2.9.2 Indirect calorimetry

Statistical significance was evaluated by a repeated measures general linear model (GLM) analysis and a Tukey multiple comparisons test when required (using SAS software). Data represented *n* values of three in each animal model. Significant outcomes between control, age- and light-matched diseased models were indicated with an asterisk (*); significant outcomes between light, age- and model-matched dark phase results were indicated with a section sign (§); and significant outcomes between 2-week, light- and model-matched 8-week models were indicated with a yen sign (¥), with a criterion of probability < 0.05.

2.9.3 Specific binding of (R)-[^{11}C]rolipram in NORM rats

Statistical significance on the specific binding was determined by One-way Analysis of Variance (ANOVA) followed by Dunnett post hoc comparisons (using SPSS software). All the statistical analysis concerning biodistribution data was performed using tissue:blood ratio for each tissue. Statistical significance (compared to control group) was indicated by asterisks (*) with a criterion of probability < 0.05.

2.9.4 (R)-[^{11}C]Rolipram baseline analyses of rat models

Statistical significance was determined utilizing the student's t-test when comparing two groups and by One-way Analysis of Variance (ANOVA) followed by Dunnett post

hoc comparisons when making multiple comparisons to control models (using SPSS software). All statistical analysis concerning biodistribution data were performed on tissue:blood ratios. Statistical significance, compared to controls, was indicated by asterisks (*) with a condition of probability < 0.05.

2.9.5 Effects of diverse treatments on in vivo (R)-[^{11}C]rolipram binding in rat models

Statistical significance was determined by One-way Analysis of Variance (ANOVA) followed by Dunnett post hoc comparisons tests (using SPSS software) in comparisons to control groups. Statistical significance was indicated by asterisks (*) when comparing NORM, DR, DIO, and citrate controls models while significance was indicated with a (+) when using DM2 as a control for its own treatments. The criterion of significant probability was < 0.05.

3.0: RESULTS

3.1 Specific binding and metabolism in NORM rats

3.1.1 Biodistribution analysis of (R)-[^{11}C]rolipram PDE4 specific binding

(*R*)-[^{11}C]Rolipram distributes in many rat tissues. As expected, saturating doses of (*R*)-rolipram (1 mg/kg) and Ro20-1724 (30 mg/kg) reduced (*R*)-[^{11}C]rolipram binding to non-specific levels in PDE4 rich tissues. Significant decreases of (*R*)-[^{11}C]rolipram binding were revealed in brain (HYPO, cerebellum, brain stem), SkM, heart (atria, right ventricle free wall, LVS), pancreas, and lung (Fig. 8A). Whereas, no reduction in (R)-[^{11}C]rolipram was observed in WAT, BAT, and liver (Fig. 8A). (*R*)-[^{11}C]Rolipram specific binding to PDE4 was found to be approximately 70-84% in brain, 39-40% in SkM, 29-40% in heart, 44-51% in pancreas, and 33-35% in lung (Fig. 8B). For clarity and simplicity of expressing this data, the HYPO and LVS are presented in future figures as representative regions of the brain and heart. The lung region has little to do with the processes associated with obesity and diabetes, and WAT and BAT contain no specific binding to PDE4 such that theses tissues were no longer considered regions of interest and are not presented further.

3.1.2 Metabolite and specific binding of (R)- and (S)-[^{11}C]rolipram in peripheral tissues using high performance liquid chromatography

HPLC tissue analyses of the organic fractions 45 minutes postinjection of (*R*)-[^{11}C]rolipram, demonstrated the presence of hydrophilic metabolites from SkM (Fig. 9A), pancreas, and BAT (Table II) in the solvent front fractions of the capture and analytical

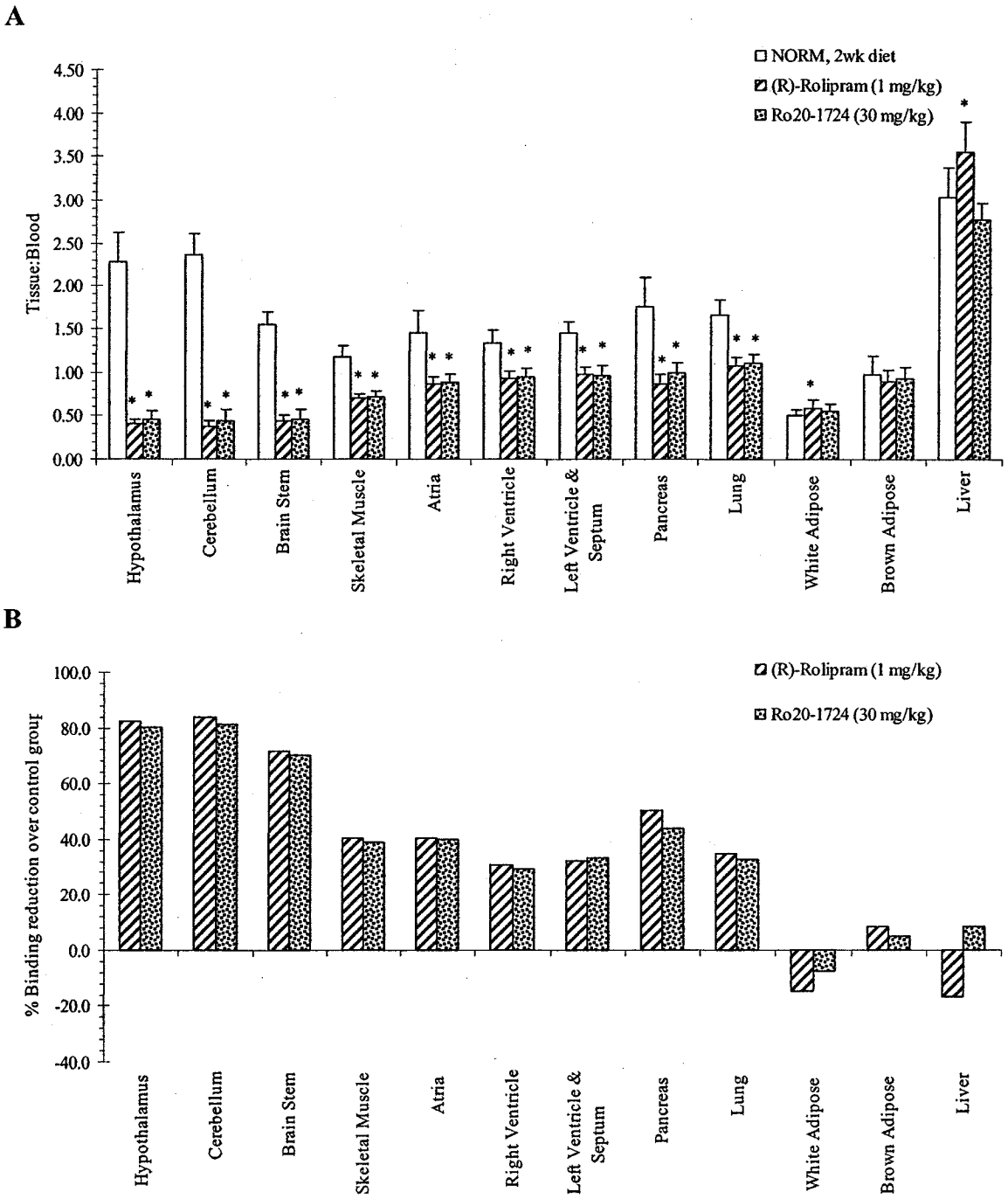

Fig. 8: Distribution of (*R*)-[^{11}C]rolipram in 2-week diet fed NORM rats 45 min following co-injection with the competitors (*R*)-rolipram or Ro20-1724 **(A)**; and percent reduction in specific radioligand binding following coinjection of competitive PDE4 inhibitors **(B)**. Data are mean tissue:blood ± SD and average % reduction in tissue:blood radioactivity following treatment over control (*$p<0.05$, One-way ANOVA with Dunnett comparisons test to short-term NORM rats; NORM: n=27, (*R*)-rolipram: n=15, Ro20-1724: n=5).

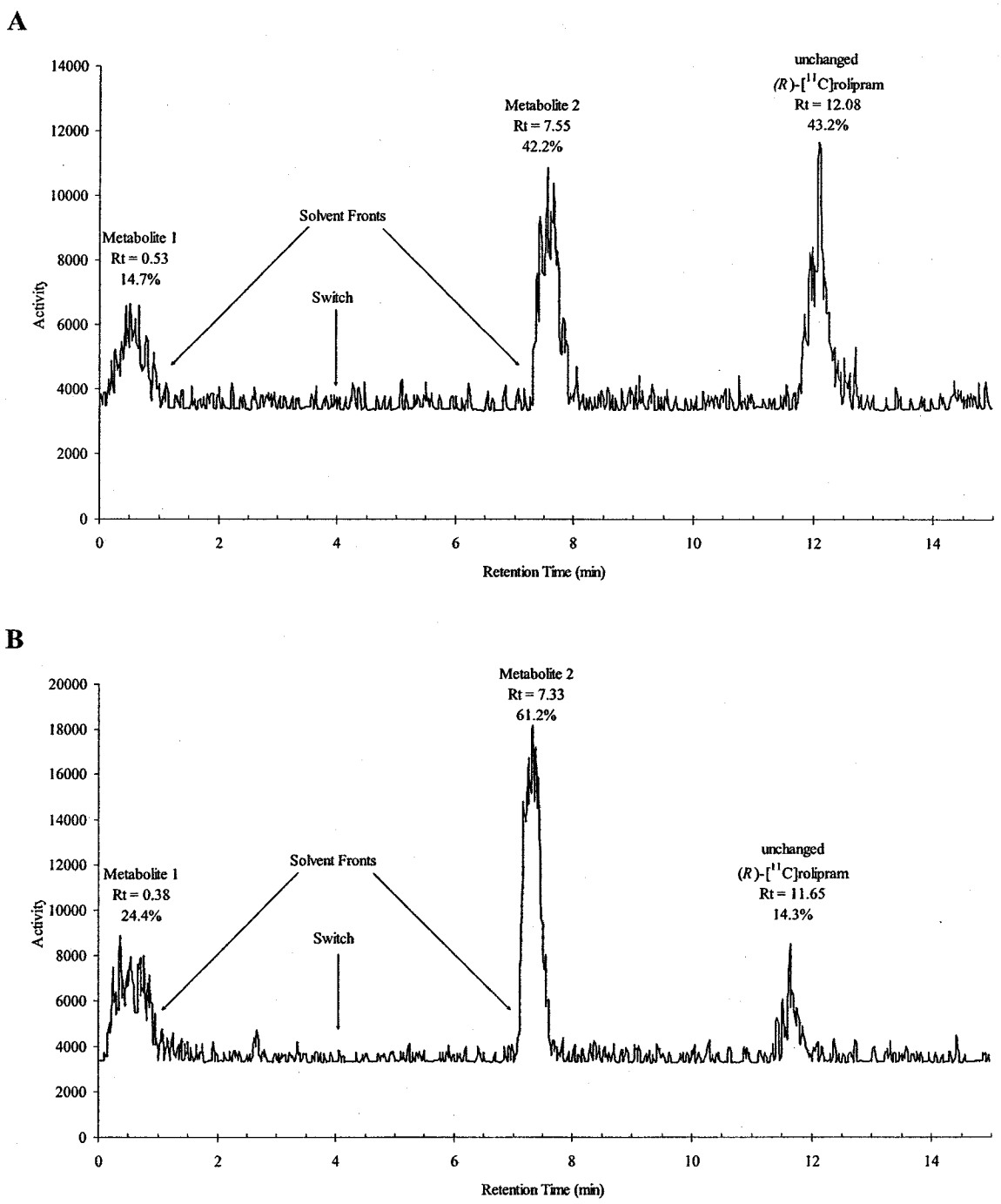

Fig. 9: Representative HPLC chromatograms of (*R*)-[^{11}C]rolipram and its ^{11}C-labeled metabolites from an individual rat skeletal muscle **(A)**, and skeletal muscle blocked by co-administration of cold (*R*)-rolipram **(B)**, injected 45 min prior to sacrifice using the "HPLC column-switch method" (0-4 min: Oasis HLB cartridge capture column traps tissue proteins, 1/99 acetonitrile/water, 2 ml/min; 4-15 min: Aqua C_{18} 5 µm Phenomenex analytical column, 45/55 acetonitrile/0.1 M ammonium formate, 1 ml/min; coincidence radiation detection).

Table II: Presence of unchanged (*R*)- & (*S*)-[^{11}C]rolipram and their ^{11}C-labeled metabolites in NORM rat skeletal muscle, pancreas, brown adipose tissues, and plasma.

	%AUC (*R*)-[^{11}C]rolipram			%AUC (*S*)-[^{11}C]rolipram		
	Hydrophilic Metabolites		unchanged (*R*)-[^{11}C]rolipram	Hydrophilic Metabolites		unchanged (*S*)-[^{11}C]rolipram
	1	2		1	2	
Skeletal Muscle	9.1 +/- 6.5	39.0 +/- 3.1	51.8 +/- 6.8	22.6 +/- 9.5	36.2 +/- 13.8	41.2 +/- 4.3
+ (*R*)-rolipram[a]	20.5 +/- 12.5	63.1 +/- 8.4	16.3 +/- 4.3	33.8 +/- 6.1	29.1 +/- 9.7	37.1 +/- 15.7
Pancreas	10.1 +/- 14.2	45.1 +/- 19.1	44.9 +/- 4.9	28.6 +/- 3.1	26.2 +/- 0.0	45.3 +/- 3.0
+ (*R*)-rolipram[a]	16.5 +/- 7.0	58.2 +/- 7.0	25.3 +/- 0.0	39.4 +/- 16.0	11.1 +/- 3.7	49.5 +/- 12.3
Brown Adipose	15.8 +/- 2.5	31.4 +/- 6.1	52.7 +/- 8.6	30.9 +/- 8.3	14.7 +/- 0.6	54.4 +/- 8.9
+ (*R*)-rolipram[a]	19.9 +/- 2.5	28.3 +/- 0.5	51.9 +/- 3.0	28.7 +/- 8.5	14.6 +/- 2.5	56.8 +/- 6.0
Plasma[b]	32.5 ± 7.4	42.5 ± 6.2	25.0 ± 4.9	55.9 ± 2.2	23.2 ± 4.3	20.9 ± 6.5
+ (*R*)-rolipram[ab]	39.5 ± 3.5	48.5 ± 3.5	12.0 ± 0.1	57.1 ± 7.6	23.6 ± 0.3	19.4 ± 7.3

[a] Blocking with (*R*)-rolipram (1 mg/kg) is representative of changes in specific binding. Minimum of n=3 in each group. [b] Plasma data obtained from experiments performed in our laboratory with Kenk *et al.* (Kenk et al., 2006a).

columns. Analysis of the radioactivity in the organic fractions of the tissue extracts in SkM (Fig. 9A), pancreas, and BAT revealed 45-53% unchanged (*R*)-[^{11}C]rolipram (Table II). Total unchanged (*R*)-[^{11}C]rolipram radioactivity was reduced to 16% in SkM (Fig. 9B) and 25% in pancreas following co-administration of (*R*)-rolipram, whereas unchanged (*R*)-[^{11}C]rolipram remained unaffected by (*R*)-rolipram in PDE4 poor BAT (Table II).

HPLC tissue analyses of SkM, pancreas, and BAT postinjection of (*S*)-[^{11}C]rolipram revealed the presence of hydrophilic metabolites in the solvent front fractions of the capture and analytical columns (Table II). Unchanged (*S*)-[^{11}C]rolipram binding was 41-54% in SkM, pancreas, and BAT. However, the unchanged (*S*)-[^{11}C]rolipram activity in SkM, pancreas, and BAT was not reduced following co-injection of (*R*)-rolipram (Table II). Studies conducted in our laboratory also found that the presence of labeled (*R*)- and (*S*)-[^{11}C]rolipram metabolites increased following administration on unlabeled (*R*)-rolipram in rat plasma (Kenk et al., 2006a).

3.2 NORM rat studies

3.2.1 Physiological measurements

HFD fed NORM rats possessed no significant differences in body weight compared to LFD fed rats following 2- or 8-week feeding periods (Table III). NORM 2-week HFD fed rats consumed significantly less diet per day and total diet than LFD controls; however, total caloric intake remained similar between HFD and LFD groups after both 2- and 8-week feeding periods. Diet had no effect on fasting blood glucose levels in NORM rats fed either HFD or LFD for 2- or 8-weeks.

Table III: Physiological measurements in 2- and 8-week diet NORM rats.

Animal Model	Final Body Weight$_{fasted}$ (g)	Total Diet Consumed (g)	Total Diet Consumed per Day (g/day)	Total Calories Consumed (kcal)	Glucose$_{fasted}$ (mmol/L)
2-week LFD NORM	296 ± 40	320 ± 29	23 ± 2.1	1246 ± 112	2.8 ± 0.4
2-week HFD NORM	294 ± 35	298 ± 25*	21 ± 1.8*	1315 ± 112	3.0 ± 0.8
8-week LFD NORM	474 ± 29	1244 ± 114	22 ± 2.0	4852 ± 444	3.2 ± 0.4
8-week HFD NORM	471 ± 16	1154 ± 66	21 ± 1.2	5087 ± 290	3.5 ± 0.3

Data are mean values ± SD (*$p<0.05$, student's t-test comparing HFD to LFD; *n* values for final body weight, total diet, total diet per day, and total calories consumed taken from complete NORM rat experiments, n=48, 48, 4, 4 respectively. Glucose measurements were taken from untreated NORM rats, n= 12, 15, 4, 4 respectively).

3.2.2 (R)-[^{11}C]Rolipram baseline analysis

Tissue retention of (*R*)-[^{11}C]rolipram 45 min postinjection was unaffected by dietary fat content in 2-week (Fig. 10A) or 8-week (Fig. 10B) diet fed NORM rats indicating dietary fat content had no effect on PDE4 levels. Data points to the ability to merge age-matched NORM LFD and HFD fed (*R*)-[^{11}C]rolipram binding results and findings are presented as merged age-matched HFD/LFD binding data so forth. Additionally, significant decreases in (*R*)-[^{11}C]rolipram binding to PDE4 were observed in HYPO and pancreas between 2- and 8-week NORM rats (Fig. 11A). There was also a significant increase in HYPO radioligand binding in the unfasted 2-week NORM rats compared to fasted NORM controls (Fig. 11B), indicating that neither (*R*)-[^{11}C]rolipram binding results could be merged from the 2- and 8-week NORM rats or results from 2-week fasted and unfasted NORMs.

3.2.3 Effects of acute treatments on in vivo (R)-[^{11}C]rolipram binding

Acute administration of DMI has been previously shown to significantly augment the regional uptake of (*R*)-[^{11}C]rolipram in brain and heart concurring with present results (Fig. 12). Additionally, administration of DMI to 2-week diet NORM rats caused significantly increased total binding (Table IV) and specific binding (Table V) of (*R*)-[^{11}C]rolipram to PDE4 in SkM. Acute increases in synaptic NA due to DMI had no effect on PDE4 in the pancreas. Pretreatment with CGP 12177 prior to DMI treatment brought the DMI-mediated increases in (*R*)-[^{11}C]rolipram binding back to NORM control levels (Fig. 13). CGP 12177 alone had no effect on tissue (*R*)-[^{11}C]rolipram binding to PDE4. Acute treatments yohimbine lead to significant (*R*)-[^{11}C]rolipram binding reductions to PDE4 in HYPO and SkM in 2-week diet NORM rats (Fig. 14, Table IV).

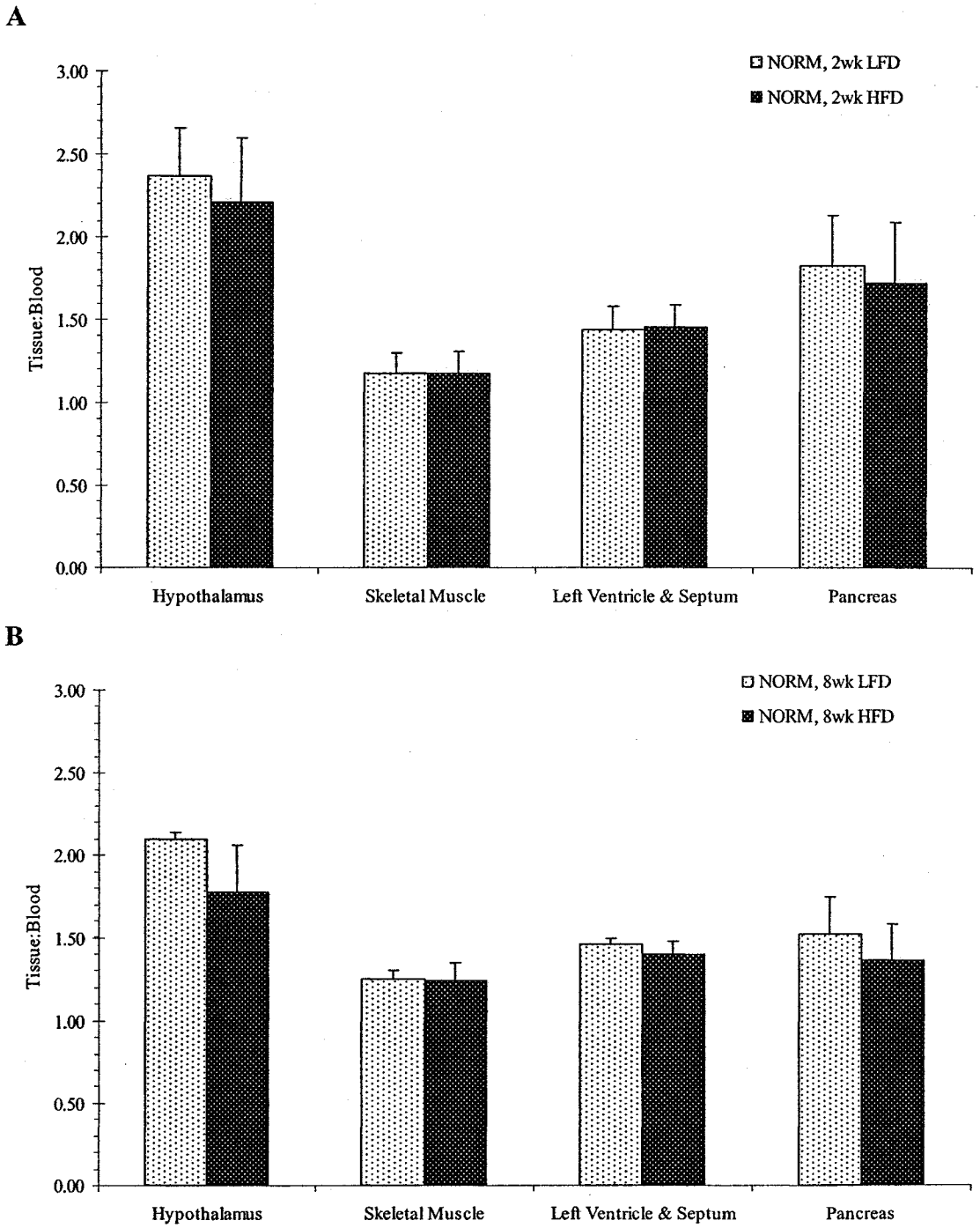

Fig. 10: (*R*)-[^{11}C]rolipram retention in LFD vs. HFD NORM rat tissues following 2-week **(A)** and 8-week **(B)** feeding periods. Data are mean tissue:blood ± SD (*$p<0.05$, student's t-test; NORM 2wk LFD: n=12, NORM 2wk HFD: n=15, NORM 8wk LFD: n=4, NORM 8wk HFD: n=4).

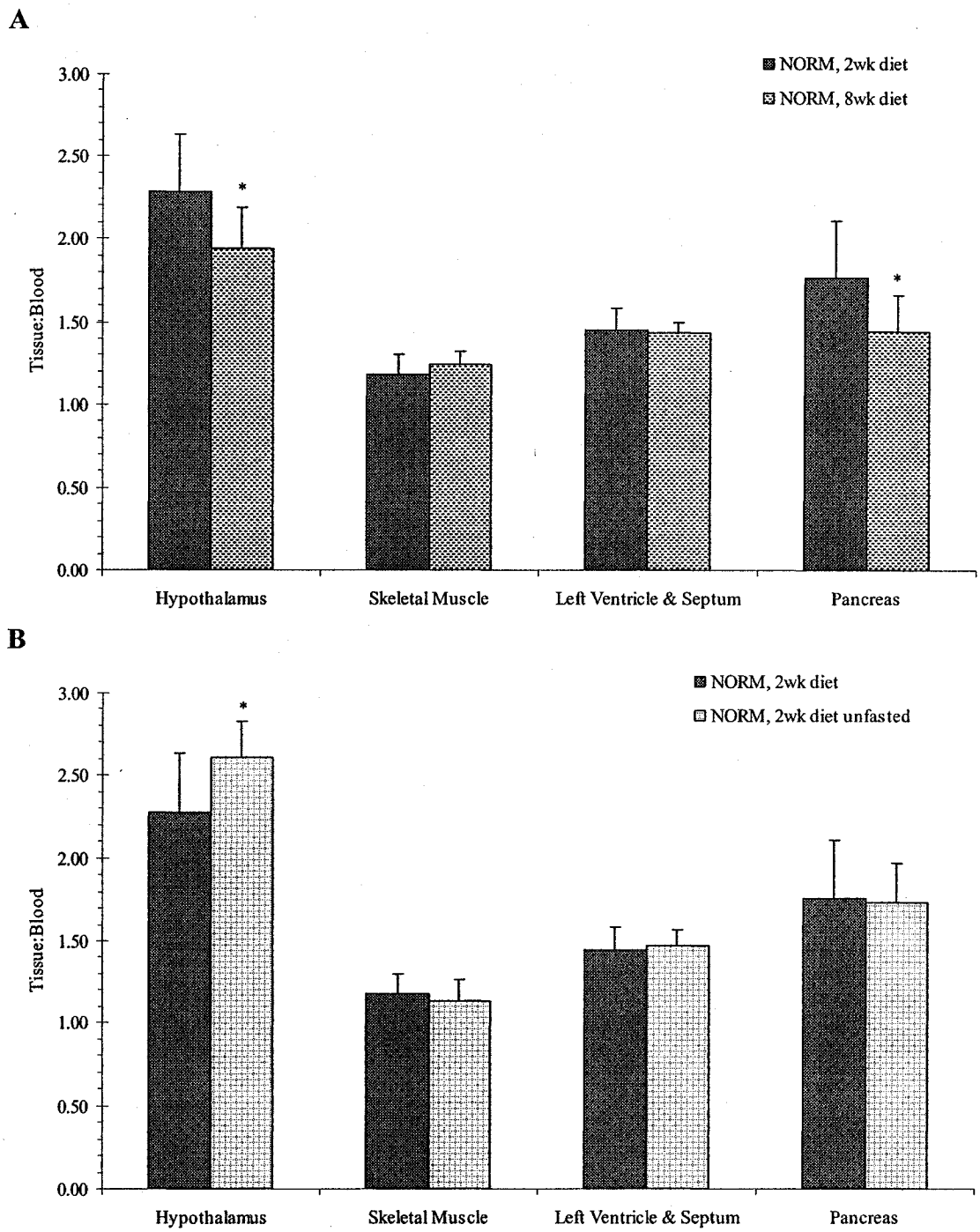

Fig. 11: Uptake of (*R*)-[^{11}C]rolipram retention of merged LFD and HFD NORM rats in 2-week and 8-week feeding periods **(A)** and comparison of tracer retention under fasting and fed conditions **(B)**. Data are expressed as mean tissue:blood ± SD (*$p<0.05$, student's t-test to NORM 2wk diet rats; NORM: n=27, NORM 8wk diet: n=8, NORM 2wk diet unfasted: n=10).

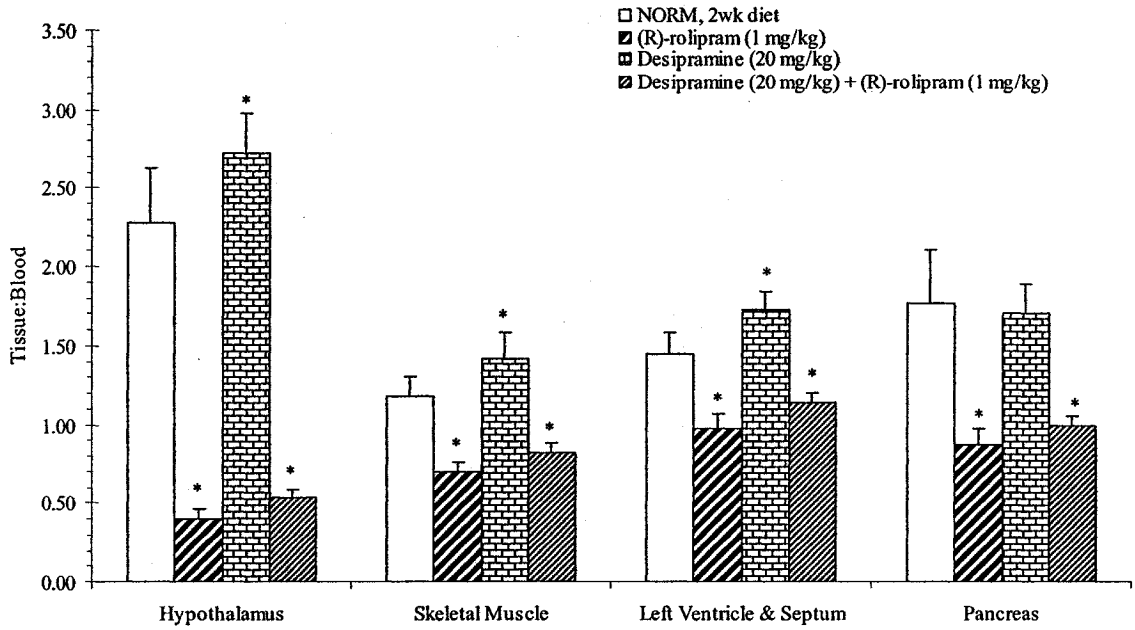

Fig. 12: Distribution of radioactivity in rat brain and periphery 45 min following (*R*)-[^{11}C]rolipram administration in 2-week diet NORM rats treated with (*R*)-rolipram (1 mg/kg coinjection), desipramine (20 mg/kg i.p. 3 h prior to radioligand injection), or desipramine (20 mg/kg i.p. 3 h prior to radioligand injection) plus (*R*)-rolipram (1 mg/kg coinjection). Data are mean tissue:blood ± SD (*$p<0.05$, One-way ANOVA with Dunnett comparisons test to 2-week diet NORM control rats; NORM: n=27, (*R*)-rolipram: n=15, desipramine: n=14, desipramine + (*R*)-rolipram: n=8).

Table IV: Percent changes[a] in (*R*)-[^{11}C]rolipram tissue retention in 2-week diet NORM rats following pharmacological treatments.

Treatment	Animal Model	(*R*)-[^{11}C]Rolipram Percent Change in Tissue			
		Hypothalamus	Skeletal Muscle	Left Ventricle & Septum	Pancreas
Acute Desipramine					
2-week diet	NORM	19	21	19	-4
Acute Yohimbine					
2-week diet	NORM	-12	-14	-7	-4
Sub-Chronic Desipramine					
2-week diet	NORM[b]	20	28	11	33

[a] Percent change in radiotracer retention (determined from tissue:blood values) between the treated rats and bank of 2-week diet NORM controls (n=27). *n* values for treatments shown in figures. [b] Compared to sub-chronic saline treated 2-week diet NORM controls.

Table V: Percent changes in (*R*)-[^{11}C]rolipram PDE4 specific binding in 2-week diet NORM rats following acute desipramine treatment increasing synaptic neurotransmission.

Treatment	Animal Model	Percent Change in (*R*)-[^{11}C]rolipram Specific Binding in Tissue			
		Hypothalamus	Skeletal Muscle	Left Ventricle & Septum	Pancreas
Acute Desipramine					
2-week diet	NORM	16	26	26	-20

Specific binding was calculated by subtracting the average tissue:blood ratio in the presence of the (*R*)-rolipram blocking dose (1 mg/kg, i.v., coinjected with the radioligand) or non-specific binding (NSB), from the total binding (T) in the absence of (*R*)-rolipram in 2-week diet NORM rats. Percent change in specific binding was calculated as follows: $((T_{desipramine} - NSB_{desipramine})-(T_{control} - NSB_{control}))/(T_{control} - NSB_{control})*100$.

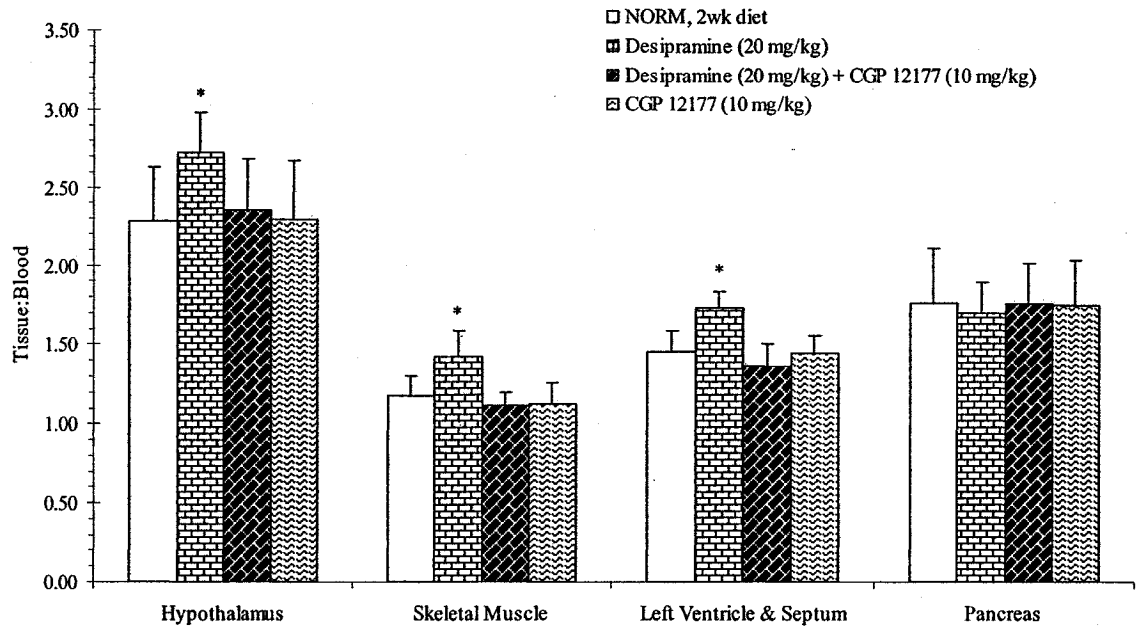

Fig. 13: Distribution of radioactivity in rat brain and periphery 45 min following (*R*)-[^{11}C]rolipram administration in 2-week diet NORM rats treated with desipramine (20 mg/kg i.p. 3 h prior to radioligand injection), desipramine (20 mg/kg i.p. 3 h prior to radioligand injection) plus CGP 12177 (10 mg/kg i.p. 3 h 15 min prior to radioligand administration), or CGP 12177 (10 mg/kg i.p. 3 h prior to radioligand) alone. Data are mean tissue:blood ± SD (*$p<0.05$, One-way ANOVA with Dunnett comparisons test to 2-week diet NORM rats; NORM: n=27, desipramine: n=14, desipramine + nadolol: n=4, desipramine + CGP 12177: n=8, CGP 12177: n=7).

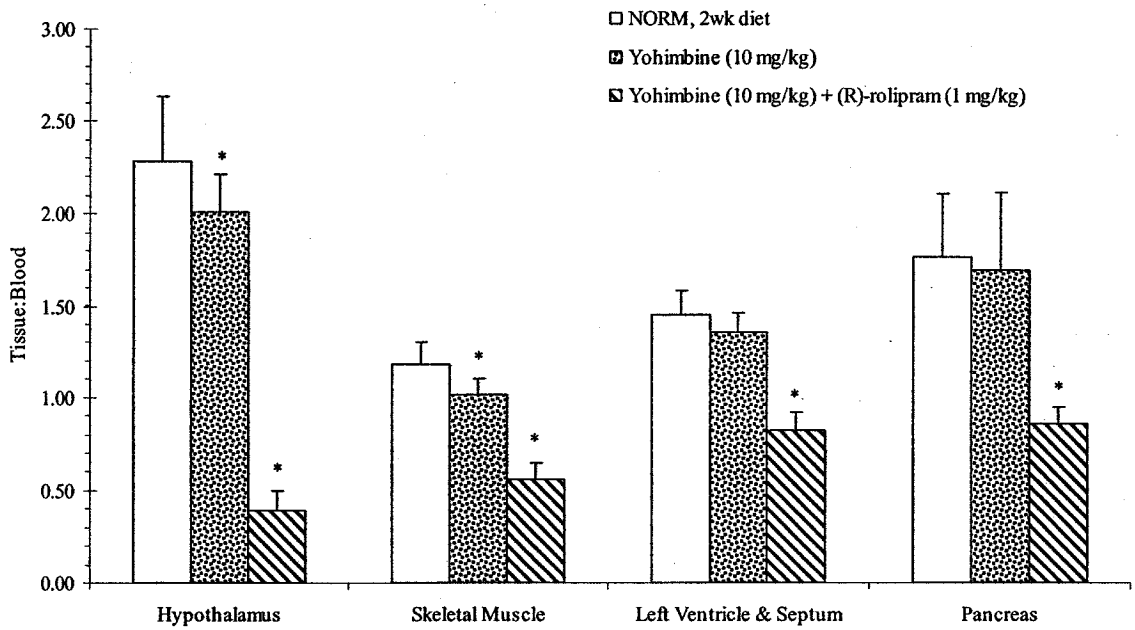

Fig 14: Distribution of radioactivity in rat brain and periphery 45 min following (*R*)-[^{11}C]rolipram administration in 2-week diet NORM rats treated with yohimbine (10 mg/kg i.p. 15 min prior to radioligand injection) or yohimbine (10 mg/kg i.p. 15 min prior to radioligand injection) plus (*R*)-rolipram (1 mg/kg coinjection). Data are mean tissue:blood ± SD (*$p<0.05$, One-way ANOVA with Dunnett comparisons test 2-week diet NORM rats; NORM: n=27, yohimbine: n=10, yohimbine + (*R*)-rolipram: n=6).

Acute yohimbine treatment to 2-week diet NORM rats was ineffective at altering (*R*)-[^{11}C]rolipram retention in heart or pancreas.

3.2.4 Effects of sub-chronic desipramine treatment on in vivo (R)-[^{11}C]rolipram binding

Sub-chronic treatment of antidepressant DMI demonstrated significantly enhanced (*R*)-[^{11}C]rolipram binding to PDE4 in HYPO, SkM and pancreas in 2-week diet NORM rats compared to saline treated controls (Fig. 15, Table IV). The LVS heart region showed a slight, although insignificant, increase in (*R*)-[^{11}C]rolipram binding to PDE4 following sub-chronic treatments of DMI. Binding of (*R*)-[^{11}C]rolipram in sub-chronic DMI treated NORM rats was significantly reduced following co-administration of unlabeled (*R*)-rolipram signifying the presence of specific binding to PDE4.

3.3 DR and DIO rat studies

3.3.1 Physiological measurements

The consumption of HFD over an 8-week feeding period caused significantly greater weight gain in DIO rats compared to DR controls (Fig. 16). Both 2- and 8-week HFD DIO rats possessed significantly greater final body weights compared to respective DR control rats (Table VI). Additionally, DIO rats consumed significantly greater amounts of total HFD, as well as diet per day, and total calories compared to DR controls in both 2- and 8-week models (Table VI). There were no significant differences between DIO and DR fasted blood glucose or plasma insulin levels in 2- or 8-week HFD models.

3.3.2 Indirect calorimetry

Twenty-four hour indirect calorimetry measurements revealed no significant differences in RER values from light or dark phases between DR and DIO rats in the 2-

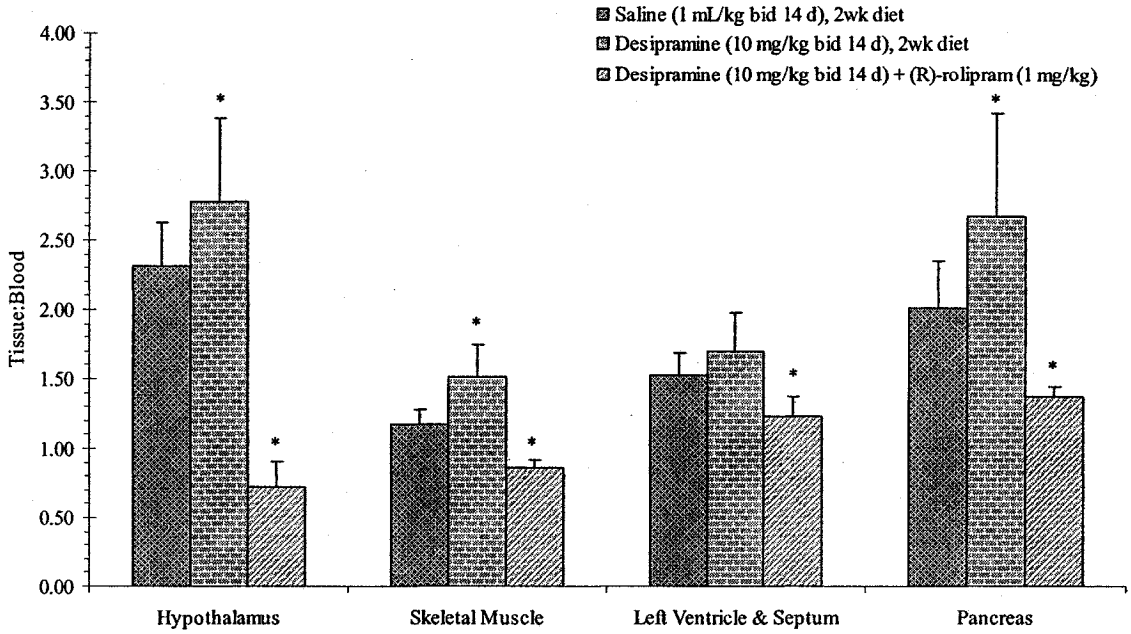

Fig. 15: Distribution of radioactivity in rat brain and periphery 45 min following (*R*)-[^{11}C]rolipram administration in 2-week diet NORM rats following 24 h washout period of treatments with saline (1 mL/kg i.p. bid, 14 days), desipramine (10 mg/kg i.p. bid, 14 days), desipramine (10 mg/kg i.p. bid, 14 days) plus (*R*)-rolipram (1 mg/kg coinjection). Data are mean tissue:blood ± SD (*$p<0.05$, One-way ANOVA with Dunnett comparisons test to 2-week diet NORM saline control rats; Saline: n=9, desipramine: n=12, desipramine + (*R*)-rolipram: n=10).

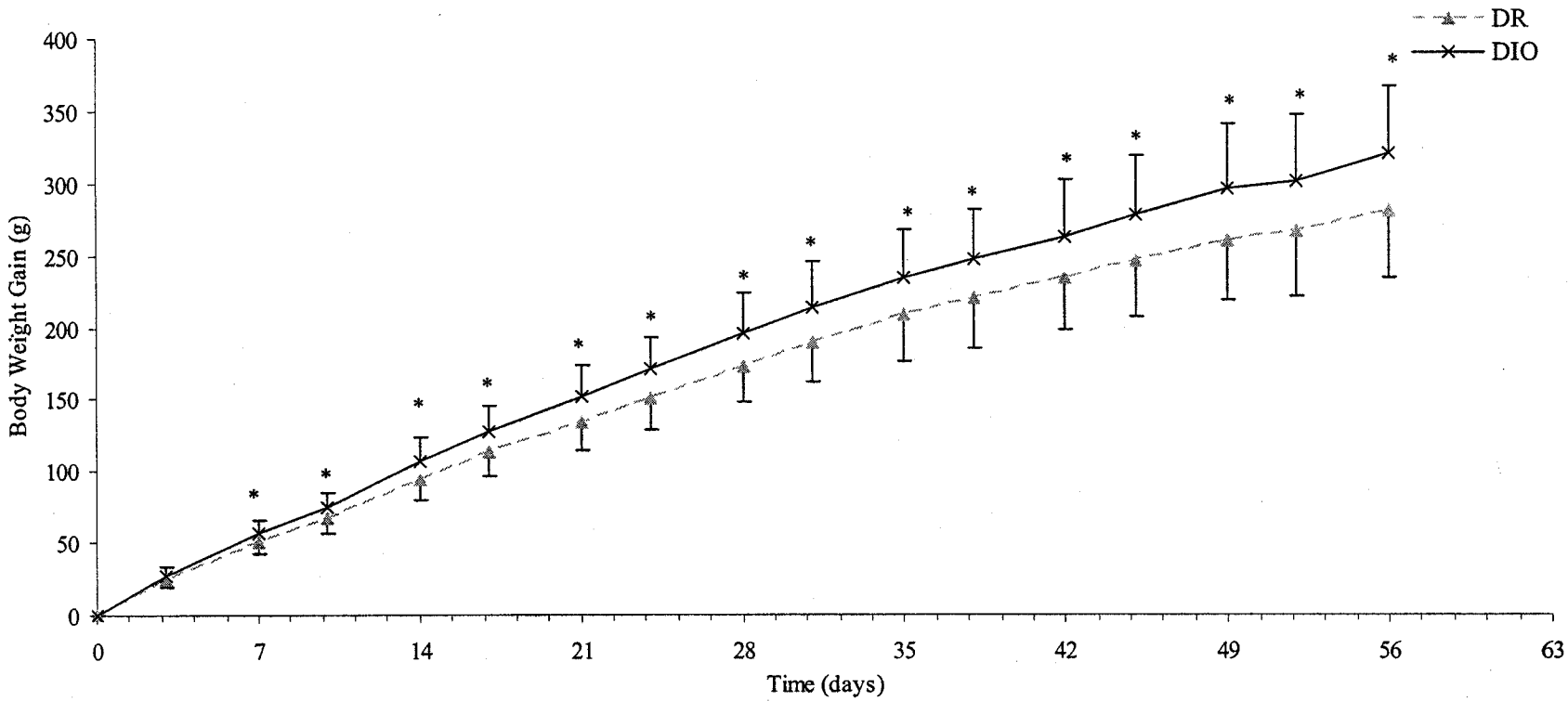

Fig. 16: Weight gain of 8-week HFD DR and DIO rats. Data are mean weight gain ± SD (*$p<0.05$, student's t-test to 8-week HFD DR controls; DR: n=17, DIO: n=17).

Table VI: Physiological measurements of DR and DIO rats.

Animal Model		Final Body Weight$_{fasted}$ (g)	Total HFD Consumed (g)	Total HFD Consumed per Day (g/day)	Total Calories Consumed (kcal)	Glucose$_{fasted}$ (mmol/L)	Insulin$_{fasted}$ (ng/mL)
2-week HFD	DR	226 ± 19	227 ± 18	16 ± 1.3	1003 ± 81	3.2 ± 0.3	0.33 ± 0.16
	DIO	248 ± 30*	258 ± 21*	18 ± 1.5*	1139 ± 91*	2.9 ± 0.3	0.28 ± 0.18
8-week HFD	DR	402 ± 52	1054 ± 117	19 ± 2.1	4647 ± 517	4.4 ± 0.3	0.63 ± 0.38
	DIO	444 ± 56*	1142 ± 91*	20 ± 1.6*	5036 ± 400*	4.5 ± 0.4	1.49 ± 0.82

Data are mean values ± SD (*$p<0.05$, student's t-test comparing DIO rats to age-matched DR controls; *n* values for final body weight, total HFD, total HFD per day, and total calories consumed taken from complete baseline and pharmacological DR and DIO rat studies, n=18, 18, 17, 17 respectively. Glucose and insulin measurements were taken from untreated DR and DIO rats, n= 5, 5, 5, 5 respectively).

or 8-week HFD models. Hence, substrate oxidation of the relative proportions of carbohydrate and fat were similar between between DR and DIO rats following both 2- and 8-week HFD feeding periods (Table VII). The 2-week HFD DIO model was found to have significantly lower $\dot{V}_{O2}$/kgBW compared to 2-week HFD DR rats in the dark phase; this observation was not found in whole body $\dot{V}_{O2}$ measurements when not normalized to body weight. During the light phase, 2-week HFD DR and DIO rats had reduced $\dot{V}_{O2}$/kgBW compared to those in the dark phase; the effect of light was only repeated in whole body $\dot{V}_{O2}$ in 2-week HFD DR rats. Both 2-week HFD DR and DIO rats in the light and dark phases had significantly augmented $\dot{V}_{O2}$/kgBW values compared to those in the 8-week HFD models; in contrast, whole body $\dot{V}_{O2}$ measurements indicated that 2-week HFD DR rats in the light phase had significantly decreased oxygen consumption compared to 8-week HFD DR rats while there were no other significant differences were observed between DR and DIO rats in 2- or 8-week models. Lastly, 8-week HFD DR rat $\dot{V}_{O2}$/kgBW in the dark phase was increased compared to 8-week HFD DIO dark phase values which was not observed in whole body $\dot{V}_{O2}$ measurements.

3.3.3 (R)-[^{11}C]Rolipram baseline analysis

Tissue retention of (*R*)-[^{11}C]rolipram 45 min postinjection was similar between 2-week HFD DR and DIO rats (Fig. 17A). Additionally, there were no differences in radioligand binding between 8-week HFD DR and DIO rats (Fig. 17B). However, significantly diminished pancreatic (*R*)-[^{11}C]rolipram binding was observed in 8-week HFD DR rats compared to 2-week HFD DRs (Fig. 18A), as well as in 8-week HFD DIO rats compared to 2-week HFD DIO rats (Fig. 18B).

Table VII: 24 hour indirect calorimetry measurements in DR and DIO rats.

Animal Model		RER[a]		$\dot{V}_{O2}$/kgBW[b] (mL/min/kg)		$\dot{V}_{O2}$[c] (mL/min)	
		Light Phase	Dark Phase	Light Phase	Dark Phase	Light Phase	Dark Phase
2-week HFD	DR	0.86 ± 0.07	0.90 ± 0.04	32.0 ± 6.7$^{\S\,¥}$	41.0 ± 7.3$^{¥}$	7.3 ± 1.6$^{\S\,¥}$	9.1 ± 1.6
	DIO	0.84 ± 0.04	0.88 ± 0.03	31.2 ± 5.9$^{\S\,¥}$	35.4 ± 5.3$^{*\,¥}$	8.7 ± 1.7	9.9 ± 1.5
8-week HFD	DR	0.81 ± 0.05	0.85 ± 0.05	25.4 ± 6.3	29.1 ± 6.3	9.1 ± 2.2	10.5 ± 2.2
	DIO	0.79 ± 0.05	0.82 ± 0.04	20.1 ± 4.2	22.5 ± 4.2*	9.7 ± 2.0	10.9 ± 2.2

[a] Respiratory exchange ratio (RER),[b] body weight corrected oxygen consumption ($\dot{V}_{O2}$/kgBW), and [c] whole body oxygen consumption ($\dot{V}_{O2}$) of 2- and 8-week HFD DR and DIO rats. Data are mean ± SD (*$p<0.05$, repeated measures GLM comparing DIO to age- and light-matched DR controls; $^{\S}p<0.05$, repeated measures GLM comparing light to dark phase age- and model-matched controls; $^{¥}p<0.05$, repeated measures GLM comparing 2-week to 8-week HFD fed light- and model-matched controls; n=3 in each group).

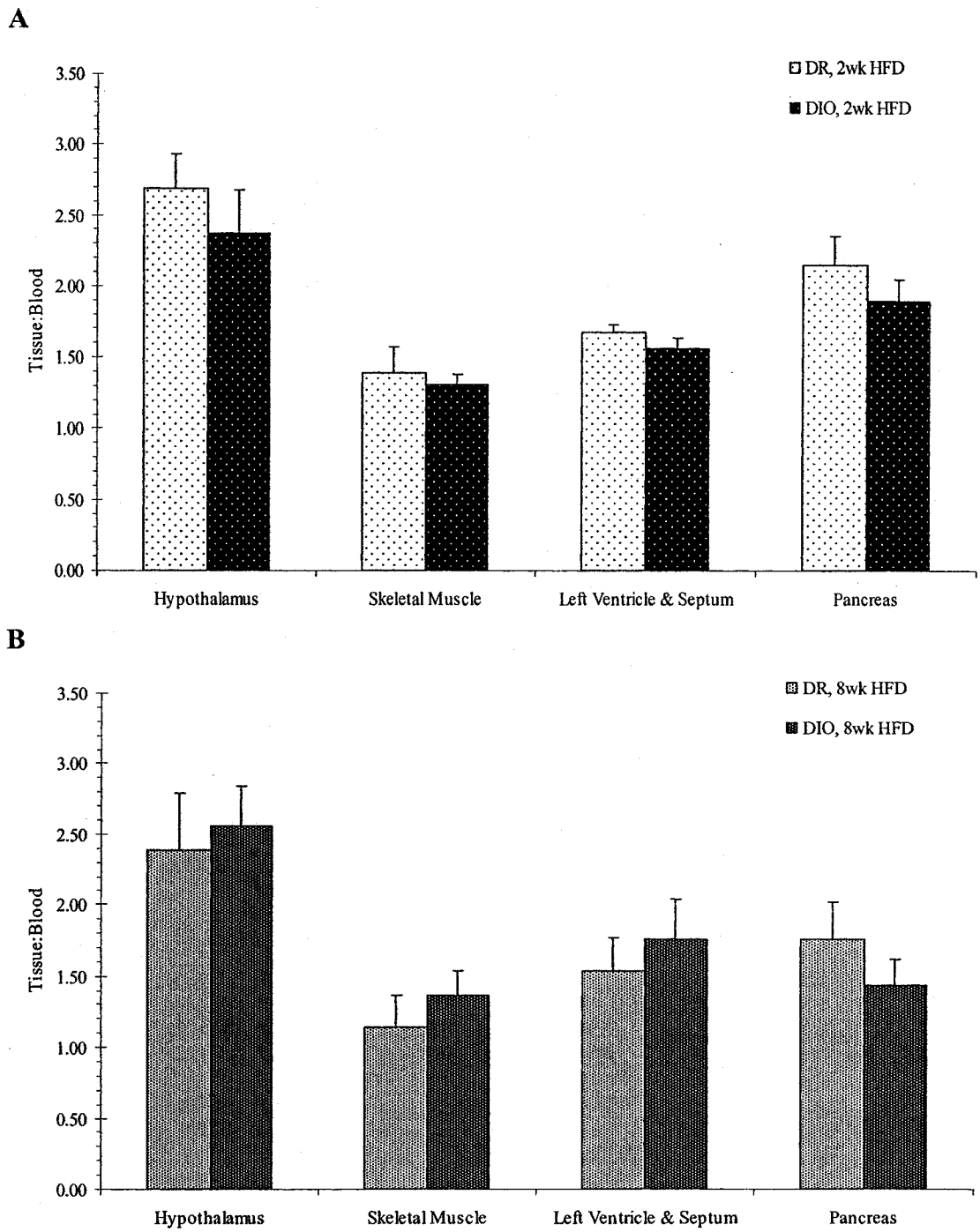

Fig. 17: Distribution of radioactivity in rat brain and periphery 45 min following (*R*)-[^{11}C]rolipram administration in 2-week HFD **(A)** and 8-week HFD **(B)** DR and DIO rats. Data are mean tissue:blood ± SD (*$p<0.05$, student's t-test to DR controls; n=5 in each group).

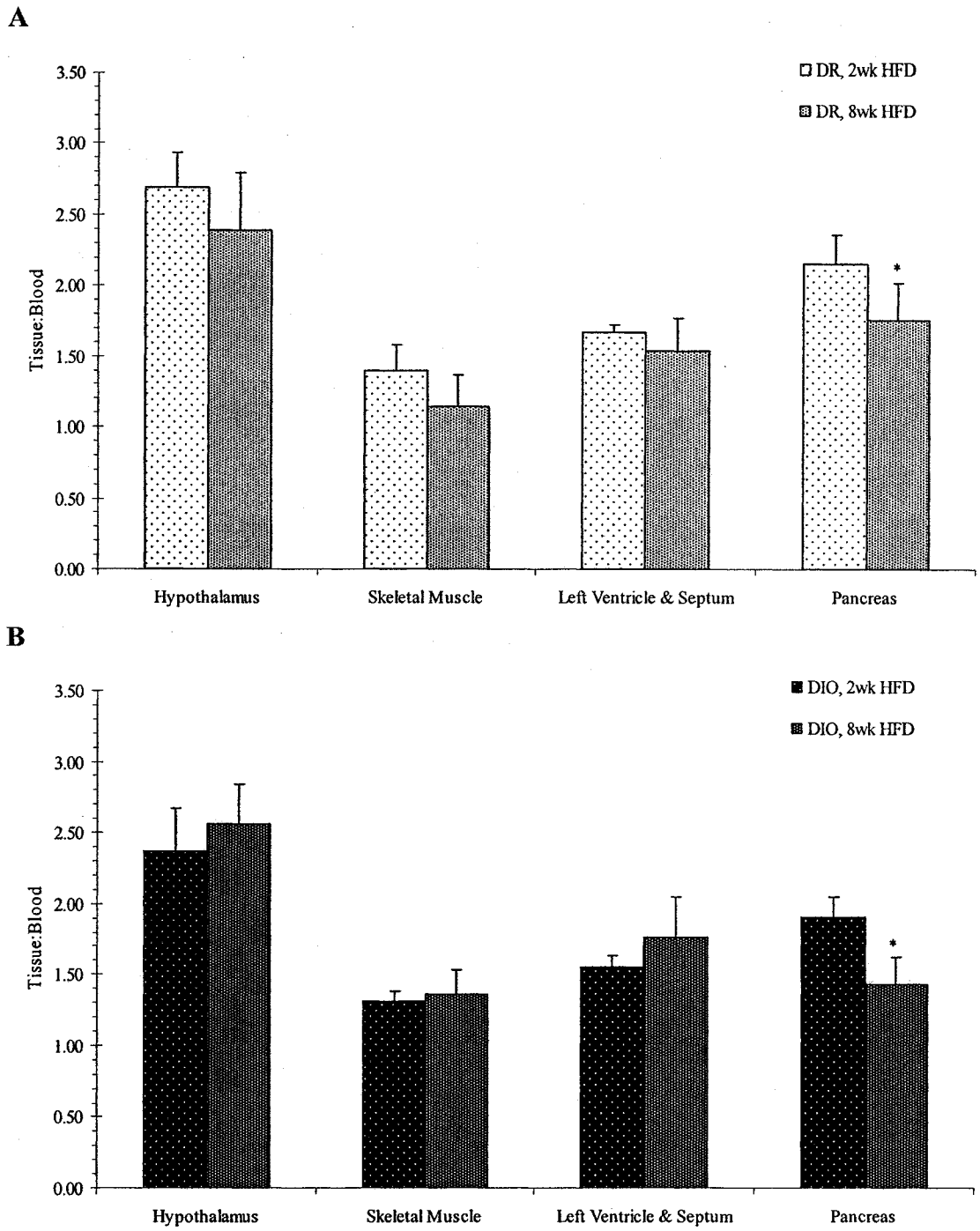

Fig. 18: Distribution of radioactivity in rat brain and periphery 45 min following (*R*)-[^{11}C]rolipram administration in 2- and 8-week HFD DR **(A)** and 2- and 8-week HFD DIO **(B)** rats. Data are mean tissue:blood ± SD (*$p<0.05$, student's t-test to 2-week HFD controls; n=5 in each group).

3.3.4 Effects of acute desipramine treatment on in vivo (R)-[^{11}C]rolipram binding

Increasing synaptic NA with DMI pretreatment had no effect on the distribution of (*R*)-[^{11}C]rolipram in 2-week HFD DR rat HYPO, SkM, or LVS (Fig. 19A). Nevertheless, pancreatic total and specific binding of (*R*)-[^{11}C]rolipram was significantly decreased (Tables VIII, IX) following DMI treatment in 2-week HFD DR rats. In contrast, acute DMI treatment to 2-week HFD DIO rats produced significantly augmented LVS total (*R*)-[^{11}C]rolipram binding (Table VIII) and specific binding (Table IX), while other tissue retentions remained unchanged (Fig. 19B).

DMI administration to 8-week HFD DR rats lead to significant amplification of total (*R*)-[^{11}C]rolipram binding in HYPO, SkM, and LVS (Fig. 20A, Table VIII). Additionally, 8-week HFD DR rat specific binding was increased following DMI in HYPO, SkM, and LVS (Table IX). Conversely, acute DMI treatment to 8-week HFD DR rats caused significant reduction in (*R*)-[^{11}C]rolipram total binding (Table VIII), and specific binding (Table IX) in pancreas (Fig 19A). Acute DMI treatment to 8-week HFD DIO rats had no effect on (*R*)-[^{11}C]rolipram binding to PDE4 (Fig. 20B).

3.4 Citrate- and streptozocin-treated rat studies

3.4.1 Physiological measurements

Both 8-week citrate- and STZ-treated citrate control and DM2 (bg<11) rats respectively, had significantly greater weight gain than 8-week STZ-treated DM2 rats over the eight week disease progression period (Fig. 21). Subsets of 2-week (Table X) and 8-week (Table XI) STZ-treated DM2 rats maintained normal blood glucose levels despite administration of the destructive β–cell alkylating agent STZ. Fasting blood

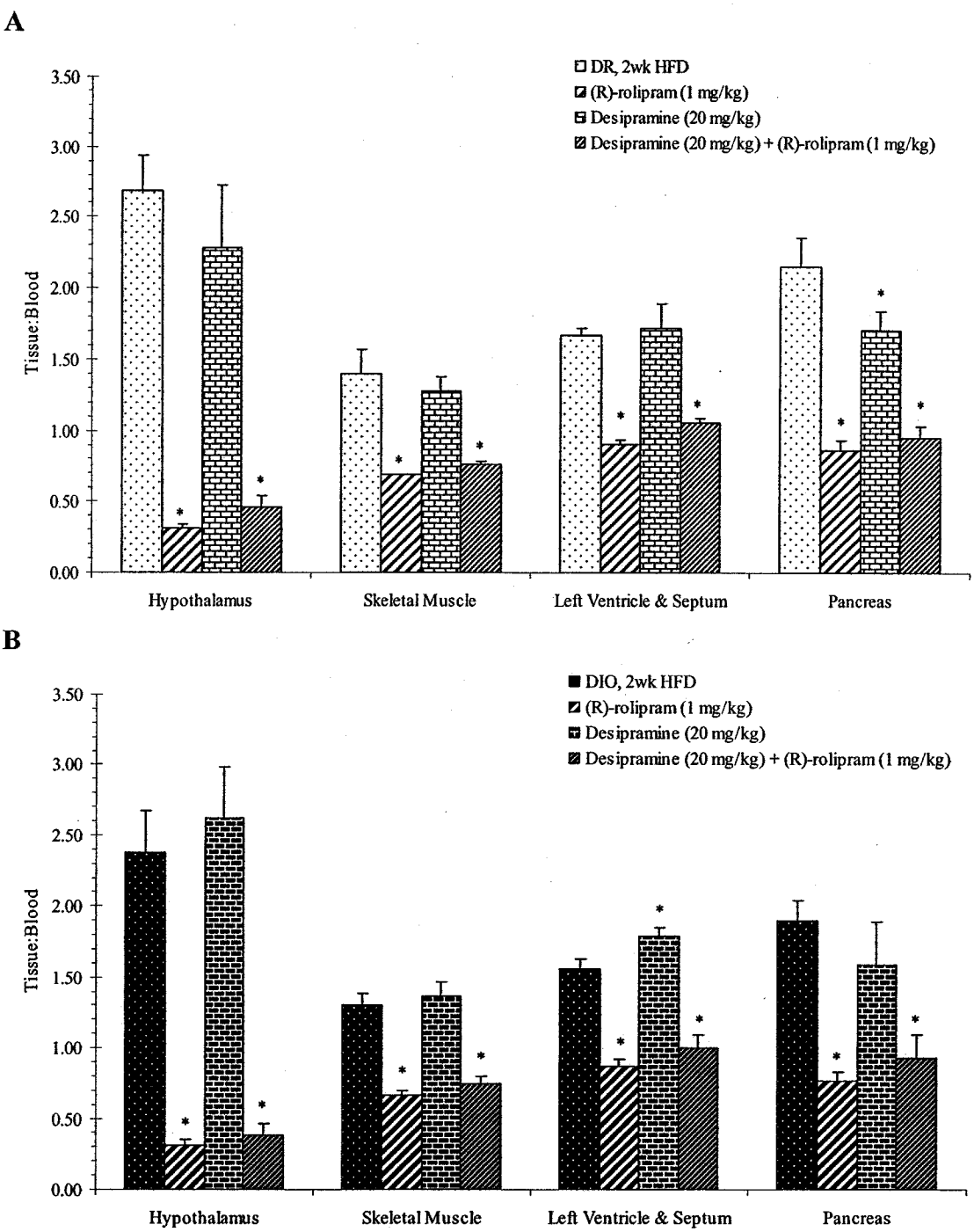

Fig. 19: (*R*)-[^{11}C]Rolipram distribution 45 min following administration in 2-week HFD DR **(A)** and DIO **(B)** rats treated with (*R*)-rolipram (1 mg/kg coinjection), desipramine (20 mg/kg i.p. 3 h prior to radioligand injection), or desipramine (20 mg/kg i.p. 3 h prior to radioligand injection) plus (*R*)-rolipram (1 mg/kg coinjection). Data are mean tissue:blood ± SD (*$p<0.05$, One-way ANOVA with Dunnett comparisons test to control 2-week HFD DR and DIO rats respectively; DR: n=5, DR (*R*)-rolipram: n=4, DR desipramine: n=5, DR desipramine + (*R*)-rolipram: n=4, DIO: n=5, DIO (*R*)-rolipram: n=4, DIO desipramine: n=5, DIO desipramine + (*R*)-rolipram: n=4).

Table VIII: Percent change[a] in (*R*)-[^{11}C]rolipram retention in 2- and 8-week HFD DR and DIO rats following acute desipramine treatment.

Treatment	Animal Model		(*R*)-[^{11}C]Rolipram Percent Change in Tissue			
			Hypothalamus	Skeletal Muscle	Left Ventricle & Septum	Pancreas
Acute Desipramine						
	2-week HFD	DR	-15	-8	3	-21
		DIO	10	4	15	-17
	8-week HFD	DR	24	24	25	-29
		DIO	1	-4	7	15

[a] Percent change in radiotracer retention (determined from tissue:blood values) between treated DR and DIO rats and banks of respective untreated controls. *n* values for treatments shown in figures.

Table IX: Percent changes in (*R*)-[^{11}C]rolipram PDE4 specific binding in 2- and 8-week HFD DR and DIO rats following acute desipramine treatment.

Treatment	Animal Model		Percent Change in (*R*)-[^{11}C]rolipram Specific Binding in Tissue			
			Hypothalamus	Skeletal Muscle	Left Ventricle & Septum	Pancreas
Acute Desipramine						
	2-week HFD	DR	-24	-27	-13	-41
		DIO	9	-4	16	-42
	8-week HFD	DR	17	43	41	-95
		DIO	-8	-23	-9	-23

Specific binding was calculated by subtracting the tissue:blood ratio in the presence of the (*R*)-rolipram blocking dose (1 mg/kg, i.v., coinjected with the radioligand) or non-specific binding (NSB), from the total binding (T) in the absence of (*R*)-rolipram in 2-and 8-week HFD DR and DIO rats. Percent change in specific binding was calculated as follows: $((T_{desipramine} - NSB_{desipramine})-(T_{control} - NSB_{control}))/(T_{control} - NSB_{control})*100$.

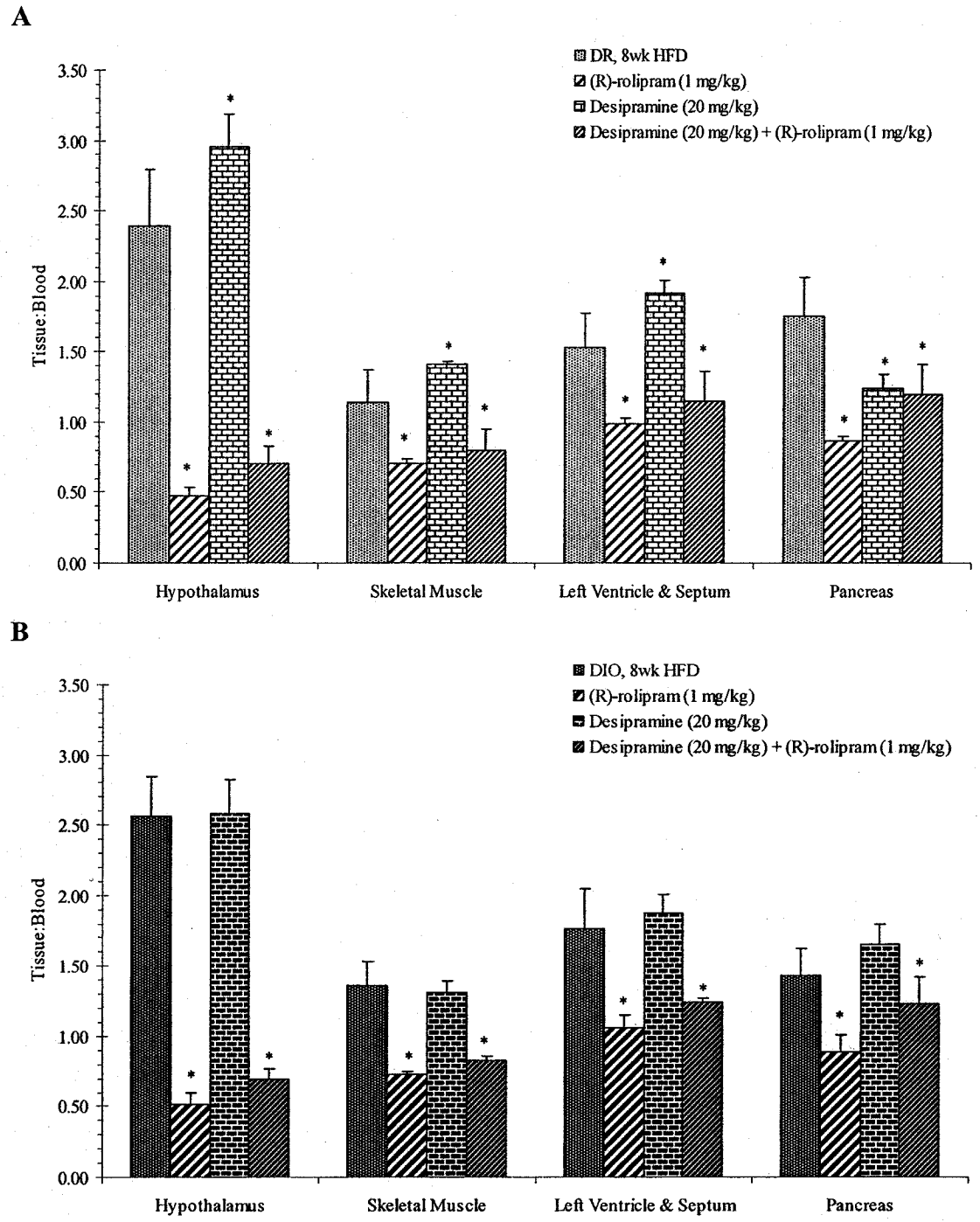

Fig. 20: (*R*)-[^{11}C]Rolipram distribution 45 min following administration in 8-week HFD DR **(A)** and DIO **(B)** rats treated with (*R*)-rolipram (1 mg/kg coinjection), desipramine (20 mg/kg i.p. 3 h prior to radioligand injection), or desipramine (20 mg/kg i.p. 3 h prior to radioligand injection) plus (*R*)-rolipram (1 mg/kg coinjection). Data are mean tissue:blood ± SD (*$p<0.05$, One-way ANOVA with Dunnett comparisons test to 8-week HFD fed control DR and DIO rats respectively; DR: n=5, DR (*R*)-rolipram: n=4, DR desipramine: n=4, DR desipramine + (*R*)-rolipram: n=4, DIO: n=5, DIO (*R*)-rolipram: n=4, DIO desipramine: n=4, DIO desipramine + (*R*)-rolipram: n=4).

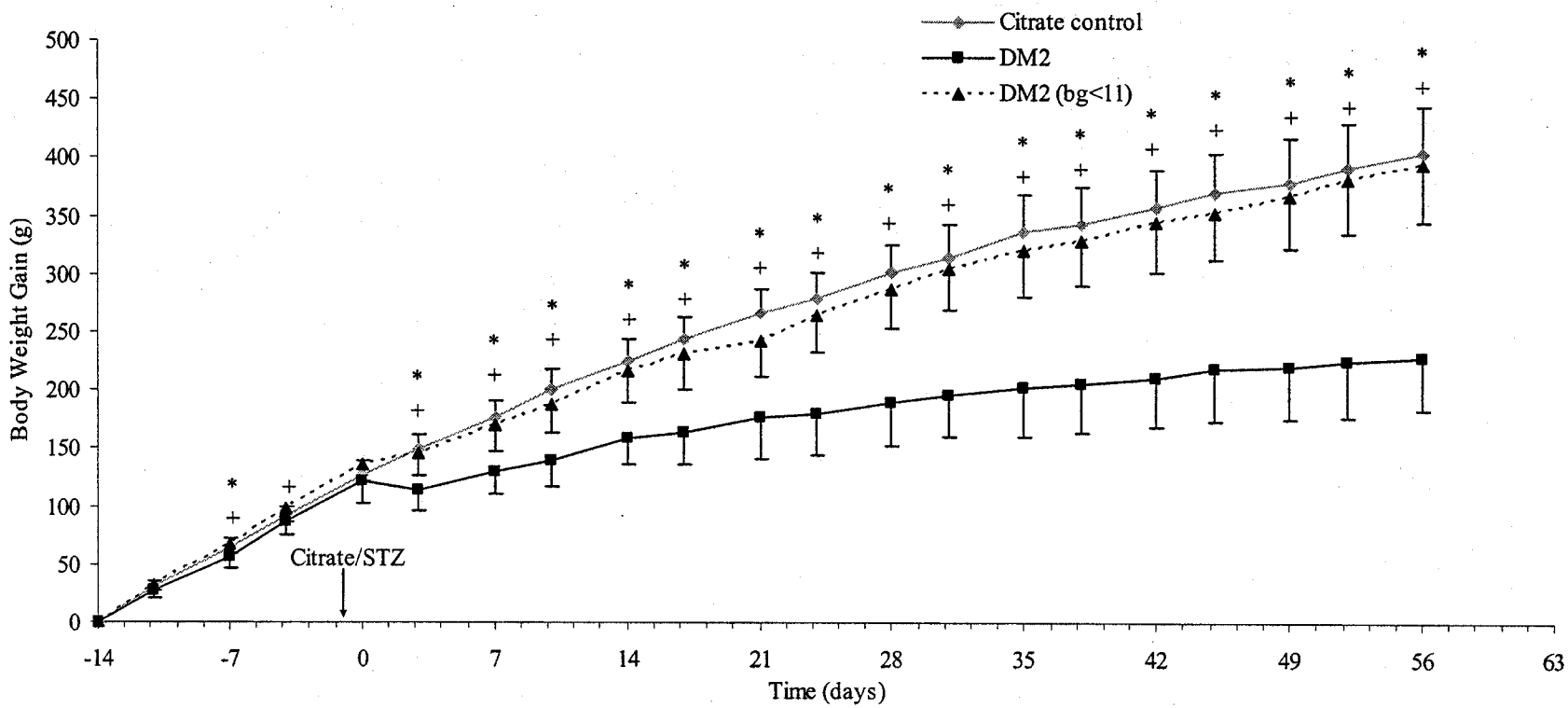

Fig. 21: Weight gain of 8-week citrate- or streptozocin (STZ)-treated citrate control, DM2, and DM2 (bg<11) rats. Data are mean weight gain ± SD (*p<0.05, One-way ANOVA with Dunnett comparisons test to 8-week STZ DM2 rats; Citrate control: n=11, DM2: n=8, DM2 (bg<11): n=8).

Table X: Two week citrate- and streptozocin-treated citrate control, DM2, and DM2 (bg<11) rat blood glucose measurements.

Animal Model	Rat #	W -2 Pre-HFD	D 0 Pre-Citrate/STZ	W 1	W 2_{fast} Biodistribution	W 2_{fast} Treatment
2-week citrate	1	7.0	6.0	5.9	3.6	-
Citrate controls	2	5.9	6.8	6.0	2.6	-
	3	5.6	6.4	6.4	3.9	-
	4	6.3	6.5	6.2	3.6	-
	5	6.3	7.0	6.7	3.9	-
	6	5.8	5.6	6.7	3.6	-
	7	6.2	6.7	6.2	3.4	-
	8	5.8	6.9	7.4	12.0	(*R*)-rolipram
	9	5.4	6.9	6.3	10.4	(*R*)-rolipram
	10	6.5	7.1	6.3	11.5	(*R*)-rolipram
	11	6.1	7.2	7.4	6.4	(*R*)-rolipram
	12	6.6	6.8	6.2	10.1	(*R*)-rolipram
	13	6.1	6.6	6.4	10.2	(*R*)-rolipram
	14	5.4	6.2	5.3	9.5	(*R*)-rolipram
2-week STZ	15	6.1	6.5	30.4	6.4	-
DM2	16	6.9	6.7	20.4	4.6	-
	17	5.9	5.9	28.9	5.9	-
	18	6.5	6.9	13.1	4.7	-
	19	5.6	5.4	15.8	3.0	-
	20	5.5	5.4	16.1	2.6	-
	21	9.1	6.1	26.9	23.2	(*R*)-rolipram
	22	6.2	6.2	22.4	19.0	(*R*)-rolipram
	23	6.3	6.1	12.0	12.0	(*R*)-rolipram
	24	6.2	6.0	28.9	14.0	(*R*)-rolipram
	25	6.2	4.9	24.9	32.8	DMI
	26	5.6	6.3	30.3	5.5	DMI
	27	6.5	6.0	26.5	3.3	DMI
	28	6.0	5.8	15.9	3.1	DMI
	29	6.0	5.6	15.3	3.7	DMI
	30	6.2	6.2	17.5	2.9	DMI
	31	7.4	5.3	12.1	9.4	DMI + (*R*)-rolipram
	32	6.4	6.0	15.9	9.9	DMI + (*R*)-rolipram
	33	6.3	6.3	12.7	10.2	DMI + (*R*)-rolipram
	34	5.6	6.3	16.2	11.9	DMI + (*R*)-rolipram
2-week STZ	35	6.7	7.0	9.7	4.3	-
DM2 (bg<11)	36	8.1	6.5	9.7	3.9	-
	37	6.3	6.7	8.9	9.9	DMI + (*R*)-rolipram

Blood glucose measures at time points -2-weeks (W), day (D) 0, 1 week following citrate- or streptozocin (STZ)-treatment, and fasting blood glucose on day of biodistribution experiment. Blood glucose not determined (nd) at early stages for some rats.

Table XI: Eight week citrate- and streptozocin-treated citrate control, DM2, and DM2 (bg<11) rat blood glucose measurements.

Animal Model	Rat #	W -2 Pre-HFD	D 0 Pre-Citrate/STZ	W 1	W 3	W 6	W 8	$W\ 8_{fast}$ Biodistribution	$W\ 8_{fast}$ Treatment
8-week citrate	1	nd	nd	nd	8.7	6.0	6.9	4.2	-
Citrate controls	2	nd	nd	nd	7.0	6.8	5.8	3.1	-
	3	nd	nd	nd	5.6	5.6	4.9	4.2	-
	4	nd	nd	nd	6.0	6.4	5.2	4.5	-
	5	nd	nd	nd	6.9	5.7	5.6	3.9	-
	6	nd	nd	nd	6.3	5.6	5.8	4.1	-
	7	6.1	7.0	6.1	6.3	6.1	5.8	3.8	-
	8	6.3	6.2	6.1	6.2	8.1	6.8	3.5	-
	9	5.6	6.4	6.4	6.1	5.8	6.0	4.1	-
	10	6.2	5.9	7.3	6.4	5.9	6.0	4.7	-
	11	6.4	6.6	6.3	5.9	5.8	5.6	3.8	-
	12	6.6	7.1	5.7	9.2	5.5	6.1	15.1	(*R*)-rolipram
	13	6.2	7.0	5.9	6.7	6.2	5.6	14.7	(*R*)-rolipram
	14	nd	nd	nd	6.2	6.8	6.2	14.2	(*R*)-rolipram
	15	6.5	6.2	7.5	7.0	6.6	5.9	12.3	(*R*)-rolipram
	16	nd	nd	nd	5.3	6.0	6.5	12.8	(*R*)-rolipram
	17	nd	nd	nd	4.9	5.1	5.8	14.3	(*R*)-rolipram
	18	6.8	7.8	7.0	6.1	6.5	7.0	12.3	(*R*)-rolipram
	19	6.2	7.4	6.1	5.9	6.7	6.2	14.7	(*R*)-rolipram
	20	7.2	6.2	6.2	6.6	6.4	6.1	12.7	(*R*)-rolipram
	21	6.6	6.1	6.6	5.8	6.1	6.6	12.7	(*R*)-rolipram
8-week STZ	22	nd	nd	nd	24.2	28.4	29.0	13.1	-
DM2	23	nd	nd	nd	24.4	27.2	29.1	23.8	-
	24	nd	nd	nd	22.5	27.9	33.4*	24.9	-
	25	nd	nd	nd	16.7	17.4	18.3	6.1	-
	26	7.4	6.3	29.0	29.3	33.2	25.9	22.0	-
	27	6.3	6.7	17.2	26.6	23.0	25.6	8.9	-
	28	6.0	6.2	19.5	32.5	23.8	26.8	18.9	-
	29	5.8	6.2	26.8	33.4*	29.5	24.3	29.5	(*R*)-rolipram
	30	6.4	5.4	23.3	27.5	28.9	23.6	19.0	(*R*)-rolipram
	31	7.2	5.9	23.1	31.0	20.5	26.7	24.3	(*R*)-rolipram
	32	5.3	6.2	19.3	22.8	20.8	23.3	20.8	(*R*)-rolipram
8-week STZ	33	nd	nd	nd	6.4	5.9	8.9	5.7	-
DM2 (bg<11)	34	6.5	6.3	9.8	7.5	6.1	6.5	4.0	-
	35	6.2	6.5	5.7	6.4	6.8	6.8	3.7	-
	36	6.2	7.1	7.2	8.7	9.2	6.0	4.7	-
	37	6.8	6.8	6.4	5.9	6.8	7.1	4.2	-
	38	6.1	6.6	6.7	12.0	5.9	5.6	4.4	-
	39	6.7	6.2	11.7	5.9	6.4	5.7	4.4	-
	40	6.5	6.3	9.2	9.3	7.3	7.7	6.3	-
	41	6.4	5.8	19.9	8.3	7.8	6.4	20.1	(*R*)-rolipram
	42	5.5	6.1	6.5	7.0	6.4	6.1	20.8	(*R*)-rolipram
	43	5.8	6.0	6.9	6.1	5.5	6.2	11.5	(*R*)-rolipram
	44	nd	nd	nd	6.2	5.4	7.1	15.5	(*R*)-rolipram
	45	nd	nd	nd	5.9	5.9	5.6	14.0	(*R*)-rolipram
	46	nd	nd	nd	5.8	5.6	6.7	15.3	(*R*)-rolipram

Glucose measures at time points -2-weeks (W), day (D) 0, 1 week following citrate- or streptozocin (STZ)-treatment at 3-, 6-, 8-weeks, and fasting glucose on day of biodistribution experiment. *Blood glucose exceeded glucometer range (>33.3 mmol/L). Blood glucose not determined (nd) at early stages for some rats.

glucose levels were also observed to be increased 45 min after (*R*)-rolipram administration in both 2- and 8-week treated citrate control and DM2 rats (Tables X, XI). Fasting plasma insulin levels of 2-week STZ DM2 rats were normal compared to 2-week citrate control rats (Table XII). However, prolonged consumption of HFD after citrate administration lead to significantly increased plasma insulin levels in 8-week citrate controls compared to 2-week citrate control rats. Additionally, 8-week STZ DM2 (bg<11) rats also possessed similar plasma insulin levels as 8-week citrate controls. However, 8-week STZ DM2 rat insulin levels were significantly reduced compared to 8-week citrate controls, indicating a hypoinsulinemic state.

3.4.2 Indirect calorimetry

Twenty-four hour indirect calorimetry measurements of 2-week citrate control and STZ-treated DM2 rats revealed no significant differences in RER from the light or dark phases (Table XIII). However, 8-week STZ DM2 rats in both the light and dark phases possessed significantly lower RERs compared to both 8-week citrate controls and 2-week STZ DM2 rats. There were no significant differences in $\dot{V}_{O2}$/kgBW or $\dot{V}_{O2}$ between citrate control or DM2 rat models.

3.4.3 (R)-[^{11}C]Rolipram baseline analysis

The process of 2-week STZ induction of DM2 had no effect on baseline tissue retention of (*R*)-[^{11}C]rolipram 45 min postinjection compared to 2-week citrate control rats (Fig. 22A). However, the effect of 8-week STZ induction of DM2 lead to significantly diminished tissue retention of (*R*)-[^{11}C]rolipram 45 min postinjection in 8-week STZ DM2 rats compared to 8-week citrate controls in HYPO and LVS (Fig. 22B). Radioligand retention in 8-week STZ DM2 rats was decreased 17 and 8% HYPO and

Table XII: Fasted plasma insulin measurements of citrate- and streptozocin-treated citrate control, DM2, and DM2 (bg<11) rats.

Animal Model		$Insulin_{fasted}$ (ng/mL)	*n*
2-week citrate	Citrate control	0.57 ± 0.31	7
2-week STZ	DM2	0.73 ± 0.31	6
8-week citrate	Citrate control	1.43 ± 0.91*	11
8-week STZ	DM2	0.32 ± 0.15+	7
8-week STZ	DM2 (bg<11)	1.29 ± 0.87	7

Insulin measured using radioimmunoassay kit from plasma obtained from citrate control and DM2 rats. Data are mean values ± SD (*$p<0.05$, One-way ANOVA with Dunnett comparisons test to 2-week citrate controls; +$p<0.05$, One-way ANOVA with Dunnett comparisons test to 8-week citrate controls; *n* values described above).

Table XIII: 24 hour indirect calorimetry measurements in 2- and 8-week citrate- and streptozocin-treated citrate control and DM2 rats.

Animal Model		RER[a]		$\dot{V}_{O2}$/kgBW[b] (mL/min/kg)		$\dot{V}_{O2}$[c] (mL/min)	
		Light Phase	Dark Phase	Light Phase	Dark Phase	Light Phase	Dark Phase
2-week citrate	Citrate Control	0.89 ± 0.06	0.93 ± 0.06	25.0 ± 7.1	29.2 ± 7.3	9.3 ± 2.5	10.8 ± 2.5
2-week STZ	DM2	0.87 ± 0.06[¥]	0.93 ± 0.06[¥]	22.0 ± 4.4	25.9 ± 4.6	7.8 ± 1.7	9.2 ± 1.8
8-week citrate	Citrate Control	0.88 ± 0.05	0.92 ± 0.04	17.5 ± 3.5	20.9 ± 3.9	10.3 ± 2.2	12.2 ± 2.4
8-week STZ	DM2	0.73 ± 0.03[*]	0.74 ± 0.03[*]	22.7 ± 5.4	25.5 ± 4.8	8.0 ± 2.1	8.9 ± 1.9

[a] Respiratory exchange ratio (RER),[b] body weight corrected oxygen consumption ($\dot{V}_{O2}$/kgBW), and [c] whole body oxygen consumption ($\dot{V}_{O2}$) of 2- and 8-week citrate- and streptozocin (STZ)-treated citrate control and DM2 rats. Data are mean ± SD (*$p<0.05$, repeated measures GLM comparing DM2 to age- and light-matched citrate controls; [§]$p<0.05$, repeated measures GLM comparing light to dark phase age- and model-matched controls; [¥]$p<0.05$, repeated measures GLM comparing 2-week to 8-week light- and model-matched controls; n=3 in each group).

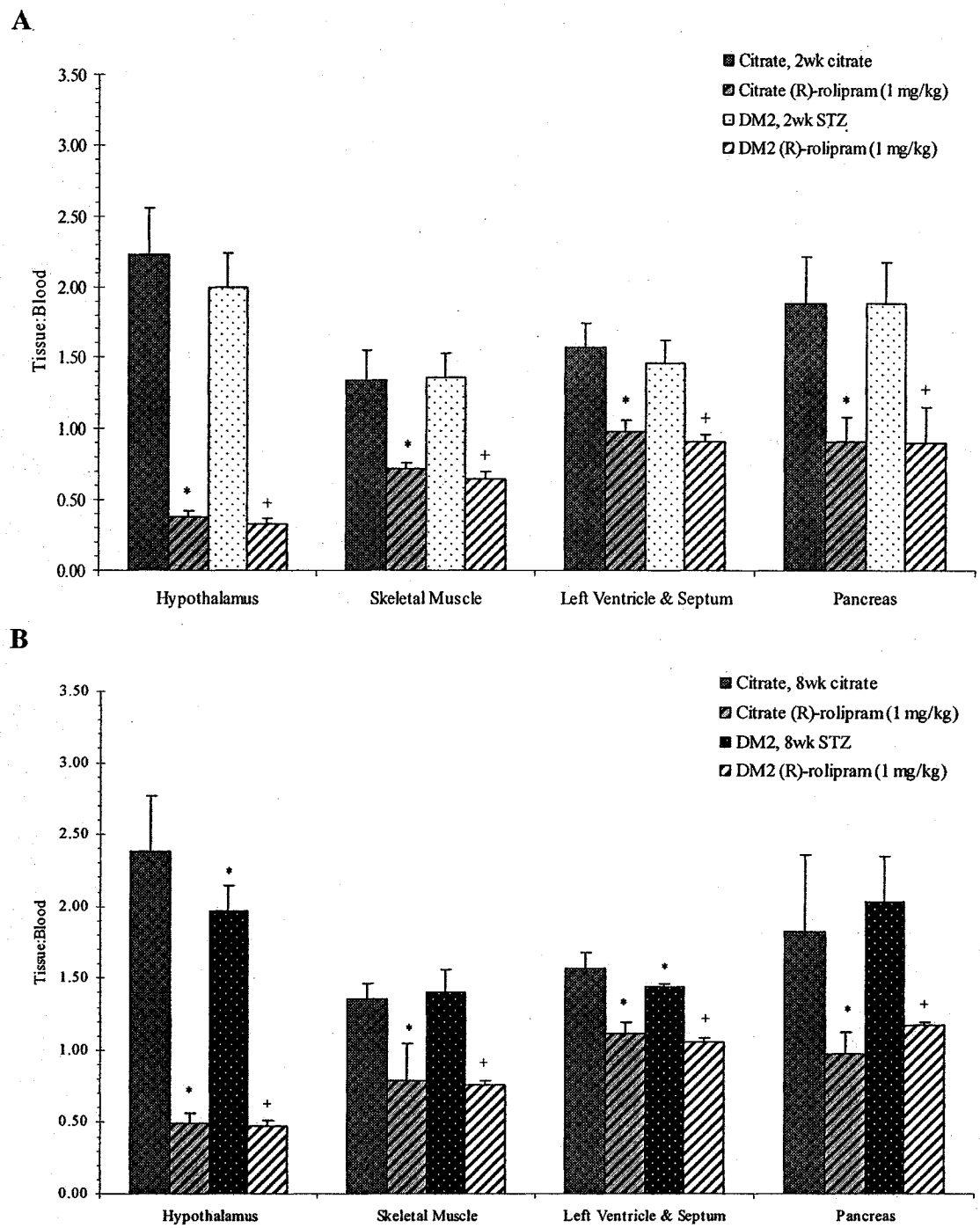

Fig. 22: (*R*)-[^{11}C]Rolipram distribution 45 min following administration in 2-week **(A)** and 8-week **(B)** citrate- or steptozocin (STZ)-treated citrate control and DM2 control rats and rats administered (*R*)-rolipram (1 mg/kg coinjection). Data are mean tissue:blood ± SD (*$p<0.05$, One-way ANOVA with Dunnett comparisons test to age-matched citrate control rats; $^{+}p<0.05$, One-way ANOVA with Dunnett comparisons test to age-matched DM2 rats; Citrate 2wk citrate: n=7, Citrate 2wk citrate + (*R*)-rolipram: n=7, DM2 2wk STZ: n=6, DM2 2wk STZ + (*R*)-rolipram: n=4, Citrate 8wk citrate: n=11, Citrate 8wk citrate + (*R*)-rolipram: n=10, DM2 8wk STZ: n=7, DM2 8wk STZ + (*R*)-rolipram: n=4).

LVS (Table XIV). Additionally, 8-week STZ-treated DM2 (bg<11) rat (*R*)-[^{11}C]rolipram binding was not significantly altered compared to 8-week citrate controls but were however significantly increased in LVS compared to 8-week STZ DM2 rats (Fig. 23).

3.4.4 Effects of acute desipramine treatment on in vivo (R)-[^{11}C]rolipram binding in 2-week citrate and streptozocin models

Following acute pretreatment of DMI, total (*R*)-[^{11}C]rolipram binding to PDE4 in 2-week STZ DM2 rats was significantly increased compared to untreated 2-week STZ DM2 rats in HYPO, SkM, and LVS (Fig. 24, Table XIV). Additionally, (*R*)-[^{11}C]rolipram specific binding to PDE4 was increased in HYPO, SkM, and pancreas (Table XV). DMI had no significant acute effect on pancreatic PDE4 levels.

Table XIV: Percent changes[a] in (*R*)-[^{11}C]rolipram retention in 2- and 8-week streptozocin-treated DM2 rat tissues at baseline and following desipramine treatment.

Treatment	Animal Model	(*R*)-[^{11}C]Rolipram Percent Change in Tissue			
		Hypothalamus	Skeletal Muscle	Left Ventricle & Septum	Pancreas
Streptozotocin					
2-week STZ	DM2[b]	-10	1	-7	0
8-week STZ	DM2[c]	-17	4	-8	12
Acute Desipramine					
2-week STZ	DM2[d]	24	23	22	4

[a] Percent change in average radiotracer retention (determined from tissue:blood values) between the treated rats and bank age-matched controls. Data compared to [b] 2-week and [c] 8-week citrate-treated citrate controls. [d] Data compared to desipramine untreated 2-week STZ DM2 controls. *n* values for treatments shown in figures.

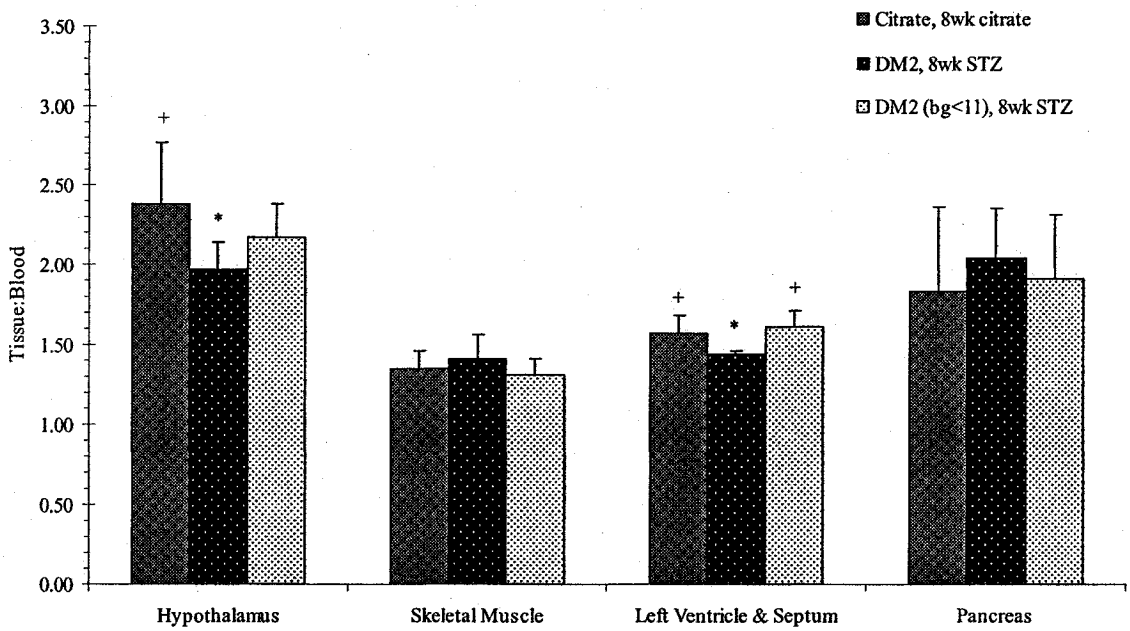

Fig. 23: Distribution of radioactivity in rat brain and periphery 45 min following (*R*)-[^{11}C]rolipram administration in 8-week citrate- and streptozocin (STZ)-treated citrate control, DM2 and DM2 (bg<11) rats. Data are mean tissue:blood ± SD (*$p<0.05$, One-way ANOVA with Dunnett comparisons test to 8-week citrate control rats; $^{+}p<0.05$, One-way ANOVA with Dunnett comparisons test to 8-week STZ DM2 rats; Citrate: n=11, DM2: n=7, DM2 (bg<11): n=8).

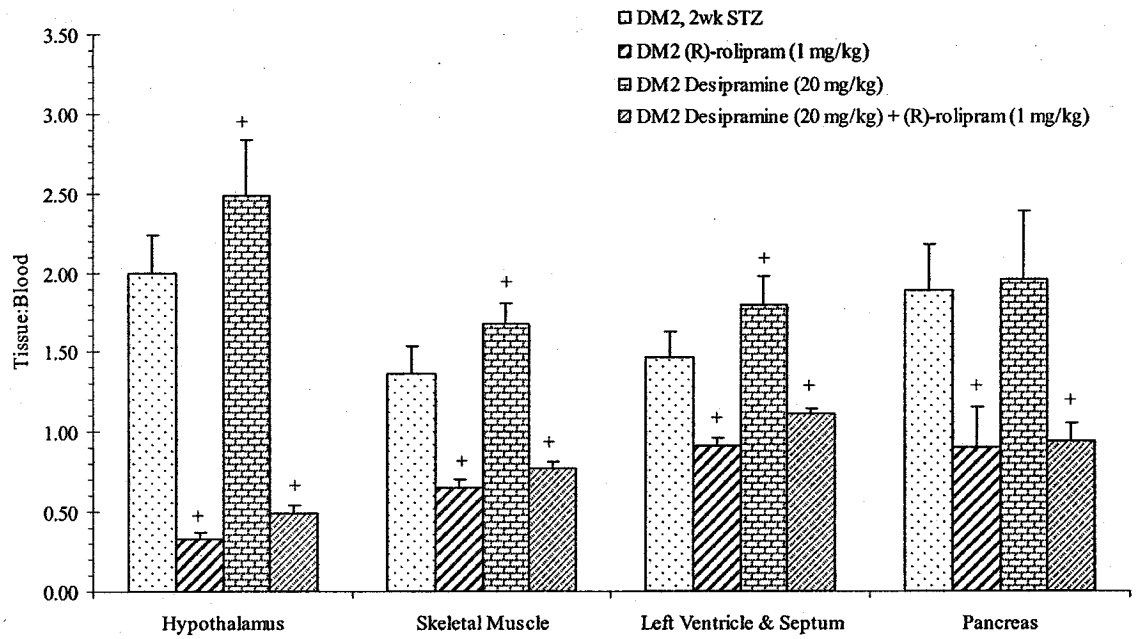

Fig. 24: Distribution of radioactivity in rat brain and periphery 45 min following (*R*)-[^{11}C]rolipram administration in 2-week steptozocin (STZ)-treated DM2 rats administered (*R*)-rolipram (1 mg/kg coinjection), desipramine (20 mg/kg i.p. 3 h prior to radioligand injection), or desipramine (20 mg/kg i.p. 3 h prior to radioligand injection) plus (*R*)-rolipram (1 mg/kg coinjection). Data are mean tissue:blood ± SD ($^{+}p<0.05$, One-way ANOVA with Dunnett comparisons test to 2-week STZ DM2 rats; DM2: n=6, DM2 (*R*)-rolipram: n=4, DM2 desipramine: n=6, DM2 desipramine + (*R*)-rolipram: n=4).

Table XV: Percent changes in (*R*)-[^{11}C]rolipram PDE4 specific binding following acute desipramine treatment in 2-week streptozocin-treated DM2 rats.

Treatment	Animal Model	Percent Change in (*R*)-[^{11}C]Rolipram Specific Binding in Tissue			
		Hypothalamus	Skeletal Muscle	Left Ventricle & Septum	Pancreas
Acute Desipramine					
2-week STZ	DM2	20	28	24	3

Specific binding was calculated by subtracting the tissue:blood ratio in the presence of the (*R*)-rolipram blocking dose (1 mg/kg, i.v., coinjected with the radioligand) or non-specific binding (NSB), from the total binding (T) in the absence of (*R*)-rolipram in 2-week streptozocin (STZ)-treated DM2 rats. Percent change in specific binding was calculated as follows: $((T_{desipramine} - NSB_{desipramine})-(T_{control} - NSB_{control}))/(T_{control} - NSB_{control})*100$.

4.0: DISCUSSION

PDE4 is an essential component of cAMP-mediated transduction that performs regulatory cell signaling functions by controlling cAMP levels formed following stimulation of GPCRs in different neurotransmitter systems of the body (Conti et al., 2003; Lourenco et al., 2006; Verde et al., 1999). The obese and diabetic disease states are known to have dysfunctional SNS signaling (Esler et al., 2001; Fisher et al., 2005; Masuo et al., 1997; Reynisdottir et al., 1994; Tentolouris et al., 2003). Recently, we have developed (*R*)-[^{11}C]rolipram as a selective PDE4 radiotracer capable of imaging cAMP-mediated signaling in the brain and periphery *in vivo* (DaSilva et al., 2002; DaSilva et al., 2001; Lourenco et al., 2001; Lourenco et al., 2006). The work described in this thesis is concerned with extended evaluation of this radiotracer in obese and diabetic rat models. The ultimate purpose of this project was to detect *in vivo* cAMP-mediated dysfunction at the PDE4 level in central and peripheral tissues of obese and diabetic animal models using (*R*)-[^{11}C]rolipram. Attaining this function required the achievement of two major objectives. The first objective was to determine the presence of PDE4 specific binding using (*R*)-[^{11}C]rolipram in tissues associated with obesity and diabetes. The second objective was to utilize animal models of obesity and diabetes at different stages of disease progression to obtain (*R*)-[^{11}C]rolipram *in vivo* binding data and determine altered intracellular PDE4 binding in cAMP-mediated signaling.

4.1 Tissue-to-blood ratios

Tissue-to-blood ratios were utilized to compensate for alterations in carrier delivery of the radiotracer caused by differences in rat body weight, tissue composition, pharmacological haemodynamics, and the presence of metabolites in the blood. Increased haemodynamic radioactivity following co-administration of (*R*)-rolipram may be explained by the observed increased presence of radiolabeled metabolites compared to unchanged (*R*)-[^{11}C]rolipram in rat plasma (Kenk et al., 2006a). Expressing data as tissue-to-blood ratios provides an attenuation correction factor in each animal, and reduces the variability of radioligand binding due to pharmacological treatments and tracer metabolism in peripheral tissues. However, it also introduces an error variable into the brain data. Peripheral tissue corrections for blood metabolites generate errors in total binding data present in the brain, which lack radiolabeled metabolites of rolipram (Lourenco et al., 1999b). Nevertheless, the amount of error introduced into the calculated brain data may be balanced by the relatively high amount of expressed PDE4 and high (*R*)-[^{11}C]rolipram specific binding present in the brain tissue compared to blood. Several groups utilize tissue-to-blood ratios as a means of improving signal attenuation; for instance, β-AR and nicotinic receptor binding studies use tissue-to-blood ratios for [^{3}H]CGP 12177 and [^{18}F]F-A-85380, respectively (Law, 1993; Picard et al., 2006). Although it is practical to express data as the commonly used %ID/g (Lourenco et al., 1999a) or %ID/g multiplied by body weight (Lourenco et al., 2006) when studying the brain alone, obtaining meaningful comparisons of (*R*)-[^{11}C]rolipram retention in peripheral tissues and brain may require application of the tissue-to-blood ratios. Therefore, results in this project were expressed as tissue-to-blood ratios. The expression

of results in this manner may best compensate for the changes in (*R*)-[^{11}C]rolipram binding owning to the presence of metabolites, body size, body composition, and systemic pharmacological effects (Law, 1993).

4.2 Specific binding and metabolism in NORM rats

4.2.1 Biodistribution analysis of (R)-[^{11}C]rolipram PDE4 specific binding

Previous studies have reported that the binding of (*R*)-rolipram to HARBS (IC_{50} ~ 2-5 nM) in the brain (Borisy et al., 1993; Zhao et al., 2003) correlates with central behavioral effects (Duplantier et al., 1996; Egawa et al., 1997; Schmiechen et al., 1990). In *in vitro* assays using PDE4 inhibitor [^{3}H]piclamilast and central or peripheral tissue homogenates, Zhao *et al.* (2003) recently reported that HARBS binding was present in abundance in central but not peripheral tissue preparations. However, in this project, the observed *in vivo* uptake of (*R*)-[^{11}C]rolipram in brain, SkM, heart, pancreas and lung highly concured with our previously published findings (DaSilva et al., 2002; Lourenco et al., 2001; Lourenco et al., 2006). Furthermore, (*R*)-[^{11}C]rolipram binding was blocked in the brain, SkM, heart, pancreatic, and lung tissues by saturating doses of (*R*)-rolipram and Ro20-1724 indicating the presence of peripheral specific binding to HARBS *in vivo*. A factor that may produce these *in vitro* and *in vivo* discrepancies of HARBS in the periphery may be the involvement of ions such as Mg^{2+} at the catalytic site of PDE4. It is known that Mg^{2+} can alter high affinity binding to the active form of PDE4 (Laliberte et al., 2000; Laliberte et al., 2002), and may represent a possible mechanism for a HARBS to LARBS shift in binding. While Mg^{2+} concentrations *in vivo* are maintained at homeostatic physiological levels, *in vitro* studies utilize non-physiological concentrations

of Mg^{2+} in tissue cultures (Zhang et al., 2006; Zhao et al., 2003), which may alter the Mg^{2+}-induced PDE4 conformation of the active holoenzyme complex. It is possible that the *in vivo* conditions occurring in the intact animals of our studies preserve the HARBS in the periphery and account for the discrepancy observed between our *in vivo* and *in vitro* results (Kenk et al., 2006b).

Investigations examining involvement of PDE activity in lipolysis and thermogenesis point to the participation of PDE2, PDE3, and PDE4 in WAT and BAT *in vitro* (Coudray et al., 1999; Nagaoka et al., 1998). However, PDE4 activity in these tissues are reportedly low (~1-9 pmol/min/mg), and PDE3 is observed to be the major contributor to cAMP hydrolysis with PDE3 to PDE4 ratios of 5:1 and 4:1 in WAT and BAT respectively (Nagaoka et al., 1998). The inability to detect *in vivo* PDE4 specific binding in adipose tissues with (*R*)-[^{11}C]rolipram may be attributed to the low PDE4 density in adipose tissues, and specific activity of the tracer that are too low to be able to study these sites without saturation.

4.2.2 Metabolite and specific binding of (R)- and (S)-[^{11}C]rolipram in peripheral tissues using high performance liquid chromatography

Conformational HPLC analyses on the identity of labeled ligand in tissues of interest further confirm the presence of (*R*)-[^{11}C]rolipram specific binding to PDE4 in SkM and pancreas, as well as non-specific binding in BAT. Rolipram biotransformation is known to degrade to at least eight metabolites in rat, rhesus monkey, and human, and these metabolites are then primarily excreted in the urine (Krause and Kühne, 1988; Krause and Kühne, 1993). The proportion of PDE4 specific binding obtained from biodistribution analysis in the brain was greater than in peripheral regions which may be

attributed to the presence of peripheral radiolabeled metabolites (Lourenco et al., 1999b). As previously shown in our laboratory, carbon-11 labeled metabolites of (*R*)-[^{11}C]rolipram do not cross the blood brain barrier of rats and are present in plasma (DaSilva et al., 2001; Lourenco et al., 1999b). The metabolism of (*R*)-[^{11}C]rolipram in peripheral tissues (Kenk et al., 2006a) indicates that approximately 50% of the radioligand signal originates from unchanged (*R*)-[^{11}C]rolipram while the remaining activity derives from hydrophilic metabolites in peripheral tissues at 45 min postinjection. Importantly, this finding reveals that the reduced total specific binding in SkM and pancreas compared to the brain is due to the presence of both unchanged (*R*)-[^{11}C]rolipram and radiolabeled metabolites. The lack of effect on the proportion of labeled metabolites present in SkM and pancreas following co-injection with a saturating dose of (*R*)-rolipram indicates that the labeled metabolites do not bind specifically to PDE4. This can be explained by the metabolites high hydrophilicity rendering them unlikely to cross the cell membrane, and structural changes that might affect binding to PDE4 (Kenk et al., 2006a).

4.3 NORM rat studies

Exploratory experiments were performed on NORM rats using different diets and drugs expected to alter cAMP-mediated signaling directly or indirectly in order to assess NORM (*R*)-[^{11}C]rolipram binding conditions that were to be used on obese and diabetic animal models. Different acute and chronic treatments were executed using previously described doses and time periods in accordance with published literature and laboratory findings.

4.3.1 Physiological measurements

Similar to a report of NORM rats fed HFD for 5 weeks with no differences in body weight gain compared to rats on a control diet (Archer et al., 2003), NORM rats fed LFD or HFD did not differ in body weight, caloric consumption, or fasted blood glucose within feeding periods. Studies of HFD induction obesity have demonstrated that following consumption of HFD for 4-6 months NORM rats become obese and insulin resistant (Brown et al., 2003; Corbett et al., 1986). Our NORM rat models on LFD or HFD had no differences in body weight or blood glucose perhaps since they were exposed to shorter periods of dietary influence.

4.3.2 (R)-[^{11}C]Rolipram baseline analysis

The regional uptake of (*R*)-[^{11}C]rolipram did not differ between LFD or HFD fed NORM rats following 2- or 8-week treatment periods. These findings are likely associated with the physiological measurement results as no significant differences in body weight, caloric consumption, or fasting blood glucose levels were found between LFD or HFD fed NORM rats. Increased dietary fat content was expected to alter PDE4 binding of (*R*)-[^{11}C]rolipram due to dietary mediated alterations in sympathetic signaling. Reports of overfeeding NORM rats with high-caloric diet with substantial fat content was found to increase BAT sympathetic activity (Young et al., 1982). Additionally, consumption of diet composed of saturated fats cause decreased β-AR binding while addition of polyunsaturated fats have shown the opposite effects (Matsuo and Suzuki, 1997; Nicolas et al., 1991). Similar binding of (*R*)-[^{11}C]rolipram in brain and periphery of HFD fed NORM, LFD fed NORM, and previous findings in normal chow fed NORM rats (Lourenco et al., 2001; Lourenco et al., 2006) suggests that the dietary fat content

does not alter NORM rat PDE4 (*R*)-[^{11}C]rolipram binding following 2- or 8-week feeding periods. These findings may be attributed to the relatively short sustained feeding periods and lack of observed dietary effects on body weight, caloric consumption or blood glucose.

Rat age or time on diet may have contributed to significant declines of (*R*)-[^{11}C]rolipram in the HYPO and pancreas in 8-week NORM rats compared to 2-week diet NORM rats. Previous studies suggest that sympathetic activation is reduced with age in humans (Hering et al., 2006; Leenen et al., 2006). In a group of young and aged hypertensive patients, plasma NA increases following dihydropyridine Ca^{2+}-blocker treatment were diminished in aged subjects (Leenen et al., 2006). It is therefore plausible that alteration in PDE4 levels in HYPO and pancreatic tissues is mediated by age dependent mechanisms in NORM rats.

Rats were required to be fasted in order to obtain reliable blood glucose and plasma insulin levels. The (*R*)-[^{11}C]rolipram increase present in the HYPO of 2-week diet unfasted rats may have been caused by excitatory SNS signaling. It is generally accepted that fasting decreases, and feeding increases SNS activity and NA release (Landsberg, 2006). Forearm SkM and adipose NA release were previously reported to be suppressed in the fasting state and increased postprandially (Patel et al., 1999; Young and Landsberg, 1977). Additionally, the HYPO is credited as a primary regulator body weight by increasing SNS signaling thermogenic tissues (Cerri and Morrison, 2005; Taniguchi et al., 2006). In contrast, other groups found that HYPO-lesioned obese rats had augmented NA response to fasting and were thought to increase SNS activation by redundant compensatory mechanisms (Balkan et al., 1992). Taken together, the ages and the fasting

state of NORM rats partly explains alterations in (*R*)-[^{11}C]rolipram binding in HYPO and pancreas and should be taken into consideration when interpreting PDE4 binding data, while dietary fat content has demonstrated no effect on PDE4 levels following 2- and 8-week feeding periods. All studies were performed with fasted rats to sustain similar (*R*)-[^{11}C]rolipram binding between experiments.

4.3.3 Effects of acute treatments on in vivo (R)-[^{11}C]rolipram binding

4.3.3.1 Acute desipramine

DMI was previously shown to increase synaptic NA levels and stimulate β-ARs, thus increasing PDE4 regulation (Esler et al., 1990; Johnson et al., 1980; Lourenco et al., 2006). The acute treatment of DMI to 2-week diet NORM rats demonstrated significant increases in (*R*)-[^{11}C]rolipram binding in HYPO, SkM, and LVS. As expected and previously demonstrated in our laboratory (Lourenco et al., 2006), acute stimulation yielded an increase of 19-21% in radioligand uptake, and a 16-26% elevation of (*R*)-[^{11}C]rolipram specific binding to PDE4 in affected PDE4 rich regions of HYPO, SkM, and LVS.

In vitro studies have shown that PDE3, 4, and 7 (Hetman et al., 2000; Parker et al., 1995) are expressed in the pancreas, however the specific function of pancreatic PDE4 remains unclear. Acute DMI treatment had no effect on pancreatic radioligand binding to PDE4 possibly suggesting some sort of compensatory mechanism in this PDE4 rich organ. Studies have identified β-ARs in pancreatic ducts (Novak, 1998) and pancreatic α-cells (Vieira et al., 2004). Adrenergic control of pancreatic amylase secretion is considered to be duel, with inhibitory actions via α_1-AR or stimulatory via β-AR (Varga et al., 1990). In the pancreas, PDE3 is considered to be a major regulator of glucose-

induced insulin secretion. Selective PDE3 inhibitors Org 9935, siguazodan, and ICI 118233 were found to augment glucose-induced secretion from rat and human islets, whereas selective inhibitors of PDE1, PDE4, and PDE5 did not (Pyne and Furman, 2003; Shafiee-Nick et al., 1995). Conversely, observations from beta-cell lines discovered that the glucose-induced insulin secretion was augmented following rolipram inhibition (Ahmad et al., 2000; Yan et al., 1995). The present results suggest that (*R*)-[^{11}C]rolipram detected an increase in PDE4 density elicited by acute DMI injection in the brain, SkM, and heart, but not the pancreas which may have compensatory mechanisms regulating PDE4 levels or be modulated by a non-NA cAMP-mediated stimulus such as glucose or insulin (Ahmad et al., 2000; Yan et al., 1995). For the above mentioned attributes, DMI was chosen to augment cAMP-mediated signaling to realize post-synaptic functionality in obese and diabetic animal models.

4.3.3.2 CGP 12177 blockade of desipramine

CGP 12177 is a non-selective β-AR antagonist leading, in theory, to inhibition of NA stimulated cAMP production (Baker, 2005; Joseph et al., 2004; Mallem et al., 2005). CGP 12177 has been shown to block *in vivo* β-ARs in peripheral tissues (Ueki et al., 1993; van Waarde et al., 1995; van Waarde et al., 2004) and brain regions at high doses (10 mg/kg) (Hjeresen et al., 1989). Increased DMI-mediated binding of (*R*)-[^{11}C]rolipram was abolished with prior CGP 12177 administration to 2-week diet NORM rats. CGP 12177 alone had no net affect on (*R*)-[^{11}C]rolipram retention. β-AR blockade of DMI-mediated changes in (*R*)-[^{11}C]rolipram retention with CGP 12177 strongly suggests the involvement of β-ARs in this process. These results concur with previous findings that incubation of cell cultures with β_2-AR agonist salbutamol increased PDE4

protein levels within 2-4 hours (Manning et al., 1996; Torphy et al., 1992b). Additionally acute stimulation of β-AR with isoproterenol in NORM rats up-regulated *in vivo* cAMP-specific PDE activity within 1 hour in the pineal gland (Oleshansky and Neff, 1975). Indeed, NA stimulation via β-ARs may employ cAMP-mediated signaling augmentation of PDE4, although further studies utilizing additional specific β-AR blockers could be used to confirm these results and identify specific β-AR isoform involvement in cAMP-mediated signaling in the future. Work towards understanding β-AR isoform involvement in cAMP-mediated signaling is currently being studied in our laboratory with mixed results.

4.3.3.3 Acute yohimbine

The presynaptic α_2-AR is negatively coupled to AC, causing decreased synthesis of intracellular cAMP upon stimulation. Antagonism of α_2-ARs by yohimbine leads to inhibition of the negative feedback in the turnover of synaptic NA, leading to rapid neuronal sympathetic discharge (McCall et al., 1983) and increased synaptic NA concentrations (Pacak et al., 1992; Szemeredi et al., 1991). Contrary to literature reports, *in vivo* yohimine administration in our study produced significant decreases in (*R*)-[^{11}C]rolipram binding in HYPO and SkM of 2-week diet NORM rats. *In vitro*, it has been reported that splice variants of PDE4 are down-regulated following the cAMP-augmention caused by AC agonist forskolin treatment (Erdogan and Houslay, 1997). Yohimbine has also been reported to display pharmacologically mediated haemodynamic effects, such as increased peripheral blood pressure (McCall et al., 1983), which may have enhanced the delivery of (*R*)-[^{11}C]rolipram in previous studies conducted in our laboratory that did not express data as a ratio to blood. Similar contradictory results with

yohimbine were also observed following lead exposure which causes increased aortic contractile response and cAMP that was blocked following yohimbine administration in rat tissues (Fazli-Tabaei et al., 2006). However, published literature predominantly states that yohimbine increases synaptic NA *in vivo* (Pacak et al., 1992), and has been linked to PDE4 as rolipram potentiates lethality in combination with yohimbine in mice (Wachtel, 1983). Due to the inconsistency of (*R*)-[^{11}C]rolipram binding data and published literature reports, yohimbine was not chosen to analyze the PDE4 cellular functional state in our rat models.

4.3.4 Effects of sub-chronic desipramine treatment on in vivo (R)-[^{11}C]rolipram binding

Sub-chronic DMI treatment to 2-week diet NORM rats significantly increased (*R*)-[^{11}C]rolipram uptake in the brain, SkM, and pancreatic regions as expected and as reported in the brain and monocytes *in vitro* (Itoh et al., 2004; Manning et al., 1996; Takahashi et al., 1999). The change in total tracer binding compared to controls was 20-33% in affected PDE4 rich tissues. Using brain tissues chronically treated with DMI, PDE4A and B, but not D expression was found to be elevated *in vitro* (Takahashi et al., 1999). PDE4 binding of (*R*)-[^{11}C]rolipram in sub-chronic DMI treated NORM rats adhere to *in vitro* reports and should mimic the hypothesized PDE4 outcomes present in chronically SNS stimulated disease states. Additional experimentation challenging sub-chronically treated rats with acute administration of DMI would provide a useful measure of the cellular functionality following sub-chronic NA augmentation.

4.4 DR and DIO rat studies

The framework of existing theories regarding obesity and energy expenditure are largely based upon a model of dysfunctional SNS signaling. In order to ascertain whether the animal models utilized were indeed obese and lean, physiological and metabolic measures were investigated. Exploratory experiments were performed on DR and DIO rats using selected drugs proven to alter cAMP-mediated signaling directly or indirectly in order to assess (*R*)-[^{11}C]rolipram binding and tissue cAMP-mediated functionality in HYPO, SkM, LVS, and pancreas. Studies were conducted on animals with similar physiological conditions that are anticipated in the human condition of obesity or DM2.

An important remark should be made regarding the methodology used to test the second and third hypotheses in the DR and DIO animals. It has never been conclusively identified that SNS dysfunction exists in this animal model, thus the second hypothesis that dysfunctional cAMP-mediated signaling is observed in obese rats was based on literature regarding the obese disease process as a whole rather than specific to the obese rat model. However, the third hypothesis that (*R*)-[^{11}C]rolipram can measure cAMP-mediated signaling in obesity is dependent upon the animal model possessing cAMP-mediated dysfunction. If the DR and DIO rats have no cAMP-mediated signaling dysfunction, then the similarity observed in (*R*)-[^{11}C]rolipram binding could be due to the model or the tracer's inability to measure differences in the obese state, thus producing a circular argument. However, results demonstrating differences in (*R*)-[^{11}C]rolipram binding between lean and obese rats would reinforce both second and third hypotheses and build a foundation upon which to formulate future theories in other disease states.

4.4.1 Physiological measurements

Both 2- and 8-week HFD DIO rats gained significantly more body weight, and consumed more HFD and more calories, than DR control rats. These findings are in agreement with published literature concerning the DR and DIO animal models. Multiple studies have demonstrated significantly increased body weight (Levin et al., 1997; Ricci and Levin, 2003) and dietary consumption in DIO rats (Farley et al., 2003; Gao et al., 2002; Levin et al., 1987). Thus, the DIO rats were indeed obese compared to the DR controls as stated in literature (Levin et al., 1997). HFD fed DR and DIO rat fasting blood glucose levels were found to be similar and correspond to published glucose levels observed in these rats (Gao et al., 2002; Levin et al., 1997; Levin and Sullivan, 1987). Reports of plasma insulin levels are varied in reports of DR and DIO rats. An investigation on DR and DIO rats fed HFD from 4-weeks of age until 10-weeks revealed no significant differences in plasma insulin levels (Ricci and Levin, 2003), whereas other studies have observed significantly increased plasma insulin levels in 9- and 10-week old DIO rats fed HFD for 2-weeks compared to DR controls (Levin et al., 1997). Our HFD fed DR and DIO fasting plasma insulin levels were observed to be similar in both the 2- and 8-week feeding periods. Alterations in (*R*)-[^{11}C]rolipram binding or cellular functionality may be produced by some non-glucose or non-insulin mediated means of cAMP signaling modification of PDE4 in this model of obesity.

4.4.2 Indirect calorimetry

Indirect calorimetry measures of 2- and 8-week HFD DR and DIO rats show no differences in energy substrate utilization, or whole body oxygen consumption, while DIO rats have reduced oxygen consumption corrected for body weight. Reports suggest

that obese rats have increased RERs indicating a state of fat storage. Obese Zucker rats fed butter or soybean diets have increased RER values compared to control rats (Rolland et al., 2002). Following consumption of HFD for a period of 4-weeks, NORM rats separated on greatest propensity to gain weight (DIO) had significantly greater 24 hour RER values compared to controls (Chang et al., 1990). Further exemplifying increased RER in DIO rats, another study showed that even when fed LFD, DIO rats have higher RERs compared to DR controls (Gao et al., 2002). Conflicting RER results may be due to our inbred models of DR and DIO rats verses NORM rat classified DR and DIO rat models or to the relatively short HFD feeding periods that our models were subjected to. The similarity between DR and DIO substrate utilization may indicate that alterations in (*R*)-[^{11}C]rolipram binding between DR and DIO models may not be produced by dietary substrate utilization.

In order to compare our results to literature reports of $\dot{V}_{O2}$ corrected for body weight, findings were expressed as both weight corrected and whole body $\dot{V}_{O2}$. Obese rodents have been found to possess reduced $\dot{V}_{O2}$ corrected for body mass (Erickson et al., 1996; Maskrey et al., 2001) or area (Pelleymounter et al., 1995) compared to lean controls. In another study, DR and DIO rats were observed to possess the same oxygen consumption corrected for body area over a two hour examination (Levin et al., 1989). However, expression of data in this manner has been challenged (Himms-Hagen, 1997) revealing that metabolic findings may be incorrectly expressed when correcting for additional adiposity associated mass that is metabolically inactive. There is also no single mass exponent that can account for varying metabolic conditions of basal rates and maximum oxygen uptake (Darveau et al., 2002; Weibel, 2002). Thus to avoid the pitfalls associated

with the practice of normalizing $\dot{V}_{O2}$ to body mass, $\dot{V}_{O2}$ per whole rat was also expressed. While our data corresponds to existing literature of body mass corrected $\dot{V}_{O2}$, conservative whole body $\dot{V}_{O2}$ data demonstrates no significant differences in energy expenditure between DR and DIO rats. Taken together, DIO rats were obese and gained significantly greater weight evident by differences in HFD consumption compared to DRs, while there was no difference between DR and DIO rat substrate utilization or whole body energy expenditures.

4.4.3 (R)-[^{11}C]Rolipram baseline analysis

As expected without extrinsic NA stimulation, baseline 2- and 8-week HFD DR and DIO rats had similar PDE4 levels observed with (*R*)-[^{11}C]rolipram binding in HYPO, SkM, and LVS. SNS signals for thermogenesis occur in response to stimuli such as cold or food rather than constitutively expressed (Dulloo, 2002; Dulloo et al., 1992), thus alterations in basal PDE4 levels were expected to be similar in basal conditions. Reduction of (*R*)-[^{11}C]rolipram binding observed in pancreata of HFD fed DR and DIO rats following increased dietary feeding period signified that 2- and 8-week PDE4 binding data could not be merged and must be analyzed separately. Pancreatic decreases of (*R*)-[^{11}C]rolipram PDE4 binding in 8-week HFD DR and DIO rats compared to the 2-week models may possibly be due to compensatory mechanisms regulating PDE4, age dependent SNS changes (Hering et al., 2006; Leenen et al., 2006), or glucose and insulin mediated modification of SNS signaling between groups (Ahmad et al., 2000; Yan et al., 1995), as previously suggested in NORM rat studies.

4.4.4 Effects of acute desipramine treatment on in vivo (R)-[^{11}C]rolipram binding

Acute treatment with DMI increasing synaptic NA was shown to augment the regional distribution of (*R*)-[^{11}C]rolipram in previous experiments with NORM rats as

well as from published literature from our laboratory (Lourenco et al., 2006). Interestingly, no effect of acute DMI was observed in PDE4 (*R*)-[^{11}C]rolipram binding in 2-week HFD DR rat HYPO, SkM, or LVS tissues, while pancreatic uptake decreased. The deficient PDE4 response to acute DMI in 2-week HFD DR rats may be partially explained by a differential response to caloric restriction compared to DIO rats. Upon caloric restriction, DIO rats reportedly exhibit a greater reduction in sympathetic activity (24 hour urine NA) compared to DR rats (Levin and Dunn-Meynell, 2000). Importantly, these findings were also observed by Levin *et al.* in chow fed NORM and HFD fed DIO rats using RIA analysis of NA and found that heart, aorta, and pancreas NA content decreased to a greater extent in HFD DIO rats (Levin et al., 1983). Dysfunctional PDE4 response to DMI in 2-week HFD DR rats may be explained by lessened sympathetic deactivation in response to fasting which may have lead to an altered cAMP-mediated response to DMI in this model.

In vivo results obtained from 8-week HFD DR rats treated with acute DMI indicates a significant augmentation of (*R*)-[^{11}C]rolipram binding in HYPO, SkM and LVS regions, and decreased retention observed in the pancreas which concur with literature. Following glucose stimulated increases in NA content in HFD DR and DIO rats, Levin et al. hypothesized that DR rats possess a dampened sympathetic activation after glucose load, possibly due to heightened end-organ responsiveness to NA (Levin and Sullivan, 1987), which is supported by our findings. The decreased pancreatic (*R*)-[^{11}C]rolipram binding in acute DMI treated 2- and 8-week HFD DR rats may be partially explained by a DMI-mediated disruption of glucose homeostasis and insulin sensitivity (McIntyre et al., 2006) that may have lead to altered PDE4 levels by compensatory mechanisms.

As anticipated from literature reports of elevated plasma NA in HFD fed DIO rats (Levin and Dunn-Meynell, 2000), 2-week HFD DIOs treated with acute DMI only had significantly increased LVS (*R*)-[^{11}C]rolipram binding with no changes in HYPO, SkM, or pancreas. Furthermore, 8-week HFD DIO rats treated with DMI had no changes in (*R*)-[^{11}C]rolipram binding to PDE4. The (*R*)-[^{11}C]rolipram binding results concerning the 2- and 8-week HFD DIO rats may be partially explained by tissue and plasma NA content. Plasma NA levels following glucose administration are lower in DR rats compared to DIOs (Levin and Sullivan, 1987). Also, high urinary excretion of NA has also been observed to be >150% in DIO rats compared to DRs prior to administration of HFD (Levin and Dunn-Meynell, 2000). Intriguingly, urinary exretion of NA in HFD DIO rats reportedly returns to normal DR levels after a 10-week HFD feeding period (Levin and Dunn-Meynell, 2000). The dysfunctional PDE4 cAMP-mediated signaling response to DMI treatment in DIO rats appears to deteriorate in a dietary-time dependent manner which may partially be explained by tissue and plasma NA levels.

The (*R*)-[^{11}C]rolipram binding data of acute DMI treated 2- and 8-week HFD DR and DIO rats support the concept that chronically elevated NA content leads to HFD DIO rat sympathetic end-organ insensitivity as observed by a dysfunctional cAMP-mediated signaling response to acute synaptic NA augmentation. The mechanism underlying the absence of a DMI mediated PDE4 effect on (*R*)-[^{11}C]rolipram binding in 2-week HFD DR rats remains unclear and more work is needed to fully understand the cAMP-mediated processes occurring at this time point. However, HYPO, SkM, and LVS tissues cAMP-mediated signaling remained functional in 8-week HFD DR rats. A functional cAMP-mediated response to increased NA may possibly explain how they remain lean by

mechanisms associated with thermogenesis. In contrast, 2-week HFD DIO rats were only responsive to DMI treatment in the LVS region, and had no functional PDE4 response to DMI in the 8-week HFD DIO rat model. This dysfunctional cAMP-mediated response in DIO rats to increased NA may partially explain their obese body compositions by damaged thermogenic responses to SNS stimulation. Ultimately, PDE4 binding and cAMP-mediated signaling were affected between the 8-week HFD DR and DIO models. Tissue NA content (by HPLC method) and β-AR density will be investigated in our laboratory to further the understanding of altered SNS signaling in obesity.

4.5 Citrate- and streptozocin-treated rat studies

Diabetes is associated with diverse systemic effects mediated by altered blood glucose and insulin levels. Modification of blood glucose and insulin levels can lead to deleterious effects on SNS signaling. In order to ascertain whether the STZ-treated rats were indeed affected by diabetic complications, physical and metabolic traits were investigated and compared to literature. Exploratory experiments were performed on citrate- and STZ-treated citrate control and STZ DM2 rats respectively, using selected drugs proven to alter cAMP-mediated signaling directly or indirectly in order to assess (*R*)-[^{11}C]rolipram binding and tissue cAMP-mediated signaling in PDE4 rich HYPO, SkM, LVS, and pancreas.

An important remark should be made regarding the methodology used to test the second and third hypotheses in the citrate control and STZ DM2 rats. It has never been conclusively identified that cAMP-signaling dysfunction exists in this animal model, thus the second hypothesis that dysfunctional cAMP-mediated signaling is observed in

diabetic rats was based on literature regarding the diabetic disease process as a whole, and reports of STZ-treated rat NA levels rather than specific to this DM2 model. However, the third hypothesis that (*R*)-[^{11}C]rolipram can measure cAMP-mediated signaling in diabetes is dependent upon the DM2 animal model possessing cAMP-mediated dysfunction. If the citrate control and STZ DM2 rats have no cAMP-mediated signaling dysfunction, then observed similarity in (*R*)-[^{11}C]rolipram binding could be due to the model or the tracer's inability to measure differences in the obese state, thus producing a circular argument. However, results demonstrating differences in (*R*)-[^{11}C]rolipram binding between citrate control and STZ DM2 rats would confirm both second and third hypotheses and build a foundation upon which to formulate future theories in other disease states.

4.5.1 Physiological measurements

Hyperglycemia greatly affected the citrate- and STZ-treated rats body weight gain. Hyperglycemic STZ-treated DM2 rats had significantly decreased weight gain compared to citrate control or normoglycemic STZ-treated DM2 (bg<11) rats. In our study, ~65% of rats treated with STZ surpassed glucose levels >11 mmol/L (Lateef et al., 2005; Sawant et al., 2004) that we used as a threshold number to screen STZ-DM2 rats concurring with other reports of low dose STZ-DM2 induction (Bidasee et al., 2001; Lateef et al., 2005; Sawant et al., 2004). Reports of low dose STZ-induced DM2 models have shown similar results between 4- and 8-weeks (Baluchnejadmojarad and Roghani, 2003; Bidasee et al., 2001; Morris and Pavia, 2004) post STZ-treatment, however early (3 day – 1 week) weight gain values are reportedly similar between controls and STZ DM2 rats (Baluchnejadmojarad and Roghani, 2003; Reed et al., 2000). Two-week STZ DM2

rat blood glucose was elevated while insulin levels were similar to citrate controls (Sawant et al., 2004). However, 8-week STZ DM2 rats had elevated blood glucose and significantly decreased insulin levels compared to citrate controls as previously reported in these models (Bidasee et al., 2001; Lateef et al., 2005; Morris and Pavia, 2004). These findings decisively emphasize the hyperglycemic diabetic disease state presented by the STZ DM2 rat model, and the need to screen rats for blood glucose levels after STZ treatment.

4.5.2 Indirect calorimetry

Indirect calorimetry revealed no differences between 2-week citrate controls and STZ DM2 rat with respect to RER, $\dot{V}_{O2}$/kgBW, or whole body $\dot{V}_{O2}$. However, 8-week STZ DM2 rats were found to have significantly diminished RERs compared to 8-week citrate controls while $\dot{V}_{O2}$/kgBW and $\dot{V}_{O2}$ measurements were again similar. Findings are in agreement with plasma insulin levels being significantly reduced in 8-week STZ DM2 rats. Calorimetry and insulin findings demonstrate the inability 8-week STZ DM2 rats to utilize glucose as an energy substrate as a consequence of reduced insulin levels and DM2 disease progression. As a result, 8-week STZ DM2 rats utilize FFA as their primary energy substrate. Reports concur with published literature stating inbred Albino Oxford rats treated with high dose (70 mg/kg) STZ demonstrate reduced resting RER and increased $\dot{V}_{O2}$/kgBW compared to controls (Houwing et al., 1995). Additionally, groups of high dose (85 mg/kg) STZ-treated dipeptidyl peptidase -/- mice had increased $\dot{V}_{O2}$/kgBW compared to wild type controls (Conarello et al., 2003). Collectively, indirect calorimetry measurements indicate STZ-induced DM2 rats correspond to literature

reports of DM2 rat models and progressively lose their ability to utilize glucose as an energy substrate over time.

4.5.3 (R)-[^{11}C]Rolipram baseline analysis

DM2 disease progression is characterized by hyperglycemia, insulin resistance and β-cell exhaustion (Saad et al., 1991). Without extrinsic NA stimulation, baseline 2-week citrate control and STZ DM2 rats had similar (*R*)-[^{11}C]rolipram binding to PDE4 as was also observed in DR and DIO models. However, 8-week STZ-treated DM2 rats had significantly reduced baseline (*R*)-[^{11}C]rolipram binding in the brain and heart regions compared to 8-week citrate controls, and were distinctly unique from STZ DM2 (bg<11) rats. Results signify reduced PDE4 binding and a capacity to hydrolyze cAMP in brain and heart of 8-week STZ DM2 rats. Interestingly, contrary findings of STZ-treated rats 5 weeks after treatment low dose (48 mg/kg) STZ had increased NA release in HYPO (Morris and Pavia, 2004). Decreased radioligand binding in 8-week STZ DM2 rats may be associated with autonomic neuropathy or decreased insulin levels. A report comparing diabetic mouse models advises that the pathogenesis of diabetic autonomic neuropathy develops slowly and only to a modest degree in STZ-induced diabetic mice (Schmidt et al., 2003). However, the suggestion implicating autonomic neuropathy as a source of reduced (*R*)-[^{11}C]rolipram binding in the 8-week STZ DM2 rat model is an unlikely mechanism as it is associated with longer term disease progression in STZ-treated rats (Schmidt et al., 2003). [^{11}C]Hydroxyephedrine was previously used to analyze *in vivo* cardiac NAT content in low dose (50 mg/kg) STZ DM2 rats and determined both proximal and distal myocardial segments were denervated after 9 months as opposed to only distally at 6 months (Schmid et al., 1999). Diminished (*R*)-

[^{11}C]rolipram retention observed in 8-week STZ DM2 rats is perhaps not linked to autonomic neuropathy, but rather reduced insulin levels or hyperglycemia and their effects on the SNS.

Zucker diabetic fatty rats demonstrate β-cell exhaustion and apoptosis 7 weeks following spontaneous development of diabetes (Corsetti et al., 2000). While fasting plasma insulin levels were determined to be low in the 8-week STZ DM2 rats, pancreatic (*R*)-[^{11}C]rolipram uptake was similar to 8-week citrate controls suggesting pancreatic functionality. Although pancreatic β-cells continued to produce insulin, the effect of hyperglycemia or hypoinsulinemia may have lead to observed reduction in HYPO and LVS (*R*)-[^{11}C]rolipram binding in 8-week STZ DM2 rats. Insulin administration has been found to increase muscle SNS activity (Muntzel et al., 1994) as well as plasma NA content (Berne et al., 1992). Studies involving hyperglycemic, hypoinsulinemic STZ-treated rats demonstrate reduced SNS HYPO response to antidiuretic hormone vasopressin administration (Bunag et al., 1982). Additionally, 8-week hyperglycemic, hypoinsulinemic STZ-treated rats have reportedly diminished responses to transmural sympathetic nerve stimulation that is abolished following insulin treatment (Sato et al., 1990). Tissue NA measurements as well as insulin-treated STZ DM2 rat experiments using (*R*)-[^{11}C]rolipram would assist the recognition of the underlying pathophysiology involved in this DM2 model. Only conjectures can be contemplated about the pathophysiology underlying the exact mechanisms producing the diminished (*R*)-[^{11}C]rolipram binding in the 8-week STZ DM2 rats without more investigation. However, (*R*)-[^{11}C]rolipram was able to detect decreased PDE4 binding suggesting reduced cAMP catabolism in 8-week STZ-treated DM2 compared to citrate control rats.

4.5.4 Effects of acute desipramine treatment on in vivo (R)-[^{11}C]rolipram binding in 2-week citrate and streptozocin models

Synaptic NA stimulating DMI has previously been shown to enhance regional distribution of (*R*)-[^{11}C]rolipram binding in NORM rats (Lourenco et al., 2006), and was repeated in 2-week diet fed NORM rats. Administration of acute DMI to 2-week STZ-treated DM2 rats produced significantly increased (*R*)-[^{11}C]rolipram retention in HYPO, SkM, and LVS, while pancreas was unaffected. These findings parallel observations of increased radioligand binding in 2-week diet NORM rats following acute DMI. Results indicate that the effect of 2-week hyperglycemia present in STZ DM2 rats did not alter DMI-mediated augmentation of (*R*)-[^{11}C]rolipram binding in 2-week STZ DM2 rats. As previously described in the DR and DIO rat section, although β-ARs are present in the pancreas, PDE4 may be affected by compensatory mechanisms or be linked to other stimuli such as glucose or insulin (Ahmad et al., 2000; Yan et al., 1995) leading to changes in (*R*)-[^{11}C]rolipram binding. In concordance with results, hyperglycemic, hyperinsulinemic Wistar fatty rats treated with α_1-AR agonist phenylephrine demonstrate enhanced renal sympathetic nerve activity compared to treated control Wistar rats (Suzuki et al., 1999). Accordingly, 2-week STZ DM2 rats may experience normal to enhanced SNS response to stimuli and are relatively unaffected by hyperglycemia. Ultimately, (*R*)-[^{11}C]rolipram was able to detect a functional PDE4 cAMP-mediated response to DMI in 2-week STZ DM2 rats.

5.0: CONCLUSION

5.1 Research conclusions

Various simple conclusions can be drawn from this thesis. First, (*R*)-[^{11}C]rolipram specific binding to PDE4 was established in the brain, SkM, heart, pancreas, and lung tissues. These results indicate the presence of HARBS binding *in vivo* in both rat brain and periphery, contrary to recent *in vitro* reports. Conversely, no PDE4 specific binding was observed in WAT, BAT, or in liver tissues. Ex *vivo* HPLC analysis of SkM, pancreas, and BAT confirmed the *in vivo* PDE4 specific binding biodistribution findings with (*R*)-[^{11}C]rolipram. SkM, pancreas, and BAT tissues were observed to contain partial non-specific radioactivity signal arising from hydrophilic metabolites, contrary to the brain which does not possess labeled metabolites. However, these hydrophilic labeled metabolites are unlikely to cross the cell membrane and they do not bind PDE4. Utilizing this knowledge of labeled metabolites, it will likely be possible to introduce a non-specific metabolite component into the compartmentalization kinetic modeling analyses for PET imaging with (*R*)-[^{11}C]rolipram. Correcting for peripheral radiolabeled metabolites would permit PET imaging of alterations in (*R*)-[^{11}C]rolipram PDE4 specific binding to be analyzed with greater accuracy. Together, these results entail the ability of (*R*)-[^{11}C]rolipram to detect PDE4 specific binding in regions associated with obesity and diabetes, *proving the first hypothesis to be true for brain, SkM, heart, pancreas, and lungs*. Second, acute DMI administration evoked modulation of (*R*)-[^{11}C]rolipram binding in 2-week diet NORM rats. β-ARs may be involved in DMI-mediated augmentation of (*R*)-[^{11}C]rolipram given that pretreatment CGP 12177 abolished DMI-

mediated effects on (*R*)-[^{11}C]rolipram binding and PDE4. Third, the DIO rat model was determined to be obese compared to lean DR rats. Comparison of baseline (*R*)-[^{11}C]rolipram binding between 2- and 8-week HFD DR and DIO rats demonstrated no difference between age-matched models. However, reduced pancreatic radioligand binding was observed within the 2- and 8-week HFD DR and DIO rats. DMI treatment had no effect on (*R*)-[^{11}C]rolipram binding in 2-week HFD DR rats; whereas, the 8-week HFD DR rat model had a functional PDE4 mediated response to DMI treatment. More work is needed to fully understand the mechanisms underlying 2-week HFD DR rat results; however, the 8-week HFD DR rat model possesses a functional PDE4 cAMP-mediated response to acute NA stimulation. In contrast, 2-week HFD DIO rats only had increased LVS (*R*)-[^{11}C]rolipram binding following DMI treatment while 8-week HFD DIO rats were totally unaffected by the treatment indicating a dysfunctional PDE4 cAMP-mediated response to acute NA stimulation. Taken together, (*R*)-[^{11}C]rolipram detected cAMP-mediated signaling differences between the DR and DIO rat models *proving the second and third hypotheses to be true in obesity*. Fourth, 2- and 8-week STZ DM2 rats were hyperglycemic and had reduced weight gain and ability to utilize glucose as an energy substrate compared to citrate control rats. Two-week STZ DM2 rat (*R*)-[^{11}C]rolipram retention was similar to citrate controls. Hyperglycemia, and normoinsulinemia in 2-week STZ DM2 rats was suggested to have no effect on 2-week STZ DM2 rat PDE4 modulation. (*R*)-[^{11}C]Rolipram was able to detect a functional PDE4 cAMP-mediated response to acute DMI treatment in 2-week STZ DM2 rats. Importantly, 8-week STZ DM2 rats were found to have significantly reduced (*R*)-[^{11}C]rolipram binding in brain and heart regions suggested to be mediated by

hyperglycemic or hypoinsulinemic effects on the SNS. Thus, (*R*)-[^{11}C]rolipram was proficient in detecting reduced PDE4 cAMP hydrolyzing ability in the 8-week STZ DM2 rats compared to citrate controls *proving the second and third hypotheses true in DM2.* Overall, the major findings were that: *(1) (R)-[^{11}C]rolipram can detect changes in PDE4 in SkM, and pancreas; (2) two- and 8-week HFD fed DIO rats have a dysfunctional PDE4 cAMP-mediated response to acute synaptic NA increase, while the 8-week DR rat PDE4 response to acutely increased NA remained functional; and (3) 8-week STZ DM2 rats have reduced (R)-[^{11}C]rolipram binding to PDE4 in brain and heart compared to citrate controls.* This study supports further development of (*R*)-[^{11}C]rolipram radiotracer for studying alterations in PDE4 present in the obese and diabetic states using PET.

5.2 Future directions

Future research stemming from this work may be aimed at *in vitro* conformational studies examining tissue NA content, as well as identifying β-AR and PDE4 mRNA isoform expression in obese and diabetic animal models. Additionally, the eventual *in vivo* serial evaluation of obese and diabetic rodent cAMP-mediated signaling using [^{11}C]hydroxyephedrine, (*S*)-[^{11}C]CGP 12177, and (*R*)-[^{11}C]rolipram with small animal micro-PET technology could be completed to identify presynaptic transporter, postsynaptic receptor, and intracellular second messenger components in these disease states. Small animal PET studies would provide a full kinetic analysis of (*R*)-[^{11}C]rolipram binding not limited to only 45 min postinjection. Such studies would provide excellent insight and further understanding of the etiology and SNS dysfunction

occurring in obesity and diabetes. Regardless of the link between the subcellular and whole organism, *in vitro* measurements do not always reflect the true nature of the intracellular interactions occurring *in vivo*. Additional investigation into the role that PDE4 serves in the hydrolysis of pancreatic cAMP would prove useful for future interpretation of *in vivo* (*R*)-[^{11}C]rolipram findings. Additonal experimentation of 8-week STZ DM2 rats should be performed with acute DMI treatments elucidating the functionality of the cAMP-mediated response to acute NA stimulation. In addition to chronic NA modulation, systemic challenges with glucose, insulin, and glucagon may assist in the elucidation of PDE4 involvement in the pancreas using (*R*)-[^{11}C]rolipram. Utilizing this thesis as a basis and the aforementioned conformational studies, future research may be aimed at evaluation of SNS dysfunction in accompanying diseases associated with obesity and diabetes such as heart failure, and depression.

5.3 Statement of research significance

The complex and astonishing mosaic of the cAMP signaling pathway, comprising multiple pieces, such as NAT, β-ARs, PKA, PDEs and others, has been part of the recent pathophysiological research focus into SNS dysfunction present in obesity and diabetes. As an important component of the cAMP-mediated signaling system, PDE4 controls the action of cAMP and contributes to the functions of this second messenger system which may be altered at various stages of the obese and diabetic states. It was established that (*R*)-[^{11}C]rolipram binds specifically to PDE4 in brain, heart, and lung tissues. For the first time, this research extends PDE4 specific binding of (*R*)-[^{11}C]rolipram to *SkM*, and *pancreas*, building premise for peripheral (*R*)-[^{11}C]rolipram PET imaging of SNS

alterations occurring in obesity and diabetes. (*R*)-[^{11}C]Rolipram is the first radioligand that shows promise for imaging obese and diabetic post-synaptic alterations of PDE4 and cAMP-mediated functionality in the brain and periphery using PET. With the future successful development of radioligands able to image NAT activity and β-AR densities, (*R*)-[^{11}C]rolipram could be utilized assess the effects of various therapies and to better understand the intricate puzzle involved with SNS dysfunction and disease progression in obesity, diabetes and many other disease states. As a result of the present research, there is now the potential for studying the role of PDE4 in obese and diabetic states before and after therapy in living small animal models using PET.

REFERENCES

Abel, E.D. 2005. Myocardial insulin resistance and cardiac complications of diabetes. *Curr Drug Targets Immune Endocr Metabol Disord.* 5:219-26.

Ahmad, M., Y.H. Abdel-Wahab, R. Tate, P.R. Flatt, N.J. Pyne, and B.L. Furman. 2000. Effect of type-selective inhibitors on cyclic nucleotide phosphodiesterase activity and insulin secretion in the clonal insulin secreting cell line BRIN-BD11. *Br J Pharmacol.* 129:1228-34.

Alvarez, R., C. Sette, D. Yang, R.M. Eglen, R. Wilhelm, E.R. Shelton, and M. Conti. 1995. Activation and selective inhibition of a cyclic AMP-specific phosphodiesterase, PDE-4D3. *Mol. Pharmacol.* 48:616 - 622.

Amegadzie, B.Y., C.R. Hanning, M.M. McLaughlin, M. Burman, L.B. Cielinski, G.P. Livi, and T.J. Torphy. 1995. Characterization of two human cAMP-specific phosphodiesterase subtypes expressed in baculovirus-infected insect cells. *Cell Biol. Int.* 19:477-484.

Anderson, E.A., R.P. Hoffman, T.W. Balon, C.A. Sinkey, and A.L. Mark. 1991. Hyperinsulinemia produces both sympathetic neural activation and vasodilation in normal humans. *J Clin Invest.* 87:2246-52.

Archer, Z.A., D.V. Rayner, J. Rozman, M. Klingenspor, and J.G. Mercer. 2003. Normal distribution of body weight gain in male Sprague-Dawley rats fed a high-energy diet. *Obes Res.* 11:1376-83.

Astrup, A., J. Bulow, J. Madsen, and N.J. Christensen. 1985. Contribution of BAT and skeletal muscle to thermogenesis induced by ephedrine in man. *Am J Physiol.* 248:E507-15.

Bachman, E.S., H. Dhillon, C.Y. Zhang, S. Cinti, A.C. Bianco, B.K. Kobilka, and B.B. Lowell. 2002. betaAR signaling required for diet-induced thermogenesis and obesity resistance. *Science.* 297:843-5.

Baillie, G., S.J. MacKenzie, and M.D. Houslay. 2001. Phorbol 12-myristate 13-acetate triggers the protein kinase A-mediated phosphorylation and activation of the PDE4D5 cAMP phosphodiesterase in human aortic smooth muscle cells through a route involving extracellular signal regulated kinase (ERK). *Mol Pharmacol.* 60:1100-11.

Baillie, G.S., S.J. MacKenzie, I. McPhee, and M.D. Houslay. 2000. Sub-family selective actions in the ability of Erk2 MAP kinase to phosphorylate and regulate the activity of PDE4 cyclic AMP-specific phosphodiesterases. *Br J Pharmacol.* 131:811-9.

Baker, J.G. 2005. The selectivity of beta-adrenoceptor antagonists at the human beta1, beta2 and beta3 adrenoceptors. *Br J Pharmacol.* 144:317-22.

Balkan, B., G. Van Dijk, J.H. Strubbe, J.E. Bruggink, and A.B. Steffens. 1992. Exercise-induced sympathetic FFA mobilization in VMH-lesioned rats is normalized by fasting. *Am J Physiol.* 262:R981-5.

Baluchnejadmojarad, T., and M. Roghani. 2003. Garlic extract attenuates time-dependent changes in the reactivity of isolated aorta in streptozotocin-diabetic rats. *Life Sci.* 73:2281-9.

Beard, M.B., A.E. Olsen, R.E. Jones, S. Erdogan, M.D. Houslay, and G.B. Bolger. 2000. UCR1 and UCR2 domains unique to the cAMP-specific phosphodiesterase family form a discrete module via electrostatic interactions. *J Biol Chem.* 275:10349-58.

Beavo, J.A. 1995. Cyclic nucleotide phosphodiesterases: functional implications of multiple isoforms. *Physiological Rev.* 75:725-748.

Beavo, J.A., and D.H. Reifsnyder. 1990. Primary sequence of cyclic nucleotide phosphodiesterase isozymes and the design of selective inhibitors. *Trends Pharmacol Sci.* 11:150-155.

Berne, C., J. Fagius, T. Pollare, and P. Hjemdahl. 1992. The sympathetic response to euglycaemic hyperinsulinaemia. Evidence from microelectrode nerve recordings in healthy subjects. *Diabetologia.* 35:873-9.

Bertin, R., and R. Portet. 1975. 3':5'-Cyclic-AMP phosphodiesterase activities in white and brown adipose tissues of cold-acclimated rats. *Can J Biochem.* 53:1301-8.

Bezaire, V., W. Hofmann, J.K. Kramer, L.P. Kozak, and M.E. Harper. 2001. Effects of fasting on muscle mitochondrial energetics and fatty acid metabolism in Ucp3(-/-) and wild-type mice. *Am J Physiol Endocrinol Metab.* 281:E975-82.

Bidasee, K.R., U.D. Dincer, and H.R. Besch, Jr. 2001. Ryanodine receptor dysfunction in hearts of streptozotocin-induced diabetic rats. *Mol Pharmacol.* 60:1356-64.

Bodnar, R.J., P.E. Mann, and E.A. Stone. 1985. Potentiation of cold-water swim analgesia by acute, but not chronic desipramine administration. *Pharmacol Biochem Behav.* 23:749-52.

Bolger, G.B., S. Erdogan, R.E. Jones, K. Loughney, G. Scotland, R. Hoffmann, I. Wilkinson, C. Farrell, and M.D. Houslay. 1997. Characterization of five different proteins produced by alternatively spliced mRNAs from the human cAMP-specific phosphodiesterase PDE4D gene. *Biochem J.* 328:539-48.

Borisy, F.F., P.N. Hwang, G.V. Ronnett, and S.H. Snyder. 1993. High-affinity cAMP phosphodiesterase and adenosine localized in sensory organs. *Brain Research.* 610:199-207.

Brodde, O.E., and M.C. Michel. 1999. Adrenergic and muscarinic receptors in the human heart. *Pharmacol Rev.* 51:651-90.

Brown, A.T., T.P. Smith, C.P. Cruz, L.A. Poirier, D. Simmons, D.K. Williams, Y. Wang, J.F. Eidt, and M.M. Moursi. 2003. Intimal hyperplasia following carotid endarterectomy in an insulin-resistant rat model. *Metabolism.* 52:834-9.

Bunag, R.D., T. Tomita, and S. Sasaki. 1982. Streptozotocin diabetic rats are hypertensive despite reduced hypothalamic responsiveness. *Hypertension.* 4:556-65.

Butcher, R.W., and E.W. Sutherland. 1962. Adenosine 3',5'-phosphate in biological materials. I. Purification and properties of cyclic 3',5'-nucleotide phosphodiesterase and use of this enzyme to characterize adenosine 3',5'-phosphate in human urine. *J Biol Chem.* 237:1244-50.

Canning, P.M., M.L. Courage, and L.M. Frizzell. 2004. Prevalence of overweight and obesity in a provincial population of Canadian preschool children. *Cmaj.* 171:240-2.

Cannon, B., and J. Nedergaard. 2004. Brown adipose tissue: function and physiological significance. *Physiol Rev.* 84:277-359.

Card, G.L., L. Blasdel, B.P. England, C. Zhang, Y. Suzuki, S. Gillette, D. Fong, P.N. Ibrahim, D.R. Artis, G. Bollag, M.V. Milburn, S.H. Kim, J. Schlessinger, and K.Y. Zhang. 2005. A family of phosphodiesterase inhibitors discovered by cocrystallography and scaffold-based drug design. *Nat Biotechnol.* 23:201-7.

Cerri, M., and S.F. Morrison. 2005. Activation of lateral hypothalamic neurons stimulates brown adipose tissue thermogenesis. *Neuroscience.* 135:627-38.

Chang, S., B. Graham, F. Yakubu, D. Lin, J.C. Peters, and J.O. Hill. 1990. Metabolic differences between obesity-prone and obesity-resistant rats. *Am J Physiol.* 259:R1103-10.

Chang, Y.-H., M. Conti, Y.-C. Lee, H.-L. Lai, Y.-H. Ching, and Y. Chern. 1997. Activation of phosphodiesterase IV during densensitization of the A_{2A} adenosine receptor-mediated cyclic AMP response in rat pheochromocytoma (PC12) cells. *J. Neurochem.* 69:1300-1309.

Charbonneau, H., N. Beier, K.A. Walsh, and J.A. Beavo. 1986. Identification of a conserved domain among cyclic nucleotide phosphodiesterases from diverse species. *Proc Natl Acad Sci U S A.* 83:9308-12.

Clapham, J.C., J.R. Arch, H. Chapman, A. Haynes, C. Lister, G.B. Moore, V. Piercy, S.A. Carter, I. Lehner, S.A. Smith, L.J. Beeley, R.J. Godden, N. Herrity, M. Skehel, K.K. Changani, P.D. Hockings, D.G. Reid, S.M. Squires, J. Hatcher, B. Trail, J. Latcham, S. Rastan, A.J. Harper, S. Cadenas, J.A. Buckingham, M.D. Brand, and A. Abuin. 2000. Mice overexpressing human uncoupling protein-3 in skeletal muscle are hyperphagic and lean. *Nature.* 406:415-8.

Colledge, M., and J.D. Scott. 1999. AKAPs: from structure to function. *Trends Cell Biol.* 9:216-21.

Collins, S., and R.S. Surwit. 2001. The beta-adrenergic receptors and the control of adipose tissue metabolism and thermogenesis. *Recent Prog Horm Res.* 56:309-28.

Communal, C., K. Singh, D.B. Sawyer, and W.S. Colucci. 1999. Opposing effects of beta(1)- and beta(2)-adrenergic receptors on cardiac myocyte apoptosis : role of a pertussis toxin-sensitive G protein. *Circulation.* 100:2210-2.

Conarello, S.L., Z. Li, J. Ronan, R.S. Roy, L. Zhu, G. Jiang, F. Liu, J. Woods, E. Zycband, D.E. Moller, N.A. Thornberry, and B.B. Zhang. 2003. Mice lacking dipeptidyl peptidase IV are protected against obesity and insulin resistance. *Proc Natl Acad Sci U S A.* 100:6825-30.

Conti, M. 2000. Phosphodiesterases and cyclic nucleotide signaling in endocrine cells. *Mol Endocrinol.* 14:1317-27.

Conti, M., S. Iona, M. Cuomo, J.V. Swinnen, J. Odeh, and M.E. Svoboda. 1995a. Characterization of a hormone-inducibe, high affinity adenosine 3'-5'-cyclic monophosphate phosphodiesterase from the rat sertoli cell. *Biochemistry.* 34:7979-7987.

Conti, M., and S.L. Jin. 1999. The molecular biology of cyclic nucleotide phosphodiesterases. *Prog Nucleic Acid Res Mol Biol.* 63:1-38.

Conti, M., G. Nemoz, C. Sette, and E. Vicini. 1995b. Recent progress in understanding the hormonal regulation of phosphodiesterases. *Endocrine Rev.* 16:370-389.

Conti, M., W. Richter, C. Mehats, G. Livera, J.Y. Park, and C. Jin. 2003. Cyclic AMP-specific PDE4 phosphodiesterases as critical components of cyclic AMP signaling. *J Biol Chem.* 278:5493-6.

Corbett, S.W., J.S. Stern, and R.E. Keesey. 1986. Energy expenditure in rats with diet-induced obesity. *Am J Clin Nutr.* 44:173-80.

Corsetti, J.P., J.D. Sparks, R.G. Peterson, R.L. Smith, and C.E. Sparks. 2000. Effect of dietary fat on the development of non-insulin dependent diabetes mellitus in obese Zucker diabetic fatty male and female rats. *Atherosclerosis.* 148:231-41.

Coudray, C., C. Charon, N. Komas, G. Mory, F. Diot-Dupuy, V. Manganiello, P. Ferre, and R. Bazin. 1999. Evidence for the presence of several phosphodiesterase isoforms in brown adipose tissue of Zucker rats: modulation of PDE2 by the fa gene expression. *FEBS Lett.* 456:207-10.

Dagogo-Jack, S.E., S. Craft, and P.E. Cryer. 1993. Hypoglycemia-associated autonomic failure in insulin-dependent diabetes mellitus. Recent antecedent hypoglycemia reduces autonomic responses to, symptoms of, and defense against subsequent hypoglycemia. *J Clin Invest.* 91:819-28.

Darveau, C.A., R.K. Suarez, R.D. Andrews, and P.W. Hochachka. 2002. Allometric cascade as a unifying principle of body mass effects on metabolism. *Nature.* 417:166-70.

DaSilva, J.N., and M.R. Kilbourn. 1992. In Vivo Binding of [^{11}C]tetrabenazine to vesicular monoamine transporters in mouse brain. *Life Sciences.* 51:593-600.

DaSilva, J.N., C.M. Lourenco, D. Hussey, K. Cheung, A.A. Wilson, and S. Houle. 1999. In vivo brain mapping of the cAMP-specific phosphodiesterase-4 inhibitor R-[^{11}C]-rolipram in healthy human subjects by PET. *J Cereb Blood Flow Metab.* 19:S344.

DaSilva, J.N., C.M. Lourenco, J.H. Meyer, D. Hussey, W.Z. Potter, and S. Houle. 2002. Imaging cAMP-specific phosphodiesterase-4 in human brain with (*R*)-[^{11}C]rolipram and positron emission tomography. *Eur J Nucl Med Mol Imaging.* 29:1680-3.

DaSilva, J.N., C.M. Lourenco, A.A. Wilson, and S. Houle. 2001. Syntheses of the phosphodiesterase-4 inhibitors [^{11}C]Ro 20-1724, *R*-, *R/S*- and *S*-[^{11}C]rolipram. *J Label Compd Radiopharm.* 44:373-384.

Degerman, E., P. Belfrage, and V.C. Manganiello. 1997. Structure, localization, and regulation of cGMP-inhibited phosphodiesterase (PDE3). *J Biol Chem.* 272:6823-6.

Dousa, T.P. 1999. Cyclic-3',5'-nucleotide phosphodiesterase isozymes in cell biology and pathophysiology of the kidney. *Kidney Int.* 55:29-62.

Dulloo, A.G. 2002. Biomedicine. A sympathetic defense against obesity. *Science.* 297:780-1.

Dulloo, A.G., J. Seydoux, and L. Girardier. 1992. Potentiation of the thermogenic antiobesity effects of ephedrine by dietary methylxanthines: adenosine antagonism or phosphodiesterase inhibition? *Metabolism.* 41:1233-41.

Duplantier, A.J., M.S. Biggers, R.J. Chambers, J.B. Cheng, K. Cooper, D.B. Damon, J.F. Eggler, K.G. Kraus, A. Marfat, H. Masamune, J.S. Pillar, J.T. Shirley, J.P. Umland, and J.W. Watson. 1996. Biarylcarboxylic acids and -amides: inhibition of phosphodiesterase type IV versus [^{3}H]rolipram binding activity and their relationship to emetic behavior in the ferret. *J. Med. Chem.* 39:120-125.

Dym, O., I. Xenarios, H. Ke, and J. Colicelli. 2002. Molecular docking of competitive phosphodiesterase inhibitors. *Mol Pharmacol.* 61:20-5.

Dzimiri, N. 1999. Regulation of beta-adrenoceptor signaling in cardiac function and disease. *Pharmacol Rev.* 51:465-501.

Egawa, T., K. Mishima, Y. Matsumoto, K. Iwasaki, K. Iwasaki, and M. Fujiwara. 1997. Rolipram and its optical isomers, phosphodiesterase 4 inhibitors, attenuated the scopolamine-induced impairments of learning and memory in rats. *Jpn J Pharmacol.* 75:275-81.

Ekholm, D., P. Belfrage, V. Manganiello, and E. Degerman. 1997. Protein kinase A-dependent activation of PDE4 (cAMP-specific cyclic nucleotide phosphodiesterase) in cultured bovine vascular smooth muscle cells. *Biochim Biophys Acta.* 1356:64-70.

Elder, D.A., R.L. Prigeon, R.P. Wadwa, L.M. Dolan, and D.A. D'Alessio. 2005. {beta}-cell Function, Insulin Sensitivity and Glucose Tolerance in Obese Diabetic and Nondiabetic Adolescents and Young Adults. *J Clin Endocrinol Metab.*

Elia, M., and G. Livesey. 1992. Energy expenditure and fuel selection in biological systems: the theory and practice of calculations based on indirect calorimetry and tracer methods. *World Rev Nutr Diet.* 70:68-131.

Enerback, S., A. Jacobsson, E.M. Simpson, C. Guerra, H. Yamashita, M.E. Harper, and L.P. Kozak. 1997. Mice lacking mitochondrial uncoupling protein are cold-sensitive but not obese. *Nature.* 387:90-4.

Engels, P., S. Abdel'Al, P. Hulley, and H. Lübbert. 1995. Brain distribution of four rat homologues of the Drosophila *dunce* cAMP phosphodiesterase. *J. Neurosci. Res.* 41:169-178.

Engels, P., K. Fichtel, and H. Lübbert. 1994. Expression and regulation of human and rat phosphodiesterase type IV isogenes. *The FEBS Letters.* 350:291-295.

Enoksson, S., E. Degerman, E. Hagstrom-Toft, V. Large, and P. Arner. 1998. Various phosphodiesterase subtypes mediate the in vivo antilipolytic effect of insulin on adipose tissue and skeletal muscle in man. *Diabetologia.* 41:560-8.

Erdogan, S., and M.D. Houslay. 1997. Challenge of human jurkat T-cells with the adenylate cyclase activator forskolin elicits major changes in cAMP phosphodiesterase (PDE) expression by up-regulating PDE3 and inducing PDE4D1 and PDE4D2 splice variants as well as down-regulating a novel PDE4A splice variant. *Biochem. J.* 321:165-175.

Erickson, J.C., G. Hollopeter, and R.D. Palmiter. 1996. Attenuation of the obesity syndrome of ob/ob mice by the loss of neuropeptide Y. *Science.* 274:1704-7.

Esler, M., G. Jennings, G. Lambert, I. Meredith, M. Horne, and G. Eisenhofer. 1990. Overflow of catecholamine neurotransmitters to the circulation: source, fate, and functions. *Physiol Rev.* 70:963-85.

Esler, M., M. Rumantir, G. Wiesner, D. Kaye, J. Hastings, and G. Lambert. 2001. Sympathetic nervous system and insulin resistance: from obesity to diabetes. *Am J Hypertens.* 14:304S-309S.

Farley, C., J.A. Cook, B.D. Spar, T.M. Austin, and T.J. Kowalski. 2003. Meal pattern analysis of diet-induced obesity in susceptible and resistant rats. *Obes Res.* 11:845-51.

Fawcett, L., R. Baxendale, P. Stacey, C. McGrouther, I. Harrow, S. Soderling, J. Hetman, J.A. Beavo, and S.C. Phillips. 2000. Molecular cloning and characterization of a

distinct human phosphodiesterase gene family: PDE11A. *Proc Natl Acad Sci U S A.* 97:3702-7.

Fazli-Tabaei, S., M. Fahim, and A. Khoshbaten. 2006. Acute lead exposure and contraction of rat isolated aorta induced by D1-dopaminergic and alpha-adrenergic drugs. *Arch Iran Med.* 9:119-23.

Feve, B., K. Elhadri, A. Quignard-Boulange, and J. Pairault. 1994. Transcriptional down-regulation by insulin of the beta 3-adrenergic receptor expression in 3T3-F442A adipocytes: a mechanism for repressing the cAMP signaling pathway. *Proc Natl Acad Sci U S A.* 91:5677-81.

Fisher, S.J., J.C. Bruning, S. Lannon, and C.R. Kahn. 2005. Insulin signaling in the central nervous system is critical for the normal sympathoadrenal response to hypoglycemia. *Diabetes.* 54:1447-51.

Flegal, K.M., D.F. Williamson, E.R. Pamuk, and H.M. Rosenberg. 2004. Estimating deaths attributable to obesity in the United States. *Am J Public Health.* 94:1486-9.

Forster, C. 1998. Autonomic Nervous System Neurotransmitters. *In* Principles of Medical Pharmacology. H. Kalant, Roschlau, W., editor. Oxford University Press, New York. 135-148.

Francis, S.H., I.V. Turko, and J.D. Corbin. 2001. Cyclic nucleotide phosphodiesterases: relating structure and function. *Prog Nucleic Acid Res Mol Biol.* 65:1-52.

Frey, K.A. 1989. Positron emission tomography. *In* Basic neurochemistry: molecular, cellular, and medical aspects. G.J. Siegel, editor. Raven Press, New York. 839-855.

Fujita, M., and R.B. Innis. 2000. Nuclear psychiatry: specialty for the twenty-first century? *Eur J Nucl Med.* 27:S39-42.

Fujita, M., S.S. Zoghbi, M.S. Crescenzo, J. Hong, J.L. Musachio, J.Q. Lu, J.S. Liow, N. Seneca, D.N. Tipre, V.L. Cropley, M. Imaizumi, A.D. Gee, J. Seidel, M.V. Green, V.W. Pike, and R.B. Innis. 2005. Quantification of brain phosphodiesterase 4 in rat with (R)-[^{11}C]Rolipram-PET. *Neuroimage.* 26:1201-10.

Gao, J., L. Ghibaudi, M. van Heek, and J.J. Hwa. 2002. Characterization of diet-induced obese rats that develop persistent obesity after 6 months of high-fat followed by 1 month of low-fat diet. *Brain Res.* 936:87-90.

Gong, D.W., S. Monemdjou, O. Gavrilova, L.R. Leon, B. Marcus-Samuels, C.J. Chou, C. Everett, L.P. Kozak, C. Li, C. Deng, M.E. Harper, and M.L. Reitman. 2000. Lack of obesity and normal response to fasting and thyroid hormone in mice lacking uncoupling protein-3. *J Biol Chem.* 275:16251-7.

Hagstrom-Toft, E., J. Bolinder, S. Eriksson, and P. Arner. 1995. Role of phosphodiesterase III in the antilipolytic effect of insulin in vivo. *Diabetes.* 44:1170-5.

Hall, J.E., M.W. Brands, D.A. Hildebrandt, J. Kuo, and S. Fitzgerald. 2000. Role of sympathetic nervous system and neuropeptides in obesity hypertension. *Braz J Med Biol Res.* 33:605-18.

Hamm, H.E. 2001. How activated receptors couple to G proteins. *Proc Natl Acad Sci U S A.* 98:4819-21.

Hammadi, A., C. Crouzel, F. Hinnen, and S. Demphel. 1994. Synthesis of [^{18}F]- or [^{11}C]-1,2-diacylglycerol. *J Lab Com Rad.* 35:144-145.

Han, P., J. Werber, M. Surana, N. Fleischer, and T. Michaeli. 1999. The calcium/calmodulin-dependent phosphodiesterase PDE1C down-regulates glucose-induced insulin secretion. *J Biol Chem.* 274:22337-44.

Harada, N., S. Nishiyama, H. Ohba, K. Sato, T. Kakiuchi, and H. Tsukada. 2002. Age differences in phosphodiesterase type-IV and its functional response to dopamine D_1 receptor modulation in the living brain: a PET study in conscious monkeys. *Synapse.* 44:139-45.

Harper, M.E., and J. Himms-Hagen. 2001. Mitochondrial efficiency: lessons learned from transgenic mice. *Biochim Biophys Acta.* 1504:159-72.

Harris, M.I., Zimmet, P. 1992. Classification of diabetes mellitus and other categories of glucose intolerance. *In* International Textbood of Diabetes Mellitus. K.G.M.M. Alberti, DeFrunzo, R.A., Keen, H., & Zimmet, P., editor. John Wiley & Sons, Chichester, UK. 3-18.

Hatano, K., Y. Sakiyama, M. Suzuki, Y. Kawasumi, T. Kato, T. Kawakita, F. Suzuki, and K. Ito. 1999. Synthesis and biodistribution of [^{18}F]KF 19316, a phosphodiesterase type 4 inhibitor. *J. Labelled Cpd. Radiopharm.* 42, Suppl. 1:S624-626.

Haynes, W.G., D.A. Morgan, A. Djalali, W.I. Sivitz, and A.L. Mark. 1999. Interactions between the melanocortin system and leptin in control of sympathetic nerve traffic. *Hypertension.* 33:542-7.

Hering, D., V.K. Somers, T. Kara, W. Kucharska, P. Jurak, L. Bieniaszewski, and K. Narkiewicz. 2006. Sympathetic neural responses to smoking are age dependent. *J Hypertens.* 24:691-5.

Herscovitch, P. 1990. Principles of positron emission tomography. *In* Functional Imaging in Movement Disorders. W. Martin, editor. CRC Press, Boca Raton. 1-46.

Hetman, J.M., S.H. Soderling, N.A. Glavas, and J.A. Beavo. 2000. Cloning and characterization of PDE7B, a cAMP-specific phosphodiesterase. *Proc Natl Acad Sci U S A.* 97:472-6.

Hilton, J., F. Yokoi, R.F. Dannals, H.T. Ravert, Z. Szabo, and D.F. Wong. 2000. Column-switching HPLC for the analysis of plasma in PET imaging studies. *Nucl Med Biol.* 27:627-30.

Himms-Hagen, J. 1997. On raising energy expenditure in ob/ob mice. *Science.* 276:1132-3.

Himms-Hagen, J., J. Cerf, M. Desautels, and G. Zaror-Behrens. 1978. Thermogenic mechanisms and their control. *Experientia Suppl.* 32:119-34.

Hjeresen, D.L., A. Francendese, and J.M. O'Donnell. 1989. Microwave attenuation of ethanol-induced interactions with noradrenergic neurotransmitter systems. *Health Phys.* 56:767-76.

Hoffmann, R., G.S. Baillie, S.J. MacKenzie, S.J. Yarwood, and M.D. Houslay. 1999. The MAP kinase ERK2 inhibits the cyclic AMP-specific phosphodiesterase HSPDE4D3 by phosphorylating it at Ser579. *Embo J.* 18:893-903.

Hoffmann, R., I.R. Wilkinson, J.F. McCallum, P. Engels, and M.D. Houslay. 1998. cAmp-specific phosphodiesterase Hspde4d3 mutants which mimic activation and changes in rolipram inhibition triggered by protein kinase a phosphorylation of Ser-54: generation of a molecular model. *Biochem J.* 333:139-49.

Holden, C.A., S.C. Chan, S. Norris, and J.M. Hanifin. 1987. Histamine induced elevation of cyclic AMP phosphodiesterase activity in human monocytes. *Agents and Actions*. 22:36-42.

Houslay, M.D. 2001. PDE4 cAMP-specific phosphodiesterases. *Prog Nucleic Acid Res Mol Biol*. 69:249-315.

Houslay, M.D., and D.R. Adams. 2003. PDE4 cAMP phosphodiesterases: modular enzymes that orchestrate signalling cross-talk, desensitization and compartmentalization. *Biochem J*. 370:1-18.

Houslay, M.D., and W. Kolch. 2000. Cell-type specific integration of cross-talk between extracellular signal-regulated kinase and cAMP signaling. *Mol Pharmacol*. 58:659-68.

Houslay, M.D., and G. Milligan. 1997. Tailoring cAMP-signalling responses through isoform multiplicity. *TIBS*. 22:217-224.

Houslay, M.D., M. Sullivan, and G.B. Bolger. 1998. The multienzyme PDE4 cyclic adenosine monophosphate-specific phosphodiesterase family: intracellular targeting, regulation, and selective inhibition by compounds exerting anti-inflammatory and antidepressant actions. *Adv Pharmacol*. 44:225-342.

Houwing, H., L. Benthem, P.T. Van Suylichem, J. Van der Leest, J.H. Strubbe, and A.B. Steffens. 1995. Islet transplantation in diabetic rats normalizes basal and exercise-induced energy metabolism. *Diabetologia*. 38:919-26.

Huai, Q., J. Colicelli, and H. Ke. 2003. The crystal structure of AMP-bound PDE4 suggests a mechanism for phosphodiesterase catalysis. *Biochemistry*. 42:13220-6.

Huai, Q., Y. Sun, H. Wang, D. Macdonald, R. Aspiotis, H. Robinson, Z. Huang, and H. Ke. 2006. Enantiomer discrimination illustrated by the high resolution crystal structures of type 4 phosphodiesterase. *J Med Chem*. 49:1867-73.

Hughes, B., D. Howat, H. Lisle, M. Holbrook, T. James, N. Gozzard, K. Blease, P. Hughes, R. Kingaby, G. Warrellow, R. Alexander, J. Head, E. Boyd, M. Eaton, M. Perry, M. Wales, B. Smith, R. Owens, C. Catterall, S. Lumb, A. Russell, R. Allen, M. Merriman, D. Bloxham, and G. Higgs. 1996. The inhibition of antigen-induced eosinophilia and bronchoconstriction by CDP840, a novel stereo-selective inhibitor of phosphodiesterase type 4. *Br. J. Pharmacol*. 118:1183-1191.

Hughes, B., R. Owens, M. Perry, G. Warrellow, and R. Allen. 1997. PDE4 inhibitors: the use of molecular cloning in the design and development of novel drugs. *Drug Discovery Today*. 2:89-101.

Itoh, T., M. Tokumura, and K. Abe. 2004. Effects of rolipram, a phosphodiesterase 4 inhibitor, in combination with imipramine on depressive behavior, CRE-binding activity and BDNF level in learned helplessness rats. *Eur J Pharmacol*. 498:135-42.

Jacobitz, S., M.M. McLaughlin, G.P. Livi, M. Burman, and T.J. Torphy. 1996. Mapping the functional domains of human recombinant phosphodiesterase 4A: structural requirements for catalytic activity and rolipram binding. *Mol Pharmacol*. 50:891-9.

Jang, I., D. Hwang, J. Lee, K. Chae, Y. Kim, T. Kang, C. Kim, D. Shin, J. Hwang, Y. Huh, and J. Cho. 2003. Physiological difference between dietary obesity-susceptible and obesity-resistant Sprague Dawley rats in response to moderate high fat diet. *Exp Anim*. 52:99-107.

Jin, S.L., T. Bushnik, L. Lan, and M. Conti. 1998. Subcellular localization of rolipram-sensitive, cAMP-specific phosphodiesterases. Differential targeting and activation of the splicing variants derived from the PDE4D gene. *J Biol Chem.* 273:19672-8.

Jin, S.-L.C., J.V. Swinnen, and M. Conti. 1992. Characterization of the structure of a low K_m, rolipram-sensitive cAMP phosphodiesterase. *J. Biol. Chem.* 267:18929-18939.

Johnson, R.W., T. Reisine, S. Spotnitz, N. Wiech, R. Ursillo, and H.I. Yamamura. 1980. Effects of desipramine and yohimbine on alpha 2- and beta- adrenoreceptor sensitivity. *Eur J Pharmacol.* 67:123-7.

Joseph, S.S., J.A. Lynham, W.H. Colledge, and A.J. Kaumann. 2004. Binding of (-)-[^{3}H]-CGP12177 at two sites in recombinant human beta 1-adrenoceptors and interaction with beta-blockers. *Naunyn Schmiedebergs Arch Pharmacol.* 369:525-32.

Kaulen, P., G. Brüning, H.H. Schneider, M. Sarter, and H.G. Baumgarten. 1989. Autoradiographic mapping of selective cyclic adenosine monophosphate phosphodiesterase in rat brain with the antidepressant [^{3}H] rolipram. *Brain Res.* 503:229-245.

Kenk, M., M. Greene, R.S. Beanlands, M. Lortie, R.A. deKemp, S. Thorn, and J.N. DaSilva. 2006a. HPLC analysis of phosphodiesterase-4 inhibitor (R)-[^{11}C]rolipram metabolites in rat plasma, brain, heart, skeletal muscle and brown adipose tissue (submitted for publication). *J Label Compd Radiopharm.*

Kenk, M., M. Greene, R.A. deKemp, M. Lortie, S. Thorn, R.S. Beanlands, and J.N. DaSilva. 2006b. In vivo selective binding of (R)-[^{11}C]rolipram to phosphodiesterase-4 provides the basis for studying intracellular cAMP signaling in the periphery (submitted for publication). *Nuclear Medicine and Biology.*

Kern, W., A. Peters, J. Born, H.L. Fehm, and B. Schultes. 2005. Changes in blood pressure and plasma catecholamine levels during prolonged hyperinsulinemia. *Metabolism.* 54:391-6.

Klein, J., M. Fasshauer, M. Benito, and C.R. Kahn. 2000. Insulin and the beta3-adrenoceptor differentially regulate uncoupling protein-1 expression. *Mol Endocrinol.* 14:764-73.

Koch, W.J., R.J. Lefkowitz, and H.A. Rockman. 2000. Functional consequences of altering myocardial adrenergic receptor signaling. *Annu Rev Physiol.* 62:237-60.

Kopka, K., M.P. Law, H.J. Breyholz, A. Faust, C. Holtke, B. Riemann, O. Schober, M. Schafers, and S. Wagner. 2005. Non-invasive molecular imaging of beta-adrenoceptors in vivo: perspectives for PET-radioligands. *Curr Med Chem.* 12:2057-74.

Kovala, T., B.D. Sanwal, and E.H. Ball. 1997. Recombinant expression of a type IV, cAMP-specific phosphodiesterase: characterization and structure-function studies of deletion mutants. *Biochem.* 36:2968-2976.

Kraegen, E.W., P.W. Clark, A.B. Jenkins, E.A. Daley, D.J. Chisholm, and L.H. Storlien. 1991. Development of muscle insulin resistance after liver insulin resistance in high-fat-fed rats. *Diabetes.* 40:1397-403.

Krause, W., and G. Kühne. 1988. Pharmacokinetics of rolipram in the rhesus and cynomolgus monkeys, the rat and the rabbit. Studies on species differences. *Xenobiotica.* 18:561-571.

Krause, W., and G. Kühne. 1993. Biotransformation of the antidepressant D,L-rolipram. II. Metabolite patterns in man, rat, rabbit, rehesus and cynomolgus monkey. *Xenobiotica*. 23:1277-1288.

Lacroix, D., P. Blier, O. Curet, and C. de Montigny. 1991. Effects of long-term desipramine administration on noradrenergic neurotransmission: electrophysiological studies in the rat brain. *J Pharmacol Exp Ther*. 257:1081-90.

Laliberte, F., Y. Han, A. Govindarajan, A. Giroux, S. Liu, B. Bobechko, P. Lario, A. Bartlett, E. Gorseth, M. Gresser, and Z. Huang. 2000. Conformational difference between PDE4 apoenzyme and holoenzyme. *Biochemistry*. 39:6449-58.

Laliberte, F., S. Liu, E. Gorseth, B. Bobechko, A. Bartlett, P. Lario, M.J. Gresser, and Z. Huang. 2002. In vitro PKA phosphorylation-mediated human PDE4A4 activation. *FEBS Lett*. 512:205-8.

Landsberg, L. 2006. Feast or Famine: The Sympathetic Nervous System Response to Nutrient Intake. *Cell Mol Neurobiol*.

Landsberg, L., M.E. Saville, and J.B. Young. 1984. Sympathoadrenal system and regulation of thermogenesis. *Am J Physiol*. 247:E181-9.

Langin, D., D. Ekholm, M. Ridderstrale, M. Lafontan, and P. Belfrage. 1992. cAMP-dependent protein kinase activation mediated by beta 3-adrenergic receptors parallels lipolysis in rat adipocytes. *Biochim Biophys Acta*. 1135:349-52.

Lateef, H., O.I. Abatan, M.N. Aslam, M.J. Stevens, and J. Varani. 2005. Topical pretreatment of diabetic rats with all-trans retinoic acid improves healing of subsequently induced abrasion wounds. *Diabetes*. 54:855-61.

Lauterio, T.J., J.P. Bond, and E.A. Ulman. 1994. Development and characterization of a purified diet to identify obesity-susceptible and resistant rat populations. *J Nutr*. 124:2172-8.

Law, M.P. 1993. Demonstration of the suitability of CGP 12177 for in vivo studies of beta-adrenoceptors. *Br J Pharmacol*. 109:1101-9.

Lee, M.E., J. Markowitz, J.O. Lee, and H. Lee. 2002. Crystal structure of phosphodiesterase 4D and inhibitor complex(1). *FEBS Lett*. 530:53-8.

Lee, M.S., I. Chang, and S. Kim. 2004. Death effectors of beta-cell apoptosis in type 1 diabetes. *Mol Genet Metab*. 83:82-92.

Leenen, F.H., E. Coletta, and R. White. 2006. Sympatho-excitatory responses to once-daily dihydropyridines in young versus older hypertensive patients: amlodipine versus felodipine extended release. *J Hypertens*. 24:177-84.

Levin, B.E., and A.A. Dunn-Meynell. 2000. Defense of body weight against chronic caloric restriction in obesity-prone and -resistant rats. *Am J Physiol Regul Integr Comp Physiol*. 278:R231-7.

Levin, B.E., A.A. Dunn-Meynell, B. Balkan, and R.E. Keesey. 1997. Selective breeding for diet-induced obesity and resistance in Sprague-Dawley rats. *Am J Physiol*. 273:R725-30.

Levin, B.E., E.K. Govek, and A.A. Dunn-Meynell. 1998. Reduced glucose-induced neuronal activation in the hypothalamus of diet-induced obese rats. *Brain Res*. 808:317-9.

Levin, B.E., S. Hogan, and A.C. Sullivan. 1989. Initiation and perpetuation of obesity and obesity resistance in rats. *Am J Physiol*. 256:R766-71.

Levin, B.E., and R.E. Keesey. 1998. Defense of differing body weight set points in diet-induced obese and resistant rats. *Am J Physiol.* 274:R412-9.

Levin, B.E., and A.C. Sullivan. 1987. Glucose-induced norepinephrine levels and obesity resistance. *Am J Physiol.* 253:R475-81.

Levin, B.E., and A.C. Sullivan. 1989. Glucose-induced sympathetic activation in obesity-prone and resistant rats. *Int J Obes.* 13:235-46.

Levin, B.E., J. Triscari, S. Hogan, and A.C. Sullivan. 1987. Resistance to diet-induced obesity: food intake, pancreatic sympathetic tone, and insulin. *Am J Physiol.* 252:R471-8.

Levin, B.E., J. Triscari, and A.C. Sullivan. 1983. Altered sympathetic activity during development of diet-induced obesity in rat. *Am J Physiol.* 244:R347-55.

Liang, L., E. Beshay, and G.J. Prud'homme. 1998. The phosphodiesterase inhibitors pentoxifylline and rolipram prevent diabetes in NOD mice. *Diabetes.* 47:570-5.

Lim, J., G. Pahlke, and M. Conti. 1999. Activation of the cAMP-specific Phosphodiesterase PDE4D3 by Phosphorylation. Identification and function of an inhibitory domain. *J Biol Chem.* 274:19677-19685.

Liu, S., F. Laliberte, B. Bobechko, A. Bartlett, P. Lario, E. Gorseth, J. Van Hamme, M.J. Gresser, and Z. Huang. 2001. Dissecting the cofactor-dependent and independent bindings of PDE4 inhibitors. *Biochemistry.* 40:10179-86.

Lobban, M., Y. Shakur, J. Beattie, and M.D. Houslay. 1994. Identification of two splice variant forms of type-IV_B cyclic AMP phosphodiesterase, DPD (rPDE-IV_{B1}) and PDE-4 (rPDE-IV_{B2}) in brain: selective localization in membrane and cytosolic compartments and differential expression in various brain regions. *Biochemical Journal.* 304:399-406.

Lourenco, C.M., J.N. DaSilva, J.J. Warsh, A.A. Wilson, and S. Houle. 1999a. Imaging of cAMP-specific phosphodiesterase-IV: comparison of [^{11}C]rolipram and [^{11}C]Ro 20-1724 in rats. *Synapse.* 31:41-50.

Lourenco, C.M., J.N. DaSilva, A.A. Wilson, and S. Houle. 1999b. Metabolism of the phosphodiesterase-4 inhibitor R-[^{11}C]rolipram in rat plasma and brain. *J. Label. Compd. Radiopharm.* 42:S663-S665.

Lourenco, C.M., S. Houle, A.A. Wilson, and J.N. DaSilva. 2001. Characterization of (*R*)-[^{11}C]rolipram for PET imaging of phosphodiesterase-4: in vivo binding, metabolism, and dosimetry studies in rats. *Nucl Med Biol.* 28:347-58.

Lourenco, C.M., M. Kenk, R.S. Beanlands, and J.N. DaSilva. 2006. Increasing synaptic noradrenaline, serotonin and histamine enhances in vivo binding of phosphodiesterase-4 inhibitor (R)-[^{11}C]rolipram in rat brain, lung and heart. *Life Sci.* 79:356-64.

Lowell, B.B., and E.S. Bachman. 2003. Beta-Adrenergic receptors, diet-induced thermogenesis, and obesity. *J Biol Chem.* 278:29385-8.

Lowell, B.B., and J.S. Flier. 1997. Brown adipose tissue, beta 3-adrenergic receptors, and obesity. *Annu Rev Med.* 48:307-16.

Lowell, B.B., S.S. V, A. Hamann, J.A. Lawitts, J. Himms-Hagen, B.B. Boyer, L.P. Kozak, and J.S. Flier. 1993. Development of obesity in transgenic mice after genetic ablation of brown adipose tissue. *Nature.* 366:740-2.

Luisi, A.J., J.A. Fallavollita, G. Suzuki, R. deKemp, M.S. Haka, S.A. Toorongian, and J.M. Canty, Jr. 2005. Regional ^{11}C-Hydroxyephedrine Uptake in Hibernating

Myocardium: Chronic Inhomogeneity of Sympathetic Innervation in the Absence of Infarction. *J Nucl Med.* 46:1368-1374.

MacKenzie, S.J., G.S. Baillie, I. McPhee, G.B. Bolger, and M.D. Houslay. 2000. ERK2 mitogen-activated protein kinase binding, phosphorylation, and regulation of the PDE4D cAMP-specific phosphodiesterases. The involvement of COOH-terminal docking sites and NH2-terminal UCR regions. *J Biol Chem.* 275:16609-17.

MacKenzie, S.J., G.S. Baillie, I. McPhee, C. MacKenzie, R. Seamons, T. McSorley, J. Millen, M.B. Beard, G. van Heeke, and M.D. Houslay. 2002. Long PDE4 cAMP specific phosphodiesterases are activated by protein kinase A-mediated phosphorylation of a single serine residue in Upstream Conserved Region 1 (UCR1). *Br J Pharmacol.* 136:421-33.

Madelian, V., and E. La Vigne. 1996. Rapid Regulation of a Cyclic AMP-Specific Phosphodiesterase (PDE IV) by Forskolin and Isoproterenol in LRM55 Astroglial Cells. *Biochem Pharmacol.* 51:1739 - 1747.

Mallem, Y., D. Holopherne, O. Reculeau, O. Le Coz, J.C. Desfontis, and M. Gogny. 2005. Beta-adrenoceptor-mediated vascular relaxation in spontaneously hypertensive rats. *Auton Neurosci.* 118:61-7.

Maltsev, V.A., G.J. Ji, A.M. Wobus, B.K. Fleischmann, and J. Hescheler. 1999. Establishment of beta-adrenergic modulation of L-type Ca^{2+} current in the early stages of cardiomyocyte development. *Circ Res.* 84:136-45.

Manning, C.D., M.M. McLaughlin, G.P. Livi, L.B. Cieslinski, T.J. Torphy, and M.S. Barnette. 1996. Prolonged beta adrenoceptor stimulation up-regulates cAMP phosphodiesterase activity in human monocytes by increasing mRNA and protein for phosphodiesterases 4A and 4B. *J Pharmacol Exp Ther.* 276:810-818.

Martinez-Merlos, M.T., M. Angeles-Castellanos, M. Diaz-Munoz, R. Aguilar-Roblero, J. Mendoza, and C. Escobar. 2004. Dissociation between adipose tissue signals, behavior and the food-entrained oscillator. *J Endocrinol.* 181:53-63.

Maskrey, M., P.R. Wiggins, and P.B. Frappell. 2001. Behavioral thermoregulation in obese and lean Zucker rats in a thermal gradient. *Am J Physiol Regul Integr Comp Physiol.* 281:R1675-80.

Masuo, K., H. Mikami, T. Ogihara, and M.L. Tuck. 1997. Sympathetic nerve hyperactivity precedes hyperinsulinemia and blood pressure elevation in a young, nonobese Japanese population. *Am J Hypertens.* 10:77-83.

Matsuo, T., and M. Suzuki. 1997. Brain beta-adrenergic receptor binding in rats with obesity induced by a beef tallow diet. *Metabolism.* 46:18-22.

Maurice, D.H., D. Palmer, D.G. Tilley, H.A. Dunkerley, S.J. Netherton, D.R. Raymond, H.S. Elbatarny, and S.L. Jimmo. 2003. Cyclic nucleotide phosphodiesterase activity, expression, and targeting in cells of the cardiovascular system. *Mol Pharmacol.* 64:533-46.

McCall, R.B., M.R. Schuette, S.J. Humphrey, R.A. Lahti, and C. Barsuhn. 1983. Evidence for a central sympathoexcitatory action of alpha-2 adrenergic antagonists. *J Pharmacol Exp Ther.* 224:501-7.

McIntyre, R.S., J.K. Soczynska, J.Z. Konarski, and S.H. Kennedy. 2006. The effect of antidepressants on glucose homeostasis and insulin sensitivity: synthesis and mechanisms. *Expert Opin Drug Saf.* 5:157-68.

McLaughlin, M.M., L.B. Cieslinski, M. Burman, T.J. Torphy, and G.P. Livi. 1993. A low-K_m, rolipram-sensitive, cAMP-specific phosphodiesterase from human brain. *J. Biol. Chem.* 268:6470-6476.

Miro, X., S. Perez-Torres, F. Artigas, P. Puigdomenech, J.M. Palacios, and G. Mengod. 2002. Regulation of cAMP phosphodiesterase mRNAs expression in rat brain by acute and chronic fluoxetine treatment. An in situ hybridization study. *Neuropharmacology.* 43:1148-57.

Molenaar, P., and W.A. Parsonage. 2005. Fundamental considerations of beta-adrenoceptor subtypes in human heart failure. *Trends Pharmacol Sci.* 26:368-75.

Monaco, L., E. Vicini, and M. Conti. 1994. Structure of two rat genes coding for closely related rolipram-sensitive cAMP phosphodiesterases. *J Biol Chem.* 269:347-357.

Morisco, C., G. Condorelli, V. Trimarco, A. Bellis, C. Marrone, J. Sadoshima, and B. Trimarco. 2005. Akt mediates the cross-talk between beta-adrenergic and insulin receptors in neonatal cardiomyocytes. *Circ Res.* 96:180-8.

Morris, M.J., and J.M. Pavia. 2004. Increased endogenous noradrenaline and neuropeptide Y release from the hypothalamus of streptozotocin diabetic rats. *Brain Res.* 1006:100-6.

Müller, B., C. Lugnier, and J.-C. Stoclet. 1990. Involvement of rolipram-sensitive cyclic AMP phosphodiesterase in the regulation of cardiac contraction. *J Cardiovasc Pharmacol.* 16:796-803.

Müller, T., P. Engels, and J.R. Fozard. 1996. Subtypes of the type 4 cAMP phosphodiesterases: structure, regulation and selective inhibition. *TIPS.* 17:294-298.

Muntzel, M.S., D.A. Morgan, A.L. Mark, and A.K. Johnson. 1994. Intracerebroventricular insulin produces nonuniform regional increases in sympathetic nerve activity. *Am J Physiol.* 267:R1350-5.

Nagai, N., N. Sakane, T. Hamada, T. Kimura, and T. Moritani. 2005. The effect of a high-carbohydrate meal on postprandial thermogenesis and sympathetic nervous system activity in boys with a recent onset of obesity. *Metabolism.* 54:430-8.

Nagaoka, T., T. Shirakawa, T.W. Balon, J.C. Russell, and Y. Fujita-Yamaguchi. 1998. Cyclic nucleotide phosphodiesterase 3 expression in vivo: evidence for tissue-specific expression of phosphodiesterase 3A or 3B mRNA and activity in the aorta and adipose tissue of atherosclerosis-prone insulin-resistant rats. *Diabetes.* 47:1135-44.

Nedergaard, J., and B. Cannon. 2003. The 'novel' 'uncoupling' proteins UCP2 and UCP3: what do they really do? Pros and cons for suggested functions. *Exp Physiol.* 88:65-84.

Némoz, G., A.-F. Prigent, M. Moueqqit, S. Fougier, O. Macovschi, and H. Pacheco. 1985. Selective inhibition of one of the cyclic AMP phosphodiesterases from rat brain by the neurotropic compound rolipram. *Biochem. Pharmacol.* 34:2997-3000.

Netherton, S.J., S.L. Jimmo, D. Palmer, D.G. Tilley, H.A. Dunkerley, D.R. Raymond, J.C. Russell, P.M. Absher, E.H. Sage, R.B. Vernon, and D.H. Maurice. 2002. Altered phosphodiesterase 3-mediated cAMP hydrolysis contributes to a hypermotile phenotype in obese JCR:LA-cp rat aortic vascular smooth muscle

cells: implications for diabetes-associated cardiovascular disease. *Diabetes.* 51:1194-200.

Nevzorova, J., B.A. Evans, T. Bengtsson, and R.J. Summers. 2006. Multiple signalling pathways involved in beta2-adrenoceptor-mediated glucose uptake in rat skeletal muscle cells. *Br J Pharmacol.* 147:446-54.

Nibuya, M., E.J. Nestler, and R.S. Duman. 1996. Chronic antidepressant administration increases the expression of cAMP response element binding protein (CREB) in rat hippocampus. *J. Neurosci.* 16:2365-2372.

Nicholson, C.D., R.A.J. Challiss, and M. Shahid. 1991. Differential modulation of tissue function and therapeutic potential of selective inhibitors of cyclic mucleotide phosphodiesterase isoenzymes. *TIPS.* 12:19-27.

Nicolas, C., D. Lacasa, Y. Giudicelli, Y. Demarne, B. Agli, M.J. Lecourtier, and C. Lhuillery. 1991. Dietary (n-6) polyunsaturated fatty acids affect beta-adrenergic receptor binding and adenylate cyclase activity in pig adipocyte plasma membrane. *J Nutr.* 121:1179-86.

Novak, I. 1998. beta-Adrenergic regulation of ion transport in pancreatic ducts: patch-clamp study of isolated rat pancreatic ducts. *Gastroenterology.* 115:714-21.

O'Donnell, J.M., and H.T. Zhang. 2004. Antidepressant effects of inhibitors of cAMP phosphodiesterase (PDE4). *Trends Pharmacol Sci.* 25:158-63.

Oleshansky, M.A., and N.H. Neff. 1975. Rat pineal adenosine cyclic 3',5'-monophosphate phosphodiesterase activity: modulation in vivo by a beta adrenergic receptor. *Mol. Pharmacol.* 11:552-557.

Pacak, K., I. Armando, S. Komoly, K. Fukuhara, V.K. Weise, C. Holmes, I.J. Kopin, and D.S. Goldstein. 1992. Hypercortisolemia inhibits yohimbine-induced release of norepinephrine in the posterolateral hypothalamus of conscious rats. *Endocrinol.* 131:1369-1376.

Palczewski, K., T. Kumasaka, T. Hori, C.A. Behnke, H. Motoshima, B.A. Fox, I. Le Trong, D.C. Teller, T. Okada, R.E. Stenkamp, M. Yamamoto, and M. Miyano. 2000. Crystal structure of rhodopsin: A G protein-coupled receptor. *Science.* 289:739-45.

Parker, C.A., J.C. Matthews, R.N. Gunn, L. Martarello, V.J. Cunningham, D. Dommett, S.T. Knibb, D. Bender, S. Jakobsen, J. Brown, and A.D. Gee. 2005. Behaviour of [^{11}C]R(-)- and [^{11}C]S(+)-rolipram in vitro and in vivo, and their use as PET radiotracers for the quantificative assay of PDE4. *Synapse.* 55:270-9.

Parker, J.C., M.A. VanVolkenburg, R.J. Ketchum, K.L. Brayman, and K.M. Andrews. 1995. Cyclic AMP phosphodiesterases of human and rat islets of Langerhans: contributions of types III and IV to the modulation of insulin secretion. *Biochem Biophys Res Commun.* 217:916-23.

Parker, J.C., M.A. VanVolkenburg, N.A. Nardone, D.M. Hargrove, and K.M. Andrews. 1997. Modulation of insulin secretion and glycemia by selective inhibition of cyclic AMP phosphodiesterase III. *Biochem Biophys Res Commun.* 236:665-9.

Pascoe, W.S., A.B. Jenkins, M. Kusunoki, and L.H. Storlien. 1992. Insulin action and determinants of glycaemia in a rat model of type 2 (non-insulin-dependent) diabetes mellitus. *Diabetologia.* 35:208-15.

Patel, J.N., G. Eisenhofer, S.W. Coppack, and J.M. Miles. 1999. Norepinephrine spillover in forearm and subcutaneous adipose tissue before and after eating. *J Clin Endocrinol Metab.* 84:2815-9.

Pelleymounter, M.A., M.J. Cullen, M.B. Baker, R. Hecht, D. Winters, T. Boone, and F. Collins. 1995. Effects of the obese gene product on body weight regulation in ob/ob mice. *Science.* 269:540-3.

Picard, F., D. Bruel, D. Servent, W. Saba, C. Fruchart-Gaillard, M.A. Schollhorn-Peyronneau, D. Roumenov, E. Brodtkorb, S. Zuberi, A. Gambardella, B. Steinborn, A. Hufnagel, H. Valette, and M. Bottlaender. 2006. Alteration of the in vivo nicotinic receptor density in ADNFLE patients: a PET study. *Brain.*

Pierce, K.L., R.T. Premont, and R.J. Lefkowitz. 2002. Seven-transmembrane receptors. *Nat Rev Mol Cell Biol.* 3:639-50.

Pillai, R., K. Kytle, A. Reyes, and J. Colicelli. 1993. Use of a yeast expression system for the isolation and analysis of drug-resistant mutants of a mammalian phosphodiesterase. *Proc. Natl. Acad. Sci. USA.* 90:11970 - 11974.

Pyne, N.J., W. Cushley, H.G. Nimmo, and M.D. Houslay. 1989. Insulin stimulates the tyrosyl phosphorylation and activation of the 52 kDa peripheral plasma-membrane cyclic AMP phosphodiesterase in intact hepatocytes. *Biochem J.* 261:897-904.

Pyne, N.J., and B.L. Furman. 2003. Cyclic nucleotide phosphodiesterases in pancreatic islets. *Diabetologia.* 46:1179-89.

Reed, M.J., K. Meszaros, L.J. Entes, M.D. Claypool, J.G. Pinkett, T.M. Gadbois, and G.M. Reaven. 2000. A new rat model of type 2 diabetes: the fat-fed, streptozotocin-treated rat. *Metabolism.* 49:1390-4.

Reynisdottir, S., H. Wahrenberg, K. Carlstrom, S. Rossner, and P. Arner. 1994. Catecholamine resistance in fat cells of women with upper-body obesity due to decreased expression of beta 2-adrenoceptors. *Diabetologia.* 37:428-35.

Riachi, M., J. Himms-Hagen, and M.E. Harper. 2004. Percent relative cumulative frequency analysis in indirect calorimetry: application to studies of transgenic mice. *Can J Physiol Pharmacol.* 82:1075-83.

Ricci, M.R., and B.E. Levin. 2003. Ontogeny of diet-induced obesity in selectively bred Sprague-Dawley rats. *Am J Physiol Regul Integr Comp Physiol.* 285:R610-8.

Richter, W., and M. Conti. 2002. Dimerization of the type 4 cAMP-specific phosphodiesterases is mediated by the upstream conserved regions (UCRs). *J Biol Chem.* 277:40212-21.

Richter, W., and M. Conti. 2004. The oligomerization state determines regulatory properties and inhibitor sensitivity of type 4 cAMP-specific phosphodiesterases. *J Biol Chem.* 279:30338-48.

Ricquier, D., C. Fleury, M. Larose, D. Sanchis, C. Pecqueur, S. Raimbault, C. Gelly, D. Vacher, A.M. Cassard-Doulcier, C. Levi-Meyrueis, O. Champigny, B. Miroux, and F. Bouillaud. 1999. Contributions of studies on uncoupling proteins to research on metabolic diseases. *J Intern Med.* 245:637-42.

Robidoux, J., T.L. Martin, and S. Collins. 2004. Beta-Adrenergic Receptors and Regulation of Energy Expenditure: A Family Affair. *Annu Rev Pharmacol Toxicol.* 44:297-323.

Robison, G.A., R.W. Butcher, and E.W. Sutherland. 1968. Cyclic AMP. *Annu Rev Biochem.* 37:149-74.

Rohrer, D.K., A. Chruscinski, E.H. Schauble, D. Bernstein, and B.K. Kobilka. 1999. Cardiovascular and metabolic alterations in mice lacking both beta1- and beta2-adrenergic receptors. *J Biol Chem.* 274:16701-8.

Rolland, V., S. Roseau, G. Fromentin, S. Nicolaidis, D. Tome, and P.C. Even. 2002. Body weight, body composition, and energy metabolism in lean and obese Zucker rats fed soybean oil or butter. *Am J Clin Nutr.* 75:21-30.

Rossner, S., C.L. Taylor, R.P. Byington, and C.D. Furberg. 1990. Long term propranolol treatment and changes in body weight after myocardial infarction. *Bmj.* 300:902-3.

Saad, M.F., W.C. Knowler, D.J. Pettitt, R.G. Nelson, M.A. Charles, and P.H. Bennett. 1991. A two-step model for development of non-insulin-dependent diabetes. *Am J Med.* 90:229-35.

Saad, M.F., W.C. Knowler, D.J. Pettitt, R.G. Nelson, D.M. Mott, and P.H. Bennett. 1989. Sequential changes in serum insulin concentration during development of non-insulin-dependent diabetes. *Lancet.* 1:1356-9.

Sasaki, T., K. Furukata, T. Iimori, S. Ikegami, S. Ide, T. Hosokami, and M. Senda. 1995. 1-Acetyl-7-deacetylforskolin: a potential non-specific inactive analog of forskolin for estimation of its specific high-affinity binding and adenylyl cyclase stimulation in vitro. *Life Sci.* 57:1367-1373.

Sasaki, T., I. Ogihara-Umeda, H. Nishigori, S. Ikegami, M. Senda, K. Kitani, K. Ogawa, and T. Nozaki. 1991. Rapid synthesis of ^{14}C forskolin by a route suitable for ^{11}C labeling. *J Lab Com Rad.* 24:557-565.

Sato, N., H. Hashimoto, Y. Takiguchi, and M. Nakashima. 1990. Effect of an aldose reductase inhibitor on altered sympathetic nerve responsiveness of isolated right atria in diabetic rats. *Arzneimittelforschung.* 40:763-6.

Sawant, S.P., A.V. Dnyanmote, K. Shankar, P.B. Limaye, J.R. Latendresse, and H.M. Mehendale. 2004. Potentiation of carbon tetrachloride hepatotoxicity and lethality in type 2 diabetic rats. *J Pharmacol Exp Ther.* 308:694-704.

Schmid, H., L.A. Forman, X. Cao, P.S. Sherman, and M.J. Stevens. 1999. Heterogeneous cardiac sympathetic denervation and decreased myocardial nerve growth factor in streptozotocin-induced diabetic rats: implications for cardiac sympathetic dysinnervation complicating diabetes. *Diabetes.* 48:603-8.

Schmidt, R.E., D.A. Dorsey, L.N. Beaudet, K.E. Frederick, C.A. Parvin, S.B. Plurad, and M.G. Levisetti. 2003. Non-obese diabetic mice rapidly develop dramatic sympathetic neuritic dystrophy: a new experimental model of diabetic autonomic neuropathy. *Am J Pathol.* 163:2077-91.

Schmiechen, R., H.H. Schneider, and H. Wachtel. 1990. Close correlation between behavioural response and binding in vivo for inhibitors of the rolipram-sensitive phosphodiesterase. *Psychopharm.* 102:17-20.

Schneider, H.H. 1984. Brain cAMP response to phosphodiesterase inhibitors in rats killed by microwave irradiation or decapitation. *Biochem Pharm.* 33:1690-1693.

Schneider, H.H., R. Schmiechen, M. Brezinski, and J. Seidler. 1986. Stereospecific binding of the antidepressant rolipram to brain protein structures. *Eur J Pharmacol.* 127:105-115.

Schudt, C., S. Winder, B. Müller, and D. Ukena. 1991. Zardaverine as a selective inhibitor of phosphodiesterase isozymes. *Biochem. Pharmacol.* 42:153-162.

Schutz, Y. 1995. The basis of direct and indirect calorimetry and their potentials. *Diabetes Metab Rev.* 11:383-408.

Schwabe, U., M. Miyake, Y. Ohga, and J.W. Daly. 1976. 4-(3-cyclopentyloxy-4-methoxyphenyl)-2-pyrrolidone (ZK 62711): a potent inhibitor of adenosine cyclic 3',5'-monophosphate phosphodiesterases in homogenates and tissue slices from rat brain. *Mol. Pharmacol.* 12:900-910.

Sedvall, G., L. Farde, H. Hall, S. Pauli, A. Persson, and F.A. Wiesel. 1988. PET Scanning - A new tool in clinical psychopharmacology. *Psychopharmacol. Ser.* 5:27-33.

Seidell, J.C. 1997. Time trends in obesity: an epidemiological perspective. *Horm Metab Res.* 29:155-8.

Seifert, R., and K. Wenzel-Seifert. 2002. Constitutive activity of G-protein-coupled receptors: cause of disease and common property of wild-type receptors. *Naunyn Schmiedebergs Arch Pharmacol.* 366:381-416.

Sette, C., and M. Conti. 1996. Phosphorylation and activation of a cAMP-specific phosphodiesterase by the cAMP-dependent protein kinase. *J. Biol. Chem.* 271:16526-16534.

Sette, C., S. Iona, and M. Conti. 1994a. The short-term activation of a rolipram-sensitive, cAMP-specific phosphodiesterase by thyroid-stimulating hormone in thyroid FRTL-5 cells is mediated by a cAMP-dependent phosphorylation. *J Biol Chem.* 269:9245-9252.

Sette, C., E. Vicini, M. Hess, and M. Conti. 1994b. Short-term activation of a rolipram-sensitive, cAMP-specific phosphodiesterase through a cAMP-dependent phosphorylation. *The FASEB Journal.* 8:A370.

Shafiee-Nick, R., N.J. Pyne, and B.L. Furman. 1995. Effects of type-selective phosphodiesterase inhibitors on glucose-induced insulin secretion and islet phosphodiesterase activity. *Br J Pharmacol.* 115:1486-92.

Shakur, Y., M. Wilson, L. Pooley, M. Lobban, S.L. Griffiths, A.M. Campbell, J. Beattie, C. Daly, and M.D. Houslay. 1995. Identification and characterization of the type-ivA cyclic AMP-specific phosphodiesterase RD1 as a membrane-bound protein expressed in cerebellum. *Biochem. J.* 306:801-809.

Sharma, A.M., T. Pischon, S. Hardt, I. Kunz, and F.C. Luft. 2001. Hypothesis: Beta-adrenergic receptor blockers and weight gain: A systematic analysis. *Hypertension.* 37:250-4.

Sharp, G.W. 1979. The adenylate cyclase-cyclic AMP system in islets of Langerhans and its role in the control of insulin release. *Diabetologia.* 16:287-96.

Snitker, S., I. Macdonald, E. Ravussin, and A. Astrup. 2000. The sympathetic nervous system and obesity: role in aetiology and treatment. *Obes Rev.* 1:5-15.

Soderling, S.H., S.J. Bayuga, and J.A. Beavo. 1999. Isolation and characterization of a dual-substrate phosphodiesterase gene family: PDE10A. *Proc Natl Acad Sci U S A.* 96:7071-6.

Soeder, K.J., S.K. Snedden, W. Cao, G.J. Della Rocca, K.W. Daniel, L.M. Luttrell, and S. Collins. 1999. The beta3-adrenergic receptor activates mitogen-activated protein kinase in adipocytes through a Gi-dependent mechanism. *J Biol Chem.* 274:12017-22.

Souness, J.E., B.K. Diocee, W. Martin, and S.A. Moodie. 1990. Pig aortic endothelial-cell cyclic nucleotide phosphodiesterases. *Biochem. J.* 266:127-132.

Souness, J.E., and S. Rao. 1997. Proposal for pharmacologically distinct conformers of PDE4 cyclic AMP phosphodiesterases. *Cell. Signal.* 9:227-236.

Steinberg, S.F., and L.L. Brunton. 2001. Compartmentation of G protein-coupled signaling pathways in cardiac myocytes. *Annu Rev Pharmacol Toxicol.* 41:751-73.

Stevens, M.J. 2001. New imaging techniques for cardiovascular autonomic neuropathy: a window on the heart. *Diabetes Technol Ther.* 3:9-22.

Storlien, L.H., D.E. James, K.M. Burleigh, D.J. Chisholm, and E.W. Kraegen. 1986. Fat feeding causes widespread in vivo insulin resistance, decreased energy expenditure, and obesity in rats. *Am J Physiol.* 251:E576-83.

Surwit, R.S., T.M. Dixon, A.E. Petro, K.W. Daniel, and S. Collins. 2000. Diazoxide restores beta3-adrenergic receptor function in diet-induced obesity and diabetes. *Endocrinology.* 141:3630-7.

Surwit, R.S., C.M. Kuhn, C. Cochrane, J.A. McCubbin, and M.N. Feinglos. 1988. Diet-induced type II diabetes in C57BL/6J mice. *Diabetes.* 37:1163-7.

Suzuki, H., M. Nishizawa, M. Ichikawa, K. Kumagai, M. Ryuzaki, H. Kumagai, T. Saruta, and H. Ikeda. 1999. Basal sympathetic nerve activity is enhanced with augmentation of baroreceptor reflex in Wistar fatty rats: a model of obesity-induced NIDDM. *J Hypertens.* 17:959-64.

Swinnen, J.V., D.R. Joseph, and M. Conti. 1989. The mRNA encoding a high-affinity cAMP phosphodiesterase is regulated by hormones and cAMP. *Proc Nat Ac Sci USA.* 86:8197-8201.

Szemeredi, K., S. Komoly, I.J. Kopin, G. Bagdy, H.R. Keiser, and D.S. Goldstein. 1991. Simultaneous measurement of plasma and brain extracellular fluid concentrations of catechols after yohimbine administration in rats. *Brain Res.* 542:8-14.

Takahashi, M., R. Terwilliger, C. Lane, P.S. Mezes, M. Conti, and R.S. Duman. 1999. Chronic antidepressant administration increases the expression of cAMP-specific phosphodiesterase 4A and 4B isoforms. *J Neurosci.* 19:610-618.

Takahashi, T., T. Ido, H. Ashino, A. Ootake, R. Iwata, and K. Yanai. 1994. [^{18}F]Labeled 1,2-Diacylglycerols ; A New Tracer for the Imaging of Second Messenger System.517-519.

Taniguchi, H., M. Tanida, N. Okumura, J. Hamada, S. Sano, and K. Nagai. 2006. Regulation of sympathetic and parasympathetic nerve activities by BIT/SHPS-1. *Neurosci Lett.* 398:102-6.

Tenor, H., and C. Schudt. 1996. Analysis of PDE isoenzyme profiles in cells and tissues by pharmacological methods. *In* Phosphodiesterase inhibitors. C. Schudt, G. Dent, and K.F. Rabe, editors. Academic Press, San Diego. 21-40.

Tentolouris, N., C. Tsigos, D. Perea, E. Koukou, D. Kyriaki, E. Kitsou, S. Daskas, Z. Daifotis, K. Makrilakis, S.A. Raptis, and N. Katsilambros. 2003. Differential effects of high-fat and high-carbohydrate isoenergetic meals on cardiac autonomic nervous system activity in lean and obese women. *Metabolism.* 52:1426-32.

Tetsuka, T., E. Kusano, S. Takeda, S. Homma, I. Yoshida, Y. Ando, and Y. Asano. 1995. Activation of protein kinase C stimulates cAMP phosphodiesterase in rat renal collecting tubule. *Am J Physiol.* 268:F808-14.

Torphy, T.J., J.M. Stadel, M. Burman, L.B. Cieslinski, M.M. McLaughlin, J.R. White, and G.P. Livi. 1992a. Coexpression of human cAMP-specific phosphodiesterase activity and high affinity rolipram binding in yeast. *J. Biol. Chem.* 267:1798-1804.

Torphy, T.J., H.-L. Zhou, and L.B. Cieslinski. 1992b. Stimulation of *beta* adrenoceptors in a human monocyte cell line (U937) up-regulates cyclic AMP-specific phosphodiesterase activity. *J Pharmacol Exp Ther.* 263:1195-1205.

Tschop, M., and M.L. Heiman. 2001. Rodent obesity models: an overview. *Exp Clin Endocrinol Diabetes.* 109:307-19.

Tseng, H., J.M. Link, J.R. Stratton, and J.H. Caldwell. 2001. Cardiac receptor physiology and its application to clinical imaging: present and future. *J Nucl Cardiol.* 8:390-409.

Tsukada, H., D. Fukumoto, S. Nishiyama, K. Sato, and T. Kakiuchi. 2004. Transient focal ischemia affects the cAMP second messenger system and coupled dopamine D1 and 5-HT1A receptors in the living monkey brain: a positron emission tomography study using microdialysis. *J Cereb Blood Flow Metab.* 24:898-906.

Tsukada, H., N. Harada, H. Ohba, S. Nishiyama, and T. Kakiuchi. 2001a. Facilitation of dopaminergic neural transmission does not affect [^{11}C]SCH23390 binding to the striatal D(1) dopamine receptors, but the facilitation enhances phosphodiesterase type-IV activity through D(1) receptors: PET studies in the conscious monkey brain. *Synapse.* 42:258-65.

Tsukada, H., T. Kakiuchi, S. Nishiyama, H. Ohba, and N. Harada. 2001b. Effects of aging on 5-HT(1A) receptors and their functional response to 5-HT(1a) agonist in the living brain: PET study with [carbonyl-^{11}C]WAY-100635 in conscious monkeys. *Synapse.* 42:242-51.

U.S. Department of Health and Human Services. 2001. The Surgeon General's call to action to prevent and decrease overweight and obesity. U.S. Department of Health and Human Services, Public Health Service, Office of the Surgeon General, Rockville, MD. 60.

Ueki, J., C.G. Rhodes, J.M. Hughes, R. De Silva, D.C. Lefroy, P.W. Ind, F. Qing, F. Brady, S.K. Luthra, C.J. Steel, and et al. 1993. In vivo quantification of pulmonary beta-adrenoceptor density in humans with (S)-[^{11}C]CGP-12177 and PET. *J Appl Physiol.* 75:559-65.

van Oene, J.C., J.B. de Vries, and A.S. Horn. 1984. The effectiveness of yohimbine in blocking rat central dopamine autoreceptors in vivo. *Naunyn Schmiedebergs Arch Pharmacol.* 327:304-11.

van Waarde, A., R.L. Anthonio, T.J. Visser, P.H. Elsinga, H. Posthumus, A.M. Weemaes, P.K. Blanksma, G.M. Visser, A.M. Paans, and W. Vaalburg. 1995. Quantification of an ^{11}C-labelled beta-adrenoceptor ligand, S-(-)CGP 12177, in plasma of humans and rats. *J Chromatogr B Biomed Appl.* 663:361-9.

van Waarde, A., W. Vaalburg, P. Doze, F.J. Bosker, and P.H. Elsinga. 2004. PET imaging of beta-adrenoceptors in human brain: a realistic goal or a mirage? *Curr Pharm Des.* 10:1519-36.

Varga, G., M. Papp, and E.S. Vizi. 1990. Cholinergic and adrenergic control of enzyme secretion in isolated rat pancreas. *Dig Dis Sci.* 35:501-7.

Verde, I., G. Vandecasteele, F. Lezoualc'h, and R. Fischmeister. 1999. Characterization of the cyclic nucleotide phosphodiesterase subtypes involved in the regulation of the L-type Ca^{2+} current in rat ventricular myocytes. *Br J Pharmacol.* 127:65-74.

Vesalainen, R.K., M. Pietila, K.U. Tahvanainen, T. Jartti, M. Teras, K. Nagren, P. Lehikoinen, R. Huupponen, H. Ukkonen, M. Saraste, J. Knuuti, and L.M. Voipio-Pulkki. 1999. Cardiac positron emission tomography imaging with [^{11}C]hydroxyephedrine, a specific tracer for sympathetic nerve endings, and its functional correlates in congestive heart failure. *Am J Cardiol.* 84:568-74.

Vicini, E., and M. Conti. 1997. Characterization of an intronic promoter of a cyclic adenosine 3',5'-monophosphate (cAMP)-specific phosphodiesterase gene that confers hormone and cAMP inducibility. *Mol Endocrinol.* 11:839-50.

Vieira, E., Y.J. Liu, and E. Gylfe. 2004. Involvement of alpha1 and beta-adrenoceptors in adrenaline stimulation of the glucagon-secreting mouse alpha-cell. *Naunyn Schmiedebergs Arch Pharmacol.* 369:179-83.

Vinik, A.I., M.T. Holland, J.M. Le Beau, F.J. Liuzzi, K.B. Stansberry, and L.B. Colen. 1992. Diabetic neuropathies. *Diabetes Care.* 15:1926-75.

Vinik, A.I., R.E. Maser, B.D. Mitchell, and R. Freeman. 2003. Diabetic autonomic neuropathy. *Diabetes Care.* 26:1553-79.

Wachtel, H. 1983. Potential antidepressant activity of rolipram and other selective cyclic adenosine 3',5'-monophosphate phosphodiesterase inhibitors. *Neuropharmacology.* 22:267-272.

Wang, P., J.G. Myers, P. Wu, B. Cheewatrakoolpong, R.W. Egan, and M.M. Billah. 1997. Expression, purification, and characterization of human cAMP-specific phosphodiesterase (PDE4) subtypes A, B, C, and D. *Biochem. Biophys. Res. Commun.* 234:320-324.

Wang, Z., Y. Kontani, Y. Sato, T. Mizuno, N. Mori, and H. Yamashita. 2003. Muscle type difference in the regulation of UCP3 under cold conditions. *Biochem Biophys Res Commun.* 305:244-9.

Weibel, E.R. 2002. Physiology: the pitfalls of power laws. *Nature.* 417:131-2.

West, D.B., and B. York. 1998. Dietary fat, genetic predisposition, and obesity: lessons from animal models. *Am J Clin Nutr.* 67:505S-512S.

Whalin, M.E., R.L. Garrett Jr., W.J. Thompson, and S.J. Strada. 1989. Correlation of cell-free brain cyclic nucleotide phosphodiesterse activities to cyclic AMP decay in intact brain slices. *Second Messengers Phosphoproteins.* 12:311-325.

Xu, R.X., A.M. Hassell, D. Vanderwall, M.H. Lambert, W.D. Holmes, M.A. Luther, W.J. Rocque, M.V. Milburn, Y. Zhao, H. Ke, and R.T. Nolte. 2000. Atomic structure of PDE4: insights into phosphodiesterase mechanism and specificity. *Science.* 288:1822-5.

Yach, D., D. Stuckler, and K.D. Brownell. 2006. Epidemiologic and economic consequences of the global epidemics of obesity and diabetes. *Nat Med.* 12:62-6.

Yan, C., A.Z. Zhao, J.K. Bentley, K. Loughney, K. Ferguson, and J.A. Beavo. 1995. Molecular cloning and characterization of a calmodulin-dependent phosphodiesterase enriched in olfactory sensory neurons. *Proc Natl Acad Sci U S A.* 92:9677-81.

Ye, Y., K. Jackson, and J.M. O'Donnell. 2000. Effects of repeated antidepressant treatment of type 4A phosphodiesterase (PDE4A) in rat brain. *J Neurochem.* 74:1257-62.

Ye, Y., and J.M. O'Donnell. 1996. Diminished noradrenergic stimulation reduces the activity of rolipram-sensitive, high-affinity cyclic AMP phosphodiesterase in rat cerebral cortex. *J Neurochem.* 66:1894-1902.

Yoshitomi, H., K. Yamazaki, S. Abe, and I. Tanaka. 1998a. Differential regulation of mouse uncoupling proteins among brown adipose tissue, white adipose tissue, and skeletal muscle in chronic beta 3 adrenergic receptor agonist treatment. *Biochem Biophys Res Commun.* 253:85-91.

Yoshitomi, H., K. Yamazaki, and I. Tanaka. 1998b. Cloning of mouse uncoupling protein 3 cDNA and 5'-flanking region, and its genetic map. *Gene.* 215:77-84.

Young, J.B., and L. Landsberg. 1977. Suppression of sympathetic nervous system during fasting. *Science.* 196:1473-5.

Young, J.B., E. Saville, N.J. Rothwell, M.J. Stock, and L. Landsberg. 1982. Effect of diet and cold exposure on norepinephrine turnover in brown adipose tissue of the rat. *J Clin Invest.* 69:1061-71.

Zhang, H.T., S.A. Frith, J. Wilkins, and J.M. O'Donnell. 2001. Comparison of the effects of isoproterenol administered into the hippocampus, frontal cortex, or amygdala on behavior of rats maintained by differential reinforcement of low response rate. *Psychopharmacology (Berl).* 159:89-97.

Zhang, H.T., Y. Zhao, Y. Huang, C. Deng, A.T. Hopper, M. De Vivo, G.M. Rose, and M. O'Donnell J. 2006. Antidepressant-like effects of PDE4 inhibitors mediated by the high-affinity rolipram binding state (HARBS) of the phosphodiesterase-4 enzyme (PDE4) in rats. *Psychopharmacology (Berl).*

Zhao, Y., H.T. Zhang, and J.M. O'Donnell. 2003. Inhibitor binding to type 4 phosphodiesterase (PDE4) assessed using [^{3}H]piclamilast and [^{3}H]rolipram. *J Pharmacol Exp Ther.* 305:565-72.

Zimmet, P., K.G. Alberti, and J. Shaw. 2001. Global and societal implications of the diabetes epidemic. *Nature.* 414:782-7.